

**THERMAL RAMPING TECHNIQUE : A FACILE
NANOWIRES SYNTHESIS TECHNIQUE FOR GAS
SENSING APPLICATIONS**

ZAINAL ABIDIN BIN ALI

**FACULTY OF SCIENCE
UNIVERSITY OF MALAYA
KUALA LUMPUR
2012**

**THERMAL RAMPING TECHNIQUE : A FACILE
NANOWIRES SYNTHESIS TECHNIQUE FOR GAS
SENSING APPLICATIONS**

ZAINAL ABIDIN BIN ALI

**DISSERTATION SUBMITTED IN FULFILMENT OF
THE REQUIREMENTS FOR THE DEGREE OF
MASTER OF SCIENCE**

**DEPARTMENT OF PHYSICS
FACULTY OF SCIENCE
UNIVERSITY OF MALAYA
KUALA LUMPUR
2012**

UNIVERSITI MALAYA
ORIGINAL LITERARY WORK DECLARATION

Name of Candidate: Zainal Abidin Bin Ali

(I.C/Passport No: 870713-09-5185)

Registration/Matric No: SGR 100014

Name of Degree: Master of Science

Title of Project Paper/Research Report/Dissertation/Thesis ("this Work"):

Thermal Ramping Technique : A Facile Nanowires Synthesis Technique For Gas Sensing Applications

Field of Study:

Material Science - Gas Sensor

I do solemnly and sincerely declare that:

- (1) I am the sole author/writer of this Work;
- (2) This Work is original;
- (3) Any use of any work in which copyright exists was done by way of fair dealing and for permitted purposes and any excerpt or extract from, or reference to or reproduction of any copyright work has been disclosed expressly and sufficiently and the title of the Work and its authorship have been acknowledged in this Work;
- (4) I do not have any actual knowledge nor do I ought reasonably to know that the making of this work constitutes an infringement of any copyright work;
- (5) I hereby assign all and every rights in the copyright to this Work to the University of Malaya ("UM"), who henceforth shall be owner of the copyright in this Work and that any reproduction or use in any form or by any means whatsoever is prohibited without the written consent of UM having been first had and obtained;
- (6) I am fully aware that if in the course of making this Work I have infringed any copyright whether intentionally or otherwise, I may be subject to legal action or any other action as may be determined by UM.

Candidate's Signature

Date : 31st December 2012

Subscribed and solemnly declared before,

Witness's Signature

Date : 31st December 2012

Name: Dr. Rustam Puteh
Designation : Assoc. Prof

ABSTRACT

Nanowires of SnO₂ have been successfully synthesized using a modified, simplified and less complicated carbothermal reduction technique, namely thermal ramping technique. This technique is developed to ease the synthesis process of nanowires for the development of gas sensing device. Contrary to conventional carbothermal reduction technique, no inert gas as a carrier is required. Distance of source material to substrates parameter is also eliminated. This new technique introduces ramping parameter to the conventional technique to compensate the elimination of the carrier gas. SnO₂ was chosen as the raw material due to its wide availability, low-cost and widely used in the sensing devices. The SnO₂ nanowires were synthesized under different controlled parameter such as heating temperature, Au catalyst and number of ramping. The morphological and crystal structure of the yielded nanowires were characterized using the field emission scanning electron microscopy (FESEM), Energy dispersive X-ray spectroscopy (EDX) and X-ray diffraction (XRD). It was discovered that nanowires density increased as the temperature increased. This could be attributed to the increased in the Sn, SnO, SnO₂ and CO/CO₂ vapour supply to the substrates. XRD results show that the nanowires yielded at 700 °C to 900 °C have tetragonal rutile structure of SnO₂, whereas at 1000 °C, the nanowires yielded were detected to be SnO₂, Sn₃O₄ and Sn₂O₃/SnO.SnO₂. The density of SnO₂ nanowires grown with Au catalyst was also observed to be significantly higher than that of SnO₂ nanowires without Au catalyst. The SnO₂ nanowires grown with and without Au catalyst can be attributed to the vapour-liquid-solid (VLS) and vapour-solid (VS) mechanism, respectively. Moreover, the density of the SnO₂ nanowires also increased as the ramp number increased. No nanowires were observed in the first ramp. The SnO₂ nanowires only started to appear in the second ramp and densified in the third ramp. In hydrogen gas sensing test, the

sensor was observed to display the optimum performance at 200 °C, with response and recovery times were approximately 20 s and 140 s, respectively. At different hydrogen concentration, the sensitivities were observed to be highest and lowest at 1000 ppm and 200 ppm, respectively. The unstable and fluctuated electrical response and sensitivities of the sensor observed at 400 ppm, 300 ppm and 200 ppm could be attributed to the presence of water vapour on the sensor and complex reaction probably occurred between the vapour with the oxygen and hydrogen.

ABSTRAK

Nanodawai SnO₂ telah berjaya disintesis menggunakan kaedah penurunan karboterma yang diubahsuai, diringkas dan kurang rumit yang dikenali sebagai teknik tanjakan terma. Teknik ini dicipta untuk memudahkan proses sintesis nanodawai bagi kegunaan sebagai pengesan gas. Bertentangan dengan teknik penurunan karboterma konvensional, teknik ini tidak menggunakan sebarang gas nadir sebagai gas pengangkut. Parameter jarak sumber bahan ke substrat telah diabaikan. Teknik baru ini memperkenalkan satu parameter iaitu tanjakan terma sebagai ganti kepada penggunaan gas pengangkut di dalam teknik karboterma konvensional. SnO₂ dipilih sebagai bahan mentah kerana ia mudah didapati, murah dan digunakan secara meluas dalam peralatan pengesan. Nanodawai SnO₂ disintesis dengan parameter kawalan yang berbeza-beza seperti suhu pemanasan, Au sebagai sistem pemangkin dan bilangan tanjakan. Morfologi dan struktur kristal nanodawai yang terhasil dicirikan menggunakan mikroskopi imbasan electron (FESEM), spektroskopi sebaran tenaga (EDX) dan belauan sinar-X (XRD). Didapati kepadatan nanodawai bertambah apabila suhu meningkat. Ini mungkin disebabkan peningkatan bekalan wap Sn, SnO, SnO₂ dan CO/CO₂ kepada substrat. Keputusan XRD menunjukkan nanodawai yang dihasilkan pada suhu 700 °C hingga ke 900 °C mempunyai struktur SnO₂ rutil tetragon, manakala pada suhu 1000 °C, nanodawai yang terhasil dikesan mempunyai SnO₂, Sn₃O₄ dan Sn₃O₃/SnO.SnO₂. Kepadatan nanodawai SnO₂ yang disintesis menggunakan Au sebagai pemangkin juga dilihat jelas lebih tinggi berbanding sintesis nanodawai SnO₂ yang tidak menggunakan Au. Mekanisma wap-cecair-pepejal (VLS) dan mekanisma wap-pepejal (VS) masing-masing mempengaruhi pertumbuhan nanodawai SnO₂ yang menggunakan Au dan tidak menggunakan Au. Selain itu, kepadatan nanodawai SnO₂ juga bertambah apabila bilangan tanjakan bertambah. Tiada nanodawai

terhasil pada tanjakan pertama. Nanodawai SnO₂ hanya muncul pada tanjakan kedua dan semakin padat pada tanjakan ketiga. Dalam ujian mengesan gas hidrogen, pengesan memberikan prestasi optimum pada suhu 200 °C, dengan masing-masing memberikan gerakbalas dan masa pemulihan dianggarkan lebih kurang 20 saat dan 40 saat. Pada kepekatan gas hidrogen yang berbeza, nilai sensitiviti tertinggi dan terendah pengesan adalah pada 1000 ppm dan 200 ppm. Gerak balas elektik dan sensitiviti yang tidak stabil dan turun naik pada 400 ppm, 300 ppm dan 200 ppm mungkin disebabkan kehadiran wap air pada permukaan pengesan dan tindakbalas kompleks yang mungkin berlaku antara wap air dengan oksigen dan hidrogen.

ACKNOWLEDGEMENTS

“In the name of Allah, the most merciful and the most beneficial”

Thanks and praises to Allah s.w.t who granted me the strength and light of guidance to complete this dissertation.

I would like to express my sincere gratitude to my supervisor, Assoc. Prof. Dr. Rustam Puteh for his immense and continuous support and motivation. His guidance, suggestion and knowledge really helped me to go through this research and thesis writing. I am forever indebted to him.

I would also like to thank Assoc. Prof. Dr. Roslan Md Nor and Prof. Dr Rosiyyah Yahya for their support, encouragement, insightful comments and assistance. Many thanks go to my senior lab mates, Mrs Wan Ahliah and Ms Farida for their helps throughout this research journey. It was their present that had made the lab's life so cheerful. My acknowledgement also goes to technicians and office staffs of Department of Physics for their cooperation.

Last but not least, I would like to thank my family, my parents, my brothers and my sisters who always stood behind me, through thick and thin. Thanks for the supports, cares and inspirations.

TABLE OF CONTENTS

ABSTRACT	ii
ABSTRAK	iv
ACKNOWLEDGEMENT	vi
TABLE OF CONTENT	vii
LIST OF FIGURES	xi
LIST OF TABLES	xiv
Chapter 1 Introduction	1
1.1 Nanostructures	1
1.2 Application of Nanostructures in Devices	2
1.2.1 Solar cell	2
1.2.2 Water treatment	3
1.2.3 Sensing Application	3
1.3 Gas Sensor	5
1.3.1 Type of Gas Sensor	5
1.3.2 Nanowires for Chemiresistor Gas Sensor	7
1.3.3 Fabrication Process of Nanowire Based Sensor	10
1.3.3.1 Electron Beam Evaporation	10
1.3.3.2 Focus Ion Beam (FIB)	11
1.3.3.3 Contact Printing	12
1.4 Metal Oxide Nanowires Gas Sensor	13
1.4.1 Categories of Metal Oxide	13
1.4.2 Sensing Mechanism of Metal Oxide Sensor	15
1.4.3 Application of Nanowire in Metal Oxide Gas Sensor	18

1.5	SnO ₂ Nanowires Sensor for Hydrogen Detection	20
1.6	Objectives	22
Chapter 2	Literature Review of Nanowires Synthesis Technique	23
2.1	Nanowires Synthesis Technique	23
2.1.1	Size Reduction Litography	24
2.1.2	Templates Method	25
2.1.3	Solvothermal Methods	27
2.1.4	Sol Gel	27
2.1.5	Vapor-Liquid-Solid (VLS) Mechanism Growth Techniques	28
2.2	Growth Mechanism of SnO ₂ Nanowires In Carbothermal Reduction Technique	31
2.3	Effect of Various Parameters towards SnO ₂ Morphology	34
2.3.1	Effect of Temperature	34
2.3.2	Source Material to Substrate Distance	35
2.3.3	Molar Ratio of SnO ₂ : C	36
2.3.4	Gold thickness	37
2.3.5	Inert Gas Flow rate	39
2.3.6	Oxygen in Argon Gas Carrier	40
2.4	Thermal Ramping As A Facile Nanowires Synthesis Technique	41
Chapter 3	Experimental Setup	43
3.1	Introduction	43
3.2	Synthesis of SnO ₂ Nanowires	44
3.2.1	Substrate preparation	44
3.2.2	SnO ₂ Nanowires Synthesis and Depositing	44

	Technique	
3.2.3	Factors Affecting Nanowires Formation	45
3.2.3.1	Number of Ramping	45
3.2.3.2	Deposition Temperature	47
3.2.3.3	Au as Growth Catalyst	47
3.2.3.4	Summary For Synthesizing Parameter	48
3.3	Characterisation of SnO ₂ Nanostructures	48
3.3.1	X-ray Diffraction (XRD)	48
3.3.2	Field Effect Scanning Electron Microscopy (FESEM)	49
3.3.3	Energy Dispersive X-ray Spectroscopy (EDX)	49
3.4	Gas Sensing Measurement	49
3.4.1	Gas Sensing Setup	49
3.4.2	Effect of Heating Temperature	50
3.4.3	Effect of Hydrogen Gas Concentration	51
Chapter 4	Results and Discussion: Synthesis of SnO₂ Nanowires	52
4.1	Introduction	52
4.2	Effect of Deposition/Ramp Up Temperature	53
4.3	Effect of Number of Ramping	57
4.4	Effect of Heating Time in Single Ramping	59
4.5	Effect of Au Catalyst Thickness (Based on ZnO precursor)	61
4.6	Effect of Au Catalyst in Thermal Ramping Technique	63
4.7	Conventional Carbothermal Technique	65
4.8	Growth Mechanism of SnO ₂ Nanowires In Thermal Ramping Technique	68
Chapter 5	Results and Discussion: Hydrogen Gas Sensing Test	72

5.1	Gas Sensing Results	72
5.1.1	Different operating temperature	72
5.1.2	Different gas concentration	74
5.1.3	Gas Sensor Sensitivity	75
5.2	Sensing Mechanism of SnO ₂ Nanowires Sensor	77
Chapter 6	Conclusion	81
	List of References	85
	List of publication	94

LIST OF FIGURES

Chapter 1 Introduction to Nanostructures and Applications

FIGURE		PAGE
1.1	Nanowire response to the atmosphere change from nitrogen to synthetic air against the nanowire radius.	8
1.2	An example of sensor using: (a) thin film nanowires[107], (b) an array of single nanowire[108] and (c) single nanowire	9
1.3	Scanning electron SEM images showing the steps of the in-situ lift-out fabrication procedure in the FIB/SEM system. (a) an intermediate ZnO nanorod on Si substrate, next to the FIB needle, (b) an intermediate ZnO nanorod – picked-up by the needle; (c) a single ZnO nanorod selected for sensor fabrication. Inset shows nanosensor substrate template (glass with Al contacts as contact electrodes); (d) a square hole cut on the glass; (e) place the ZnO nanorod over the hole; (f) single nanorod welded to both electrode/external connections as final sensor.	11
1.4	Schematic of the process flow for contact printing of nanowire arrays	13
1.5	Schematic diagram of band bending after chemisorptions of charged species (here the ionosorption of oxygen) EC, EV, and EF denote the energy of the conduction band, valence band, and the Fermi level, respectively, while Λ_{air} denotes the thickness of the space-charge layer, and eV surface denotes the potential barrier. The conducting electrons are represented by e^- and $+$ represents the donor sites.	16
1.6	Structural and band models of conductive mechanism upon exposure to reference gas.(a) with or (b) without CO	17

1.7	(a) Schematic depiction of the major process taking place at a SnO ₂ nanowire/nanobelt surface when exposed to O ₂ . (b) Band diagram of the pristine SnO ₂ nanostructure and in the vicinity (and beneath) a Pd nanoparticle. The radius of the depletion region is determined by the radius of the spillover zone.	18
1.8	A schematic of tetragonal unit cell of SnO ₂	21

Chapter 2 Literature Review of Nanowires Synthesis Technique

2.1	Schematic of photo lithography using UV light to pattern the resist layer.	24
2.2	(a) The SEM image of AAO membrane surface (from Ref. [107]) and (b) AAO membrane uses a template to make nanowires by electroplating.	26
2.3	The furnace diagram of VLS nanowire synthesis method.	29
2.4	VLS diagram illustrating the growth of nanowires	32
2.5	FESEM images of the morphology of SnO ₂ nanowires obtained at different heating temperature: (a) 871 °C (b) 843 °C and 648 °C	34
2.6	SEM images showing the typical morphologies of the as-synthesized SnO ₂ nanostructures: (a) wide nanobelts; (b) narrow nanobelts, inset showing a closer inspection of one curved SnO ₂ nanobelt; (c) thick nanowires; (d) thin nanowires.	35
2.7	Schematic diagram showing the formation temperatures of these morphologies	36
2.8	SEM images of grown nanostructures using different SnO ₂ : C ratios of (a) 1:2 at ×3000, (b) 1:2 at ×10,000, (c) 1:4 at ×10,000 and (d) 1:4 at ×30,000	37
2.9	FESEM images of SnO ₂ nanowires grown on different gold thin film thickness; a) 2nm, b) 5nm c) a 10nm and d) a 15nm. The average diameters of nanowires are 50 nm, 70 nm, 90 nm and 140 nm, respectively.	38
2.10	SEM images of ZnO nanowires grown at different thickness of Au film: a) 50 nm, b) 10 nm.	39
2.11	ZnO nanowires grown on Au-coated Si substrates with different Ar flowrate ; (a) 10 sccm, (b) 25 sccm and (c)	40

150 sccm.

2.12	(a), (b) ZnO combs and nanosheets fabricated by a MOCVD process. (c) SnO ₂ nanowires obtained under a flow of O ₂ (0.01%)/Ar gas and (d) SnO ₂ nanoribbons fabricated under a flow of O ₂ (1%)/Ar gas.	41
------	--	----

Chapter 3 Experimental Setup

3.1	Thermal ramping profile for 900 °C	45
3.2	Heating pattern ; (a) Single ramp , (b) Double ramp, and (c) Long-Single ramping profile.	46
3.3	Cross section of the sensing chamber	50

Chapter 4 Result and Discussion: Synthesis of SnO₂ Nanowires

4.1	FESEM images of SnO ₂ nanowires grown on Si substrates at different deposition/ramp up temperature; (a) 600 C, (b) 700 °C, (c) 800 °C, (d) 900 °C and (e) 1000 °C	53
4.2	Comparison of XRD patterns of SnO ₂ nanowires synthesized at different ramp up temperatures to the SnO ₂ powder used as the precursor.	56
4.3	FESEM images of nanowires synthesized at different ramp number; (a) Single ramp (1R), (b) Double ramp (2R) and (c) Triple ramp (3R).	57
4.4	Nanowires yielded from single ramp ; (a) 30 minutes at 900 °C, (b) 30 minutes and (c) 110 minutes at 1000 °C	59
4.5	Nanowires synthesized using different Au thickness; (a) 10 nm and (b) 25 nm.	61
4.6	Figure 4.6: XRD pattern of nanowires formed using ZnO as the precursor.	62
4.7	FESEM images of SnO ₂ nanowires synthesized (a) with and (b) without Au catalyst. Images of nanowires (c)	63

	with Au catalyst at 3000 x magnification	
4.8	FESEM images of nanowires synthesized using the conventional carbothermal technique with the distance of source material to substrates was varied ; (a) 10 cm and (b) 15 cm	65
4.9	Presence of droplets at the tip of the nanowires confirmed the growth was governed by VLS mechanism.	67
4.10	VLS diagram illustrating the growth of nanowires.	69
4.11	Schematic examples of possible nanowire structures formed under a variety of growth conditions. S1, S2 and S3 are the cone shaped structures whereas S4 is due to the vapour diffusion via nanowires sidewall.	70

Chapter 5 Results and Discussion: Hydrogen Gas Sensing Test

5.1	Electrical response at different operating temperature and constant hydrogen concentration (1000ppm).	73
5.2	Figure 5.2: Electrical response of SnO ₂ nanowires thin film towards hydrogen gas at different concentration and constant operating temperature (T= 200 °C).	75
5.3	Sensitivity of SnO ₂ nanowires sensor at different operating temperature	76
5.4	Sensitivity of SnO ₂ nanowire sensor at different gas concentrations	76

LIST OF TABLES

Chapter 1 Introduction to Nanostructures and Applications

TABLE		PAGE
1.1	Comparison of gas sensing properties of thin film nanowires and single nanowires gas sensor.	9
1.2	Categories of metal oxide based on their electrical structure	14

Chapter 3 Experimental Setup

3.1	All parameters used in the synthesization experiment	48
-----	--	----

Chapter 4 Results and Discussion: Synthesis of SnO₂ Nanowires

4.1	The weight ratio of the SnO ₂ nanowires obtained by EDX analysis	54
-----	---	----

Chapter 5: Results and Discussion: Hydrogen Gas Sensing Test

5.1	The response and recovery times of SnO ₂ nanowires sensor upon gas sensor exposure	74
-----	---	----

Chapter 1

Introduction

1.1 Nanostructures

Nanostructure has been things of interest to researchers ever since it was observed. It is physically very small, which is one-billionth of a meter and can be further classified into several categories according to their dimensionalities; zero dimensional (0D) (eg: quantum dots), one dimensional (1D) (eg: nanowires, nanobelts and nanotubes), two dimensional (2D) (eg: thin film) and three dimensional (3D) (eg: plates and flower like).

In general nanostructure exhibits different properties compared to its bulky counterpart. For example, the structural miniaturization enhances the optical properties of silver nanoparticles; absorption and scattering of light [1-2]. This is because these properties depend on the size and the shape of the particles [3]. Nanosized-structures possess absorption band which is not present in the bulky size structures. Should the light incident on the nanostructures, the scattering and reflectivity would be very different compared to the bulky structures. This gives rise to the intense colours of suspensions or sols because only nanosized-structures respond to the incident light. This phenomenon is known as local surface plasmon resonance (LSPR).

In term of mechanical properties for example, most metals are made up of small crystalline grains; the boundaries or interfaces between the grain slow down or resist the propagation of defects when the material is stressed, which signifies its strength. If these grains can be made very small, or nanoscale in size, the interface area within the material would be greatly increased, therefore enhances its strength. For example, nanocrystalline nickel is as strong as hardened steel [4].

1.2 Application of Nanostructures in Devices

Realising the unique behaviours and properties of a nanosize material could possess, tremendous efforts have been put to use nanostructures as elements in devices. This is probably when the term nanotechnology started to gain popularity. Although the term has had several definitions, the U.S. National Nanotechnology Initiative defines nanotechnology as a manipulation of anything smaller than 100 nm for their novel applications. Capability to apply nanotechnology would open the door of possibility to enhance and improve the performance of devices according to our desire. Among the most common research in nanotechnology are solar cell, water treatment and sensor.

1.2.1 Solar cell

Performance and efficiency of a solar cell can be enhanced by modifying its surface structures [5-6]. Creating different nanostructures on the surface offers several advantages for solar cells including; (i) high scattering effect so that light beams have to travel longer distance hence producing more electrons [6] and (ii) improve absorption [7]. Absorption can be improved by changing the surface structures using ultrafast pulsed laser irradiation [8]. Researchers have demonstrated that this irradiation has successfully makes nanospike patterns on the silicon surface, which capable of reducing reflection of light from the surface [9]. Therefore more light will be absorbed. Low cost in producing solar cell can be achieved by using self-assembled nanostructures method [10] instead of current wet chemical processing approach, used in the solar industry.

1.2.2 Water treatment

Nanostructured materials exhibit several advantages over conventional microstructured materials for water purification, including larger relative surface areas. Yi Cui et al. [11] explain that most typical water purifiers work by trapping bacteria in tiny pores of filter material. Forcing water through those filters requires electric pumps which consume quite significant amount of energy. In addition, the filters could get clogged and must be maintained regularly. The new material, in contrast, has relatively huge pores, which allow water to flow through easily. In addition it kills bacteria right away, instead of just trapping them. It is known that bacteria can be killed when in contact with silver or electricity [12], and decided to combine both approaches. Sub-microscopic silver nanowires are spread onto cotton, and then added a coating of carbon nanotubes, which give the filter extra electrical conductivity. Tests on E. coli-tainted water showed that the electrified cotton/silver could kill up to 98 percent of the bacteria. The filter material no longer clogged, and water have flown through it very quickly without any need for a pump. This could lower the cost of a wide array of filtration technologies for water, food, air, and pharmaceuticals where the need to replace filters regularly is a large cost. Moreover, these chlorine-free water purification methods are better since carcinogenic disinfection byproducts could be formed when components of natural water interact with chlorines.

1.2.3 Sensing Application

Nanostructures make good sensors because their small dimensions enhance the sensitivity of the sensors. For example, consider nanowire sensors that detect chemicals and biologicals molecules in medical field like virus and protein. The similarity of average diameter that nanowires and protein enables the creation of tool for detection

and treatment of disease[13]. Silicon nanowires have been used for single-stranded DNA detection where negatively charge polyanionic macromolecule binding towards the p-type nanowire surface leads to an increase in conductance value [14].

Nearly all modern, commercial, low-cost, combustible gas sensors are made of conductive thin films of metal oxides. An exposure to a volatile compound like benzene, for example, will cause a reaction which alters the current running through the film, thereby triggering an alarm. Thin-film sensors are effective, but require heat to operate. Frequent heating can degrade the materials that make up the films and contacts, causing reliability problems [15]. Moreover, most thin-film sensors work within a narrow range; might detect a small amount of toluene in the air, but fail when gas is in massive release, according to [16]. By using nanowire, the range of the new sensors runs from just 50 parts per billion up to 1 part per 100, or 1 percent of the air in a room [16]. Each nanowire is a defect-free single crystal, rather than the conglomeration of crystal grains in thin-film sensors, so they're less prone to degradation.

In a report [17], Lu explains that a small amount of NO₂ gas on a thin film can diminish the current by only 2 percent, compared to 50 percent decrease observed in a zinc oxide nanowire. Nanowires also can be more quickly reset to begin sensing again. For films, elaborate methods are needed to cleanse the surface, requiring from half an hour to many hours. With nanowires, a voltage signal to the transistor drives away the chemical, restoring the original sensing condition in a matter of minutes [18].

Many more reports have been published on the advantages of using nanomaterials in solar cell [19-21] and water treatment [22-24], however only the sensing technology is of our interest and will be discussed in the next part.

1.3 Gas Sensor

1.3.1 Type of Gas Sensor

There is various type of gas sensor available. It is classified based on its working mechanism. Listed below are some of them.

a) Piezoelectric Gas Sensor

This type of sensor relies on mass changes to detect the gas molecules or analyte. Analyte adsorbed onto the sensor will result in a mass change which is registered through the wave velocity or resonant frequency of the sensor. A surface acoustic wave (SAW) device is an example of a piezoelectric sensor that detects changes in its wave velocity. The SAW devices operate between 30 and 300 MHz [25], higher frequencies than quartz crystals, which rely on changes in its resonant frequency. The sensor is usually coated in order to modulate its selectivity to different gaseous species. Piezoelectric gas sensor has been used as the building block in attempts to create electronic nose applications where by using an array of sensors, it can emulate the mammalian nose that can simulate mammalian olfactory responses to various aromas.

b) Infrared gas sensor

The detection principle utilizes infrared light to interact with gas molecules. Infrared light lies between the visible and microwave portions of the electromagnetic spectrum. It has a frequency range of 1 to 4 THz. When interacts with gas molecules, part of the infrared energy which has the same frequency as the gas molecule's natural frequency will be absorbed while the rest of the radiation will be transmitted. The larger the molecules, the more modes of natural frequencies they have. Natural frequencies are also determined by the molecular structure of the chemicals. They are always the same for a given molecule and bonding structure. As the gas molecules absorb this radiation,

the molecules gain energy and vibrate more vigorously. This vibration results in a rise in the temperature of the gas molecules. The temperature increases in proportion to gas concentration, and is detected by the detector. In contrast, the radiation absorbed by the gas molecules at the particular wavelength will cause a decrease in the original source strength. This radiation energy decrease may as well be detected as a signal. Infrared detectors then convert the electromagnetic radiation energy or temperature changes into electrical signals.

c) Chemiresistor/Conductometric Gas Sensor

When a sensor is exposed to analytes, analytes molecules will be chemically adsorbed on the sensor surface. This adsorption will alter the surface states and hence changes the sensor resistance. A sensor that detects analytes by monitoring this change is called chemiresistors or conductometric. Sensitivity, response and recovery time, and limit of detection (LOD) are among the important performance parameters and the definition is given as follow [26]. The sensitivity of the chemiresistor sensors is defined as the ratio of the device's resistance when exposed to target species to that in ambient air, exactly R_g/R_a (where R denotes resistance, the subscript 'g' denotes target gas, and 'a' denotes ambient air). Response (recovery) time is defined as the time period needed for the device to undergo resistance changing from 10% (90%) to 90% (10%) of the value in equilibrium upon exposure to an oxidizing (reducing) analyte. LOD gives the lowest detection of the sensor. To enhance the performance, many studies have focused on reducing the size of the sensing element in the form of nanorods and nanowires.

1.3.2 Nanowires for Chemiresistor Gas Sensor

The use of nanowires in various gas sensing applications is increasing rapidly as they offer ultrahigh detection ability or sensitivity towards various chemical species [27]. Nanowires have a high aspect ratio. This favours the adsorption of gases on the sensor and increases the sensitivity of the sensor because the interaction between the analytes and the sensing part is higher. The improvement is also manifested by shorter response time [28]. With the small size of nanowires or nanorods, a few gas molecules are sufficient to change the electrical properties of the sensing elements [29]. This allows the detection of a very low concentration of chemical vapors.

However, compared to thin film chemiresistors sensor, nanowires based sensor will only exhibit improved sensitivity when their diameter is approximately 25nm or less [30]. F. Hernandez-Ramirez concluded this based on his study using SnO₂ single nanowire (refer Fig.1). In the case of thin film sensor, most of them are typically in the form of polycrystalline materials with nanosized grains [31]. The interface between the grains forms a potential barrier which electrons must overcome to transport from one grain to another. Adsorption of analyte molecules on the grain boundaries alters the surface state and this potential barrier, which changes the conductance [32]. Therefore smaller grains and larger surface-to-volume ratio would result in a higher sensitivity. Nanowires for example, only when their diameters are comparable to or smaller than the grain size of the thin film, can we observe a higher sensitivity. Electrons inside this small size nanowire have a quasi one-dimensional transport which also contributes to this higher sensitivity [33].

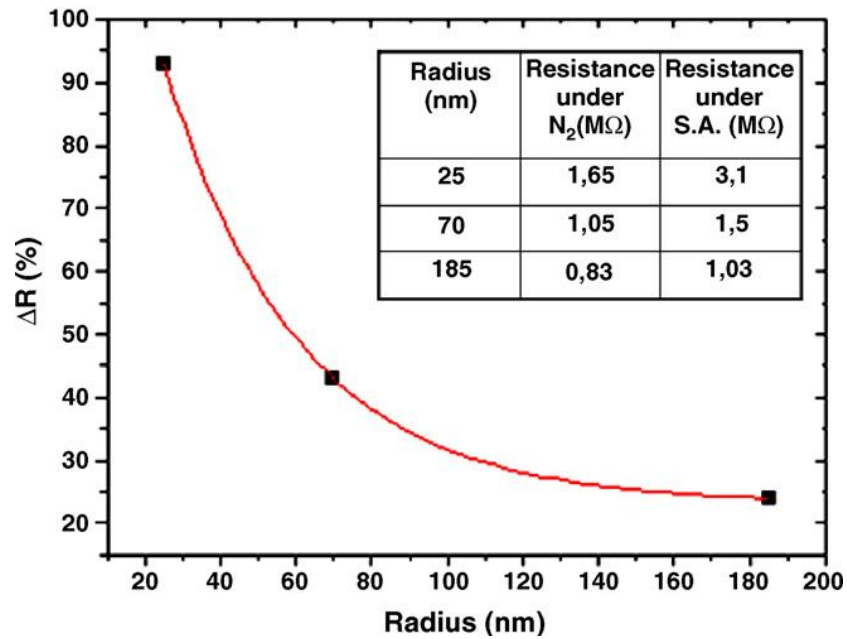


Figure 1.1: Nanowire response to the atmosphere change from nitrogen to synthetic air against the nanowire radius. (from [29,30])

Nanowire can be used in a sensor whether as; (a) nanowires dispersed on a substrate equipped with electrodes (called thin film nanowires) or (b) a single nanowire/an array of single nanowire (refer Fig. 2). They exhibit different performance level. In general, gas sensitivities of single nanowire are far less than the thin film gas sensor [26], although in some cases single nanowire demonstrated better performance. Comparison can be seen in Table 1. The superior performance by the thin film of nanowires is attributed to enhanced sensitivity associated with nanowire/nanowire junctions, which are found only in multiwire devices [34]. However, it should be noted that using an individual nanowire as a single nanocrystal has more advantages from the point of view of stability, repetitivity and reliability as there is not grain boundaries [30].

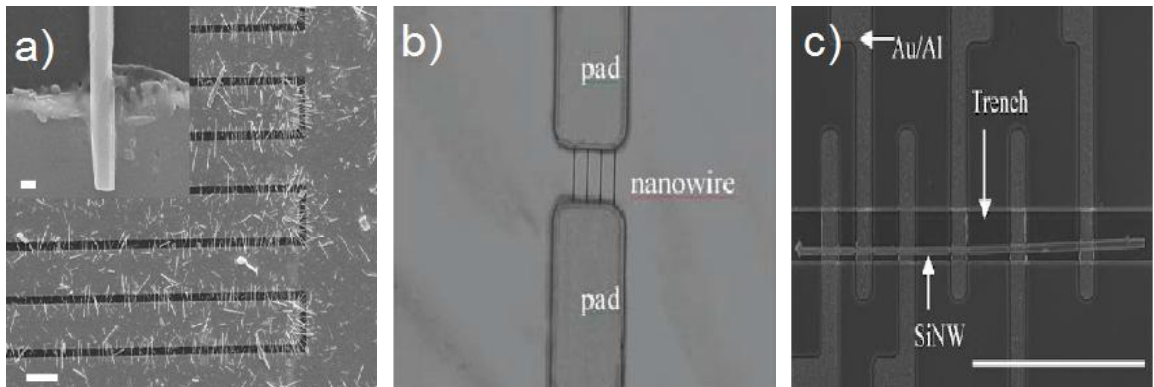


Figure 1.2: An example of sensor using: (a) thin film nanowires[35], (b) an array of single nanowire[36] and (c) single nanowire [37]

Table 1.1: Comparison of gas sensing properties of thin film nanowires and single nanowires gas sensor.

Material		Target gas	Lowest detection concentration	Response /Recovery time	Reference
SnO ₂	Thin film of nanowhiskers	H ₂	10 ppm	N/A	[38]
	Single nanowire	H ₂	100 ppm	N/A	[39]
ZnO	Thin film of nanowires	H ₂	500 ppm	10 mins/ N/A	[40.]
	Single Nanowire	H ₂	200 ppm	30 s/ 50-90 s	[41]
In ₂ O ₃	Thin film of nanowires	H ₂ S	200 ppb	2-3 mins/ N/A	[42]
	Single nanowire	H ₂ S	1 ppm	48 s/ 56 s	[43]

*N/A = not available

1.3.3 Fabrication Process of Nanowire Based Sensor

Fabrication is an assembly process to produce a working sensor. It covers from synthesizing nanowires to establishing the connection between electrodes or contact pads to the nanowires thin film. The good quality of the process ensures the device has a good electron flow and no bias effect to the sensing nanowire.

Nanowires would first be synthesized using various bottom-up or top down approach such as spin coating [44], vapour-liquid-solid [45] and others [46-48]. Then the contact pads could be attached or created to the nanowires using technique such as electron beam evaporation and focus ion beam. Contact printing is used to transfer the nanowires from the growth substrates to the intermediate and sensing substrates.

1.3.3.1 Electron Beam Evaporation

Electron Beam evaporation is a form of physical vapor deposition in which a target anode is bombarded with an electron beam given off by a charged tungsten filament under high vacuum. This electron beam causes atoms from the target to transform into the gaseous phase. These atoms are later precipitate into solid form, coating a thin layer of the anode material. In fabricating sensing devices, the target anode, aurum or aluminium is deposited using E-beam Evaporator onto the surface of the fabricated nanowires (synthesized prior to the fabrication). Gold is used as it has a good reliability contact and a very good conductivity. This ensures the device has a good electron flow and no bias effect to the sensing nanowires [35]. The layer is then coated and patterned using photolithography process to form the contact point. A chemical is used for etching off the pattern. Finally, the photo resist layer is removed to expose the gold pad for contact.

1.3.3.2 Focus Ion Beam (FIB)

Focus ion beam (FIB) machine is typically used to make electrical contact with the single nanowire in gas sensing studies. Usually, synthesized nanowires are transferred from grown substrates to transit or intermediate substrates such as Si/SiO₂ in order to avoid charging problems in the FIB system. This can be accomplished by contact printing technique. Once transferred, single nanowire can be located and selected by FIB needle with the help of a magnification system. The tip of FIB needle is then brought to one end of the single nanowire. The needle is moved until it touches the nanowire. Then the nanowire is attached to the end of the FIB needle as shown in Fig. 3b by depositing a small amount of Pt. This step is repeated for another end of the nanowire. The single nanowire is then raised away from the substrates

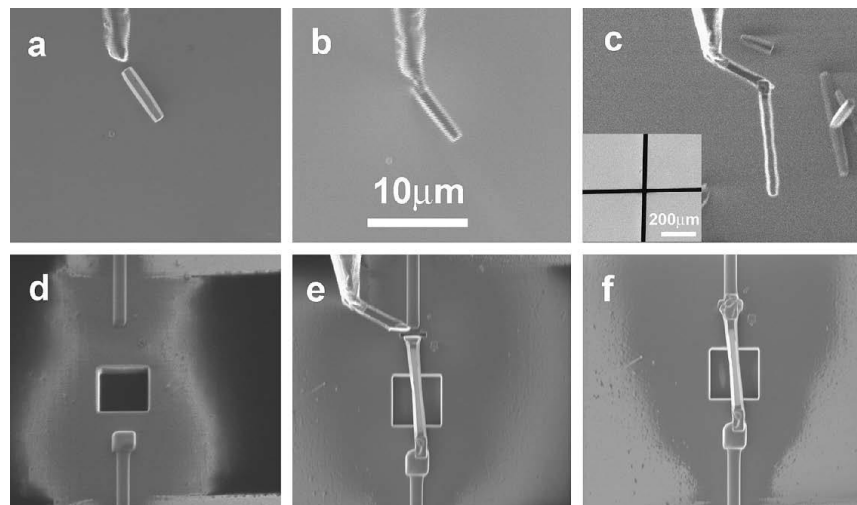


Figure 1.3: Scanning electron SEM images showing the steps of the in-situ lift-out fabrication procedure in the FIB/SEM system. (a) an intermediate ZnO nanorod on Si substrate, next to the FIB needle, (b) an intermediate ZnO nanorod – picked-up by the needle; (c) a single ZnO nanorod selected for sensor fabrication. Inset shows nanosensor substrate template (glass with Al contacts as contact electrodes); (d) a square hole cut on the glass; (e) place the ZnO nanorod over the hole; (f) single nanorod welded to both electrode/external connections as final sensor. (from [49])

A receiver substrate intended for the sensing device is prepared to house the single nanowire. Glass substrate could be used and Al electrodes are deposited as template with external electrodes/connections [49]. Using micromanipulator, the nanowire is carefully positioned over the substrates. The nanowire is fixed to one of the pre-deposited electrodes/external contacts. The nanowire is cut and the needle is raised away from the substrate.

1.3.3.3 Contact Printing

It is a method of transferring nanowires from growth substrates to intermediates or receiver substrates intended for sensing applications. The nanowires are detached off the growth substrates by directionally sliding with the receiver substrates. The detachment is caused by the van der Waals interactions with the surface of the receiver substrate; therefore, resulting in the direct transfer of aligned wires to the receiver. The alignment is due to the lithographically patterned resist coating the receiver substrates. Maintaining nanowire-substrate interactions is essential for the assembly process where dynamic friction is a key for alignment of nanowires and the detachment of nanowires from the donor substrate. Lubricants can be applied to reduce friction which could result in the grinding and breaking of nanowires hampering the alignment. After nanowires printing, the spacer resist is removed by a standard lift-off process using acetone, leaving behind the nanowires that were directly transferred to the patterned regions of the substrate. Details explanation can be found in Zhiyong Fan et al work [50].

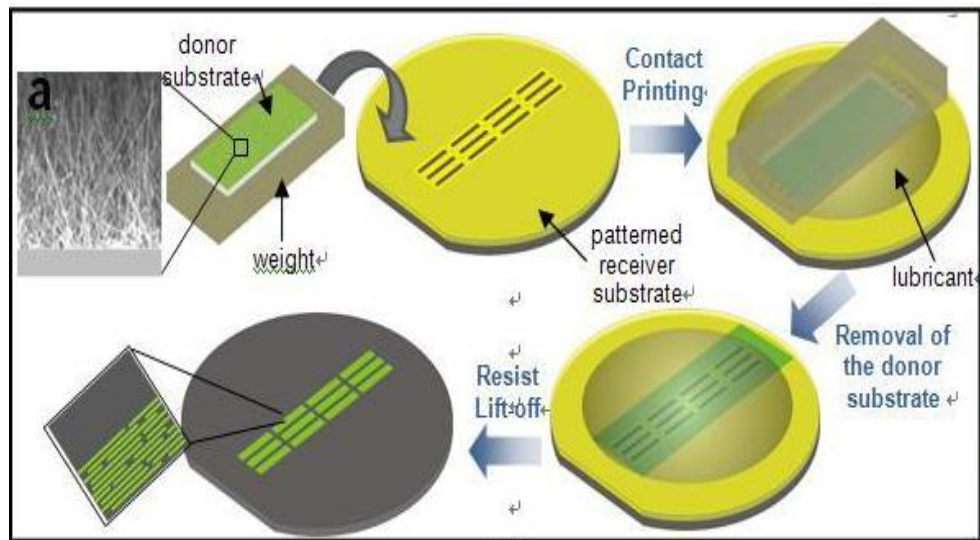


Figure 1.4: Schematic of the process flow for contact printing of nanowire arrays [from 50]

1.4 Metal Oxide Nanowires Gas Sensor

In 1962 Seiyama *et al* discovered that the electrical conductivity of ZnO could be dramatically changed by the presence of reactive gases in the air [51]. Since then, there have been tremendous reports on the applications of semiconducting metal oxides as gas sensors due to their low-cost, high sensitivity and stability [52-53] as well as high compatibility with microelectronic processing. This type of sensor that relies on the change of the conductivity when operating is known as conductimetric sensor.

1.4.1 Categories of Metal Oxide

Many metal oxides are suitable for detecting combustible, oxidizing or reducing gases by conductive measurements, owing to their deviation from stoichiometry and defects such as interstitial vacancies. The following oxides show a gas response in their conductivity: Cr_2O_3 , Mn_2O_3 , Co_3O_4 , NiO , CuO , In_2O_3 , SrO WO_3 , TiO_2 , V_2O_3 , GeO_2 , Fe_2O_3 , Nb_2O_5 , MoO_3 , Ta_2O_5 , La_2O_3 , CeO_2 , Nd_2O_3 [51, 54]. Suitability of metal oxides

selected for gas sensors can be determined from their electronic structure. Considering the fact that metal oxides have a wide range of electronic structure, hence they can be divided into the following categories [55]:

Table 1.2: Categories of metal oxide based on their electronic structure

Transition metal	Non transition metal	
<ul style="list-style-type: none"> • Any element in d-block in the Periodic Table • Ranges from group 3 to 12 • Examples : Fe₂O₃, NiO, Cr₂O₃ 	Pre Transition	Post transition
	<ul style="list-style-type: none"> • Elements in position before Transition element in the Periodic Table • Example : MgO 	<ul style="list-style-type: none"> • Elements in the position after the transition elements in the Periodic Table • Example : ZnO, SnO₂

Pre-transition-metal oxides are almost inert. This owes to their large bandgaps. For example, MgO has 7.8 eV whereas 10.6 eV. Neither electrons nor holes can easily be formed. Hence contributes to insignificant electrical conductivity change's when expose to gases. Probably due to this reason the pre-transition metal oxides are rarely used to develop sensors. Transition-metal oxides behave differently because the energy difference between a cation dn configuration and either a $dn+1$ or $dn-1$ configurations is often rather small [56]. They can change forms in several different kinds of oxides, which means they are more sensitive than pre-transition-metal oxides to the environment. However, instability of its structure and non-optimality of other parameters important for conductometric gas sensors limit their application field. Only

transition-metal oxides with d^0 and d^{10} electronic configurations find their real gas sensor application [55]. The d^0 configuration is found in binary transition-metal oxides such as TiO_2 , V_2O_5 , WO_3 whereas d^{10} configuration is found in post-transition-metal oxides, such as ZnO and SnO_2 . The post-transition-metal oxides may be reduced, but not oxidized [55]. However, the reaction with oxidizing species such as O_2 will occur provided that the samples have been bulk reduced or where the surfaces have been made oxygen deficient [57-58].

1.4.2 Sensing Mechanism of Metal Oxide Sensor

Adsorption is a process where molecules of gas are bounded to a surface material. The adsorption itself can be divided into physisorption and chemisorptions. Physisorption describes the physical attachment of the gas molecules to the surface, whereas chemisorptions involve the exchange of electrons between the adsorbed molecules and surface materials. The former is exothermic whereas the latter is endothermic process. In gas sensing application, it relies mainly on the surface reaction occur between the molecules adsorbed and the surface material. The chemical reaction would alter the surface conductivity by reducing or increasing the charge carriers or electrons number in the conduction band of the material. Depending on the type of gas, reducing gases or electron donor (i.e., H_2 , CO , H_2S) will extract away the electrons from the surface thereby reducing the conductivity of the surface in n-type material, whereas oxidizing gases (i.e., NO_2 , O_2) will increase the conductivity in the n-type material. In p-type material, both cases are however reversed.

Generally, at room temperature the surface of the metal oxide is covered or adsorbed by oxygen molecules from surrounding. Oxygen is a reducing agent and has an electronegativity character. It would capture and trap electrons from the conduction band, E_c of the metal oxide to form richer electron molecules or ionic oxygen

molecules, hence creating a negatively charge surface. O_2^- , O^- and O^{2-} are the charged molecules formed [59] and their total amount is limited by Weisz limitation [60]. These negative charge molecules induce band bending and create electron- depleted region (so called space-charge layer) in the material thereby reducing surface conductivity in the n-type material.

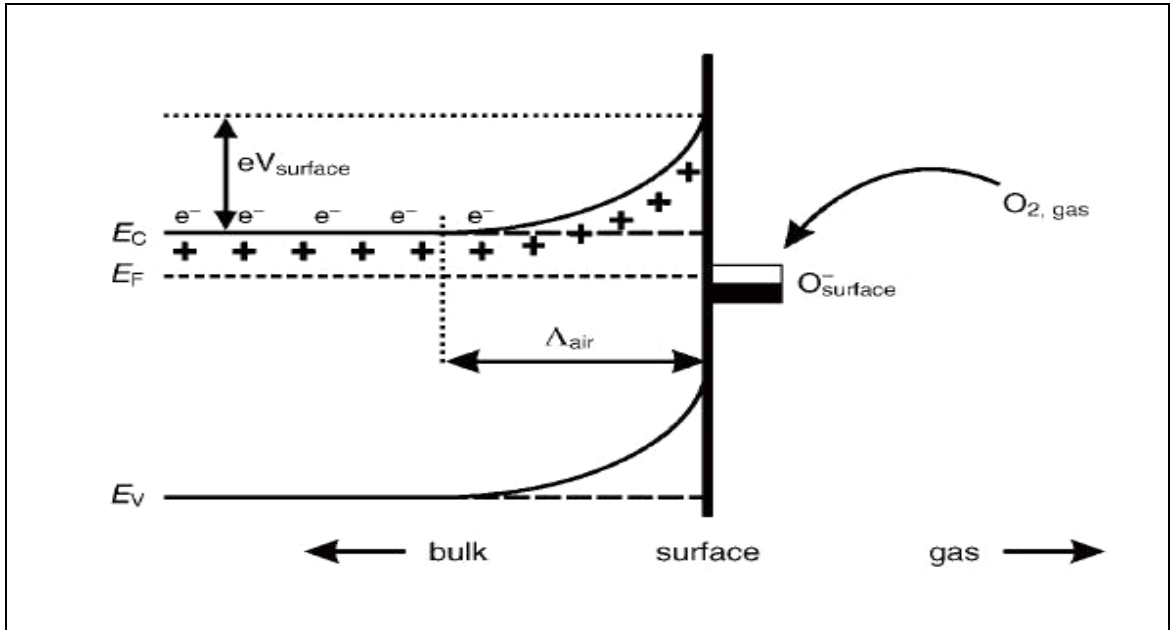


Figure 1.5: Schematic diagram of band bending after chemisorptions of charged species (here the ionosorption of oxygen) E_C , E_V , and E_F denote the energy of the conduction band, valence band, and the Fermi level, respectively, while Δ_{air} denotes the thickness of the space-charge layer, and eV_{surface} denotes the potential barrier. The conducting electrons are represented by e^- and $+$ represents the donor sites (adapted from [61]).

Reaction of these charged oxygen species with reducing gases or a competitive adsorption and replacement of the adsorbed oxygen by other molecules can decrease and reverse the band bending, resulting the conductivity to increase. Most of the studies model and explain the mechanism using CO as the reducing gas [57, 62]. When gas sensors are exposed to the reducing gas, CO is oxidized by O^- and released electrons to the bulk materials. With the decrease of the number or amount of O^- on the surface, the thickness of space-charge layer will also decrease. Then the Schottky barrier between two grains is lowered and it would be easy for electrons to conduct in sensing layer

through different grains. Figure 6 schematically shows the structural and band model of conductive mechanism when exposed to reference gas with or without CO.

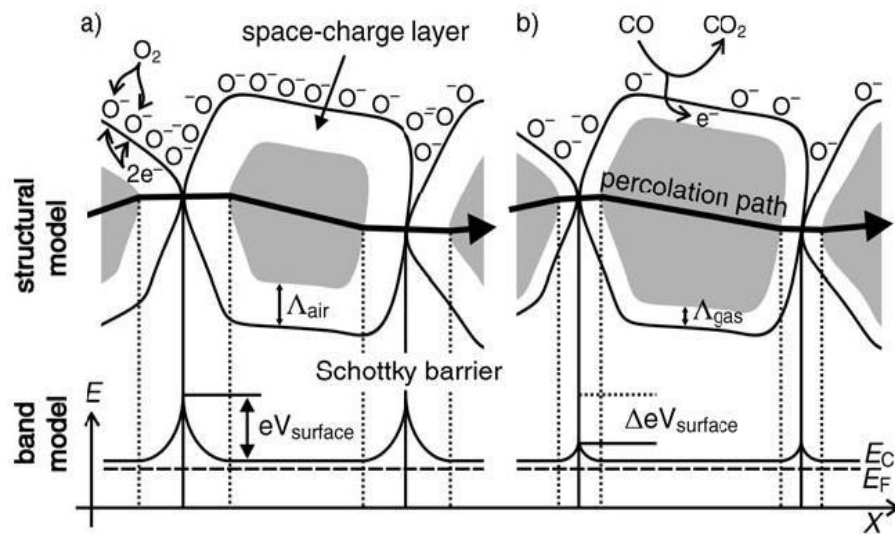


Figure 1.6: Models of structural and band of conductive mechanism upon exposure to reference gas (a) with or (b) without CO (adapted from [61, 63]).

Since the sensing mechanism of metal oxides depends directly on the reduction or oxidation reaction, which is a chemisorptions process and very sensitive to the temperature, therefore the sensor must be heated before detection can be carried out. Reports have shown a temperature range of 100 °C to 300 °C [38, 41-42, 64]. The optimum performance is also a temperature dependent. For example, a report [65] demonstrated SnO₂ based sensor work in the range of 100 °C to 300 °C, but shows the highest sensitivity to NO₂ at 200 °C.

There are reports on the efforts to reduce the dependency to the temperature by noble metals doping [66-69]. Palladium and platinum are commonly used. They work as oxidation catalyst, easing the chemisorptions process. The mechanism can be explained chemically using Pd on SnO₂ surface [70]. Pd is a far better oxygen dissociation catalyst than SnO₂. Therefore it catalytically activates the dissociation of molecular oxygen (as depicted in Figure 6a, process no. 1). Then the diffusion of atomic

products to the metal oxide takes place (as shown in Figure 6a process-2). Moreover, molecular oxygen does not necessarily dissociate on Pd surface (in process 2). It is believed that oxygen molecules can reside briefly on an oxide support and diffuse to a catalyst particle before it has had an opportunity of desorption [71]. This is the so-called “back-spillover effect” (process-3 in Figure 6a). There is an effective “capture radius” (R_c in Figure 6b) around the Pd particles. An effective oxygen delivery system forms if the whole surface of metal oxide covered by this oxygen “collect zones” [72]. The net results of process 2 and 3 significantly enhance the probability of oxygen ionosorption on metal oxides and hence improve the sensitivity.

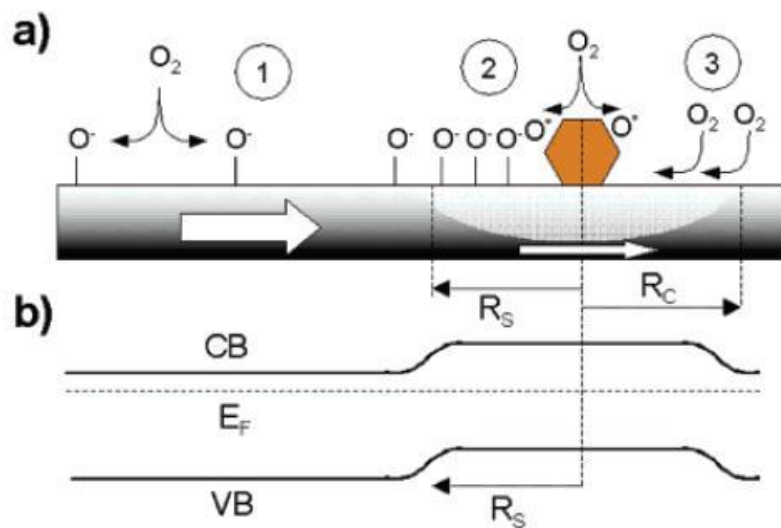


Figure 1.7: (a) Schematic depiction of the major process taking place at a SnO₂ nanowire/nanobelt surface when exposed to O₂. (b) Band diagram of the pristine SnO₂ nanostructure and in the vicinity (and beneath) a Pd nanoparticle. The radius of the depletion region is determined by the radius of the spillover zone (adapted from [49]).

1.4.3 Application of Nanowire in Metal Oxide Gas Sensor

Apart from increasing the surface area of the metal oxide sensor, nanowires with diameter smaller than 25nm [30] which is comparable to the grain size in thin film sensors could result into a better sensitivity, as demonstrated with In₂O₃ nanowires for NH₃ detection[73].

Lu *et al.* [74] have indicated that the SnO₂-based sensor response to 500 ppm CO increases drastically if the particle diameter becomes smaller than 10 nm. In₂O₃ nanowires with diameter of 10nm were reported to detect the lowest concentration for NO₂ [75]. Studies of SnO₂ nanoparticle sensor layers exposure to H₂ [76] indicated that gas response using 20 nm particles was about 10 times more sensitive than that of using 25-40 nm particles. For small grains and narrow necks, when the size of the grain is less than twice the thickness of surface charge layers, the grain will be fully involved in the space-charge layer [77]. Then a surface influence on free charge carrier's mobility should be taken into consideration. This happens due to the number of collisions experienced by the free charge carriers in the bulk of the grain becomes comparable with the number of surface collisions. The latter could probably be influenced by adsorbed species acting as additional scattering centers [78]. This case is favourable because the sensitivity of metal oxide gas sensors can be enhanced significantly by this method [78-82].

However smaller crystal size of nanocrystals does not necessarily mean the enhancement in gas response. Studies [83] indicated that the sensor sample based on SnO₂ nanocrystals (~50 nm) produced by gel combustion method showed higher response and shorter response time than the one prepared from hydrothermal-synthesized SnO₂ nanocrystals (12–13 nm). This can be attributed to the more porous nanocrystalline microstructure of SnO₂ nanocrystals produced by gel combustion method than that offered by hydrothermal-synthesized SnO₂ nanocrystals which are smaller in size but tend to agglomerate into large entities.

Nanowire enables the possibility of producing self-heated gas sensor. No external heater is required as Kolmakov *et al.* [84] have demonstrated the fabrication of self-heating gas sensor towards oxygen and hydrogen gas. The nanowire itself dually functions as the sensing element and the heater. They carefully bias the sensor to a

condition where the supplied current can be used by the nanowires to warm it up to a temperature just sufficient for surface reaction. This reduces the power consumption.

1.5 SnO₂ Nanowires Sensor for Hydrogen Detection

Hydrogen is expected to replace hydrocarbons and becomes fuel of the future. As it is an invisible, odourless, and flammable gas, it is necessary to detect and prevent any hydrogen leakage to the environment. Hence, there is a strong need to develop novel hydrogen sensors for: solid oxide fuel cells [85-86], hydrogen engine cars [87], transportation and storage of H₂ [88] or other applications. Nowadays, hydrogen is used as the fuel for the internal combustion engines and fuel cells in aerospace industries that could probably soon flood into the automotive industry and customers houses due to the potential for substantially cleaner emissions than internal combustion engines. To control the energy conversion processes in such engines and fuel cells will require numerous hydrogen sensors for each unit. It is apparent that the cost, compactness, reliability, sensitivity and selectivity along with technical requirements on such devices are major specifications which have to be considered when sensors were developed. There have been numerous efforts to produce a compact, reliable, inexpensive, and low power consumption sensor device that can detect hydrogen [85, 89-91].

SnO₂ is one of the most promising and useful materials for gas sensors, especially for H₂ sensing. There are two factors that drive the study of SnO₂ as gas sensing material; (i) its suitable physicochemical properties, for example, it has a high reactivity to reducing gases at low operating temperatures. This is attributed to the easy adsorption of oxygen at its surface because of the natural non-stoichiometry of SnO₂. (ii) SnO₂ has a lower cost when compare to other available materials for similar applications.

SnO₂ is an n-type semiconductor due to its oxygen vacancies act electronically as electron donor. The band gap is 3.6 eV. As a mineral, SnO₂ is also called Cassiterite. It

has the same rutile structure as many other metal oxides, such as TiO_2 , RuO_2 , GeO_2 , MnO_2 , and VO_2 . The rutile structure has a tetragonal unit cell with space group symmetry of $P4_2/mnm$. The lattice constants are $a = b = 4.7374 \text{ \AA}$ and $c = 3.1864 \text{ \AA}$ [65]. In the bulk all Sn atoms are sixfold coordinated to threefold coordinated oxygen atoms.

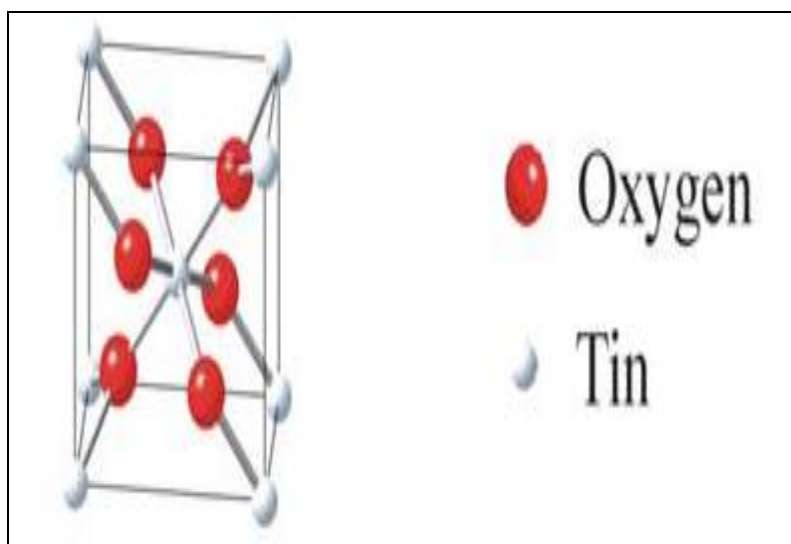


Figure 1.8: A schematic of tetragonal unit cell of SnO_2 (adapted from [92])

Several nanowire- SnO_2 -based H_2 sensors have also been reported. There are pure and Pd-coated multiple SnO_2 nanorods [93-94], Pt doped SnO_2 nanowire [95], SnO_2 nanorod arrays [96], sensor based on single nanowires of SnO_2 [97], metallic catalyst coatings (Pd, Pt, Au, Ag, Ti and Ni) on multiple SnO_2 nanorods [98]. However, for mass scale production purpose, an inexpensive and simple synthesis process is required [99-101]. Moreover, it has been pointed out that there are disadvantages of nanorods/nanowires currently used in sensors [102], including complexity to increase in term of sample preparation and device fabrication, time consuming analysis, as well as lack of selectivity. On the other hand, the features of the nanowire synthesis method desired by industry must be of low-cost materials and processing, well controlled

process parameters, environment friendly reagents, etc. [101]. To overcome some of these limitations and to bridging between the laboratory and industry, this work focus on the synthesis technique of SnO₂ nanowires as the building block for a high selectivity H₂ sensor.

Therefore, the main goal of this master research is to describe a new method based on the modified carbothermal reduction technique to synthesis SnO₂ nanowires for hydrogen gas sensing device.

1.6 Objectives

In this study, the main objective is to develop a new nanowire synthesis technique for H₂ gas sensing application and to demonstrate that this technique is suitable and at par with other nanowires synthesis technique. SnO₂ is chosen as the material due to its low cost and availability. In detail the objective can be further expanded as follows; (i) to study the effects of temperature towards the formation of SnO₂ nanowires, (ii) to study the effect of ramp parameter, (iii) to study the effect of Au thickness towards nanowires morphology, (iv) to synthesize nanowire with and without Au catalyst and (v) to analyse the hydrogen sensing performance of the SnO₂ nanowires .

Chapter 2

Literature Review of Nanowires Synthesis Technique

2.1 Nanowires Synthesis Technique

To date, there have been various nanowires synthesis technique developed. Some are simple yet powerful, some are complex. In general, all these techniques can be classified into two; bottom up and top down approach. In top down approach, the process starts with bulk materials and undergoes miniaturization into desired size (mostly via etching). In contrast, the bottom up approach is an assembly process where smaller particles join to make a larger structure. Although both approaches produce nanowires, each has its own advantages and disadvantages.

The advantages [103] of the bottom up approach are the possibility of selective doping (n- or p-type) of the nanowires by controlled injection of the dopant precursor gas and secondly, high quality single crystalline nanowires with well-controlled composition and electronic properties can be produced. However, controlling diameter and orientation of the nanowires require tedious and tons trial and error experiments before acquiring the right parameter setup. This impedes the success of reproducing high degree of nanowires in different setup as there are lot of parameter need to be considered.

In top down approach, well aligned nanowires with high uniformity can be produced. This approach is perfect for providing high quality nanowires to be used in devices (eg; electronic circuit and sensor). The diameter of the nanowires can also be controlled but to obtain high precision is still a challenge [104]. Numerous steps involve to yield the desired nanowires contributes to the complexity of this approach and put a barrier for the mass production [41].

Therefore in this part, we will review one of the widely used top down approach which is size reduction lithography technique and several other techniques which can be categorised as bottom up approach.

2.1.1 Size Reduction Litography

Lithography is a process of transferring pattern using masks to a material. There are two types of lithography widely used, conventional lithography and unconventional lithography such as photo lithography and electron beam lithography, respectively. The resolution achieves by the latter is better than the former because of the limitation by the wavelength of light used for the exposure in photo lithography [105]. Photo lithography uses UV light whereas electron beam lithography uses a beam of electrons to shine through a mask onto a resist layer which cover our material (eg; polymer, metal oxide). The mask stops some of the light from proceeding onto the resist. A resist is a thin layer used to transfer a pattern to the material which it is deposited upon. For electron beam lithography, the resists used are usually polymers dissolved in a liquid solvent.

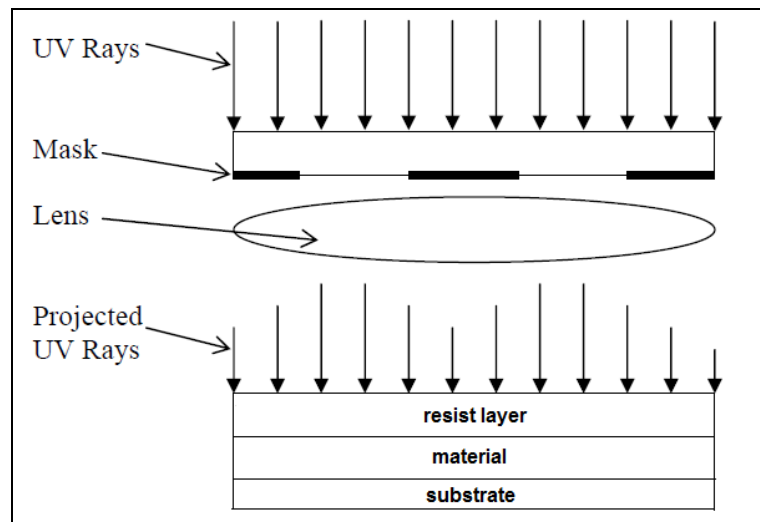


Figure 2.1: Schematic of photo lithography using UV light to pattern the resist layer. Adapted from [106]

In typical procedure, a thin layer of the resist liquid is spun on to the desired material before being baked to evaporate all the residual solvent. The masks are then placed on top or close to the resist layer. Prior to this process, the masks are designed

with patterns using designing software such as AUTOCAD and GDS II Editor [107]. The masks can be created by several ways, but one of the most common and accurate method is using an electron beam [106]. This is to etch desired designs to the masks. Finally, UV light or electron beam is shone on the setup (refer Fig. 1). The resist (negative type) layer which is exposed to UV light or electron beam would undergo reaction which polymerizes it. The unexposed part would then decompose and removed by etching reagent, thereby leaving behind a set of resist patterns. The patterns formed can be fabricated or transferred into the underlying material to form nanowires by using reactive ion etching or wet etching. Although, uniformity and morphology can be controlled, the precision is still a challenge as some work reports that there is about 40 nm diameter difference between the size of the nanowire design and the fabricated one [107].

2.1.2 Templates Method

The templating method is a second powerful way to synthesize nanowires for use in electronic devices. The idea is to fill materials into a nanoporous template (mostly by electrochemistry) to form nanostructures that can be released by dissolving the template. The template method has been accomplished using a variety of templates such as polycarbonate membranes [108] and nanochannel alumina (NCA) [109]. However, nanoporous anodic aluminum oxide (AAO) membranes are the most extensively used templates for nanowire synthesis [110-112]. The AAO membranes are fabricated by anodizing aluminum foils in acids at a voltage higher than 15V [113]. The pores inside the membrane are perpendicular to the surface and positioned in the form of a hexagonal lattice (See figure 3a). The pore size is proportional to the anodizing voltage.

To synthesize nanowires, materials have to be filled into the nanopores in some way. Electrochemistry is an effective method for such applications and has been used to synthesize nanowires consisting of metals [114-117], conducting polymers [118], nonconductive metal oxides [111, 113, 119-121] and semiconductors [122]. It is straightforward to fill metals and conducting polymers into the template by electrochemistry, while semiconducting and non-conducting materials can only be filled into the nanopores in an indirect way. This is described by [108].

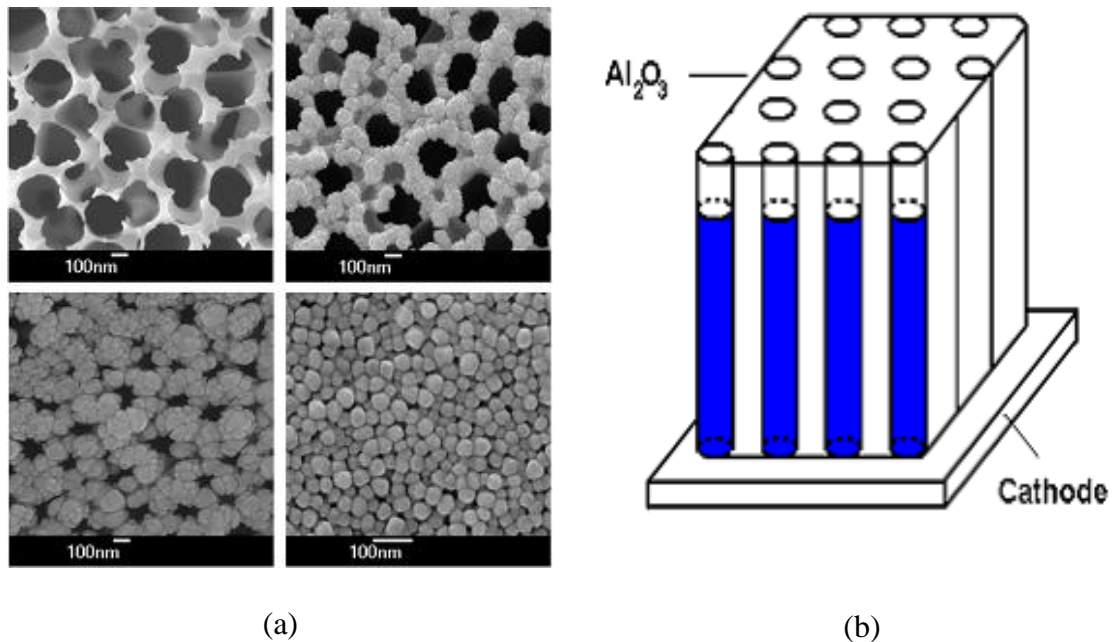


Figure 2.2: (a) The SEM image of AAO membrane surface (from [123]) and (b) AAO membrane uses a template to make nanowires by electroplating [32].

2.1.3 Solvothermal Methods

Solvothermal synthesis method involves the use of a solvent under pressure and certain temperature to increase the solubility of solids and speed up reaction their reaction. Autoclave is used to achieve the desired and elevated pressure and temperature. If water is used as the solvent, it is called hydrothermal method. The advantage of this method is that almost all of materials can be made soluble with a proper used of solvent, suitable temperature and pressure, therefore broadening the scope of synthesizing nanowire from any solid material [124].

Heath et al [125] pioneered this method by demonstrating that Ge nanowires could be synthesized from GeCl_4 or phenyl GeCl_3 with sodium in an alkane solvent heated and pressurized at 275 C and 100 atm. Single-crystalline nanowires with a diameter of 7-30 nm and length up to 10 μm were obtained. Qian et al later utilized this technique to demonstrate its versatility with the synthesis of wires [126], tubes [127] and whiskers [128] from various materials. Although it seems that the technique is versatile, the products were often characterized by low yield, low purity and poor uniformity in size and morphology. The solvents involved are also not environmentally friendly.

2.1.4 Sol Gel

The sol-gel process is a solution process used to synthesis various nanowires [129-131]. Sol-gel process involves the transition of a solution system from a liquid "sol" (mostly colloidal) into a solid "gel" phase. The starting materials used in the preparation of the "sol" are usually inorganic metal salts or metal organic compounds such as metal alkoxides. In a typical sol-gel process, the precursor is subjected to a series of hydrolysis and polymerization reactions to form a colloidal suspension, or a

"sol". Further processing of the "sol" makes it possible to make materials in different forms.

Thin films consist of nanowires can be deposited on a substrate by spin-coating [132] or dip-coating [129,133]. When the "sol" is cast into a mold, a "wet gel" will form. With further drying and heat treatment, the "gel" is converted into dense materials. If the liquid in a wet "gel" is extracted under a supercritical condition, a highly porous and extremely low-density material called "aerogel" is obtained. As the viscosity of a "sol" is adjusted into a given viscosity range, fibers can be drawn from the "sol". Different type of solvent may produce nanowires with different morphology [134-136].

2.1.5 Vapor-Liquid-Solid (VLS) Mechanism Growth Techniques

Vapor-liquid-solid (VLS) method is widely used to synthesize nanowires. Nanowires of SnO₂ [135-137], ZnO[138-140], In₂O₃[141-142], V₂O₅[143-144], Ge[145] and Si [146-148] are among the material that have been grown using this method. The growth process is typically carried out in a low pressure and high temperature furnace (Figure 1). The temperature near the source is elevated sufficiently to melt the source material so they may evaporate. In some cases, the source material is mixed with carbon in order to lower the vaporising temperature of the source material. This technique is called carbothermal reduction. A carrier gas flow brings the vapor to the substrate where nanowires grow with the assistance of catalysts. The catalyst material may be pre-deposited on the growth substrate, or it may form spontaneously during the VLS growth process.

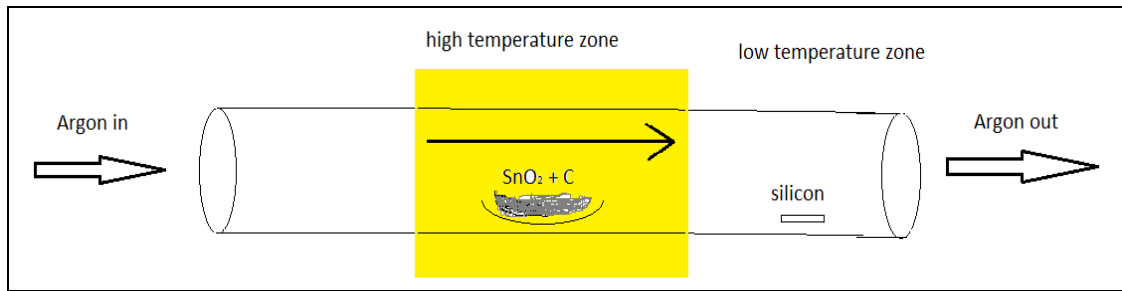


Figure 2.3: The furnace diagram of VLS nanowire synthesis method.

The catalyst metals commonly used are Au [149], Fe [150] and Ni [151] as catalysts. The metal catalysts can be mixed with the source material or spread on the substrate where the nanowires grow. These nanoparticles react with the source vapor forming solution droplets on the substrate serving as a preferential site for absorption of reactant, since there is a much higher sticking probability on liquid than the solid surfaces [152]. When the droplets become supersaturated, they are the nucleation sites for crystallization. Preferential 1D growth occurs in the presence of reactant as long as the catalyst remains liquid [153]. During this process, the catalyst particle tends to remain at the tip of the growing nanowire (Figure 2). The mechanism of the nanowire growth by VLS was first explained Wagner and Ellis in 1964 [154].

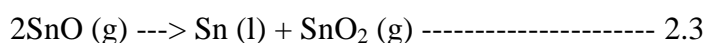
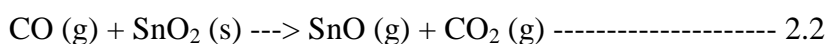
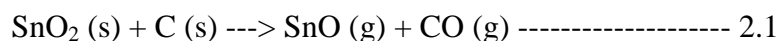
The size of the catalyst particles that used in the nanowires synthesis depends on the preparation process. Common methods include thin film deposition of the metal catalyst on the substrate by sputtering [155-156] or thermal evaporation [66]. The catalyst thin film will congregate into small droplets or particles when heated up to the growth temperature. Alternatively, prefabricated catalyst nanoparticles are deposited on the substrate instead of the thin film [73, 157,158]. These nanoparticles have uniform size, therefore the nanowires formed would be more uniformly in diameter [73].

Commonly used carrier gases include argon and nitrogen [159-160]. Oxidizing gases may be mixed in the carrier gas, depending on the source material and the desired composition of the nanowires. For example, when growing metal oxide nanowires with the metal powder source, O₂ is often mixed in the carrier gas [161]. Flow rate [162] of the inert gas and percentage of O₂ [163] may as well affect the morphology of the nanowires.

If we categorize the VLS method in terms of the preparation system, it can be classified as thermal evaporation [164], laser ablation [165] and inductive heating assisted synthesis [166], which differ only in the heating source. Some of the heating sources have advantages over the others. For example, laser ablation may enhance the uniformity of the nanowire diameter [165]. The inductive heating assisted synthesis can be more effectively heating up samples than the conventional thermal evaporation, which leads to a much shorter synthesis time [166].

2.2 Growth Mechanism of SnO₂ Nanowires In Carbothermal Reduction Technique

Carbothermal reduction method uses carbon to lower the vaporising temperature of the source material, SnO₂ powder so that vapour may be formed at lower heating temperature. Rafael Padila [166] outlined that this is possible because SnO₂ will be reduced by C at any temperature above 903 K or 630 °C. The products of the redox reaction, SnO (1080 °C) has lower vaporising temperature than the SnO₂ (1800 °C – 1900 °C). Therefore, the SnO will be the one to get evaporated and proceeds in the next chemical reaction for the nanowire growth of SnO₂.



As has been mentioned, the SnO₂ powder is first reduced by carbon to yield SnO and CO in the form of gaseous. Then, the CO will react with other remaining SnO₂ powder to form SnO and CO₂. Due to its metastability, SnO decomposes into Sn and SnO₂. Normally, the phase transformation from SnO to SnO₂ occurs at temperature above 600 C. Considering the low melting point of Sn (231.9 °C), Sn particles are still liquid at this reaction temperature. These Sn droplets could fell on the substrate and provide the energetically favoured sites for adsorption of SnO₂ vapor [167].

Considering that the substrate is coated by Au thin film, at elevated temperature, the Au will melt and form liquid droplets. Therefore Sn droplets and SnO₂ will be adsorbed on the Au surface before diffuse to the liquid/solid interface. During the diffusion and adsorption on the Au surface, both Sn and SnO₂ can coexist. However, there is also a probability that all the Sn will get oxidised by O₂ presence in surrounding

to form SnO_2 [168, 209]. At liquid/solid interface, the SnO_2 will get supersaturated and solidified. This solid will be the seed for the initiation of the nanowire growth, in which its position is just underneath the tip of the Au droplets. Continuous supplies of SnO_2 vapor and Sn liquid will continue the process of adsorption and diffusion of the vapour from the Au surface to the liquid/solid interfaces (which is now is the nanowire seed that has been formed previously). Subsequently, solidification will increase the length of the nanowires vertically.

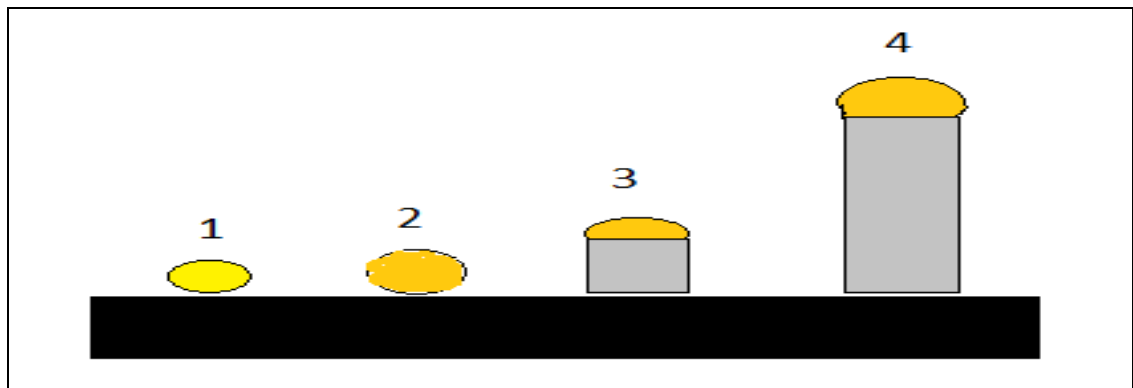


Figure 2.4: VLS diagram illustrating the growth of nanowires

In some cases, elements of Sn_3O_4 or Sn_2O_3 , AuSn_4 are also detected along with the SnO_2 . The Sn_3O_4 and Sn_2O_3 are intermediate oxidation states when SnO oxidizes to SnO_2 through indirect transition. They are not formed if transition is direct from SnO to SnO_2 . It was suggested [169-170] that if the $d(\text{nm})$ values of two sets of parallel planes belonging to the separate phases SnO and SnO_2 are nearly the same, then the direct phase transformation from SnO to SnO_2 occurs without the involvement of intermediate oxidation states Sn_2O_3 or Sn_3O_4 . According to [171], the deposition parameters such as annealing temperature and duration are the factors. They must be sufficiently high and long, respectively. For AuSn_4 , there is no detail explanation on how it coexists with the

SnO₂ nanowires except that during the adsorption, the Sn dissolve in Au droplets to form AuSn₄ alloy [172]. Probably this reaction is less favourable compare to the reaction between Sn and O₂ to form SnO₂.

In VLS mechanism, the diameter of the nanowire produced is dependent on the surface tension energy of the gold droplets. This surface tension energy is actually dependence to the gold droplets radius. This relation has been demonstrated by Wagner and Ellis [173] who determined that the limitation of VLS whisker lower diameters is the consequence of the dependence of liquid surface energy upon the change of liquid droplet radius. According to J. Weyher [174], surface tension energy can be controlled during VLS growth, by vapour phase composition, substrate type and its crystallographic orientation, growth temperature, liquid phase composition and liquid phase initial amount. For example, increasing the growth temperature will increase the droplets diameter. Larger wire size is produced. Therefore, different values of the surface tension energy can result in different crystal morphology, and structure (or structure perfection).

Apart from SnO₂ powder, reports [175-176] have shown that SnO and Sn powder can as well be used as the source material for the nanowire synthesis. In typical cases, carbothermal reduction is used for the former whereas simple thermal evaporation for the latter.

2.3. Effect of Various Parameters towards SnO₂ Morphology

There are a wide variety of parameters that can contribute to the different in morphology and distribution of the SnO₂ nanowires. Various studies have been carried out to analyse the effect of all the parameters towards the nanowires synthesized.

2.3.1 Effect of Temperature

Heating temperature is an important factor in the synthesis of nanowires as it affects the vapour pressure of the source material. The vapour pressure is exponentially increased with temperature. High temperature will result in high concentration of vapour produced. More vapour produced then will speed up the supersaturation of the liquid droplets so that the nanowires nucleation may occur in VLS growth technique. M.K. Fung et al demonstrated that morphology of SnO₂ nanowires grown is dependence on the heating temperature [177], although there was no specific relation between the temperature and the morphology (eg; diameter, distribution) is concluded in the report. In another report, Pho Nguyen et al. [178] stated that by increasing the temperature from 850 C to 880 C, the diameter of the SnO₂ nanowires were reduced from 81 nm ± 64 nm to 49 nm ±52 nm [178]. Moreover nanobelts were also observed.

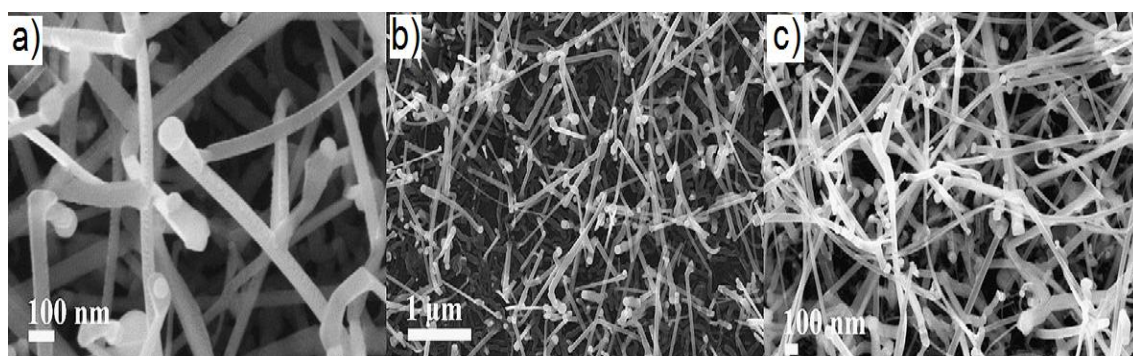


Figure 2.5: FESEM images of the morphology of SnO₂ nanowires obtained at different heating temperature: (a) 871 °C (b) 843 °C and 648 °C (from [177])

2.3.2 Source Material to Substrate Distance

Substrates are usually placed in the upstream of the furnace or at certain distance with regard to the source material. The upstream has lower temperature than the source material heating zone. This is known as temperature gradient. Therefore, the vapour of the material produced can be condensed and fall on top of the substrates due to the lower temperature environment. Condensation helps feeding the liquid droplets/gold droplets (or any catalyst used) with the source material so as to achieve supersaturation level and nucleation of nanowire may start. Depending on the type of the furnace, the degree of temperature changes or gradient in each furnace is different. For example, some may differ by 100 °C by 5 cm distance whereas some are not that too significant, 5 °C in 5 cm. As the distance is more towards the end of the furnace, the cooler the temperature would be. Therefore by varying the distance, it is as if indirectly allows us to control the amount of vapour condensed. This affects the morphology of the structures formed.

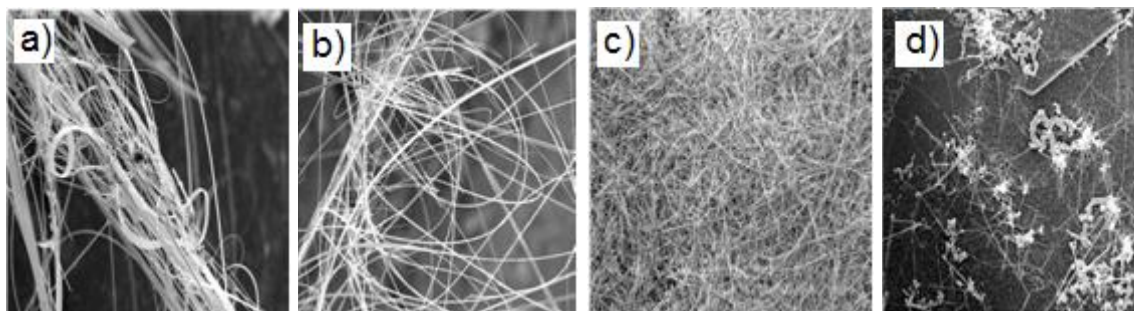


Figure 2.6 : SEM images showing the typical morphologies of the as-synthesized SnO₂ nanostructures: (a) wide nanobelts; (b) narrow nanobelts, inset showing a closer inspection of one curved SnO₂ nanobelt; (c) thick nanowires; (d) thin nanowires. (from [179])

S H Sun et al [179] reported that nanobelts and nanowires were observed when the distance is varied (refer Fig. 6). SnO₂ nanobelts and SnO₂ nanowires grew mainly in the temperature range of 1000 °C – 850°C and 850 °C – 600°C, respectively. The

diameter of the nanowires is a temperature dependent, in which the temperature is affected by the distance of the substrates in the furnace. They conclude that the temperature of the substrates and the concentration of oxide vapour were among the critical experimental parameters for the formation of different morphologies of SnO₂ nanostructures.

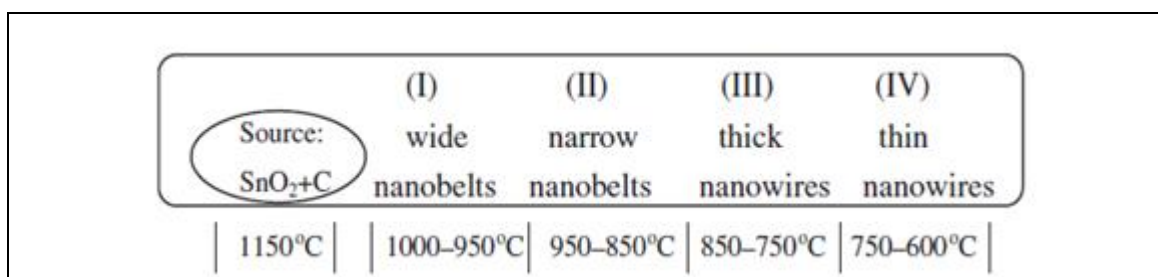


Figure 2.7: Schematic diagram showing the formation temperatures of these morphologies (adapted from [179])

2.3.3 Molar Ratio of SnO₂: C

The main advantage of mixing carbon with source material is that the source material, SnO₂ powder can be vaporised at lower vaporising temperature. Therefore various reports have demonstrated the synthesis of SnO₂ nanowires at temperature range far less than the SnO₂ vaporising temperature [180-181]. Apart from that, M. Salehi reported [182] that the ratio of carbon mixed with the SnO₂ powder has as well affected the diameter and length of the nanowires formed. By using higher carbon ratio (SnO₂: C = 1:4) instead of (SnO₂: C = 1:2), the diameter and length were decreased and increased respectively. The density of the nanowires also increases as higher carbon ratio was used (Figure 7b and 7c). They concluded that an increase in the activated carbon to SnO₂ ratio have led to higher Sn vapour pressure being produced by carbothermal reaction. Thus, increase in the Sn vapour pressure resulted in a smaller nanotube diameter.

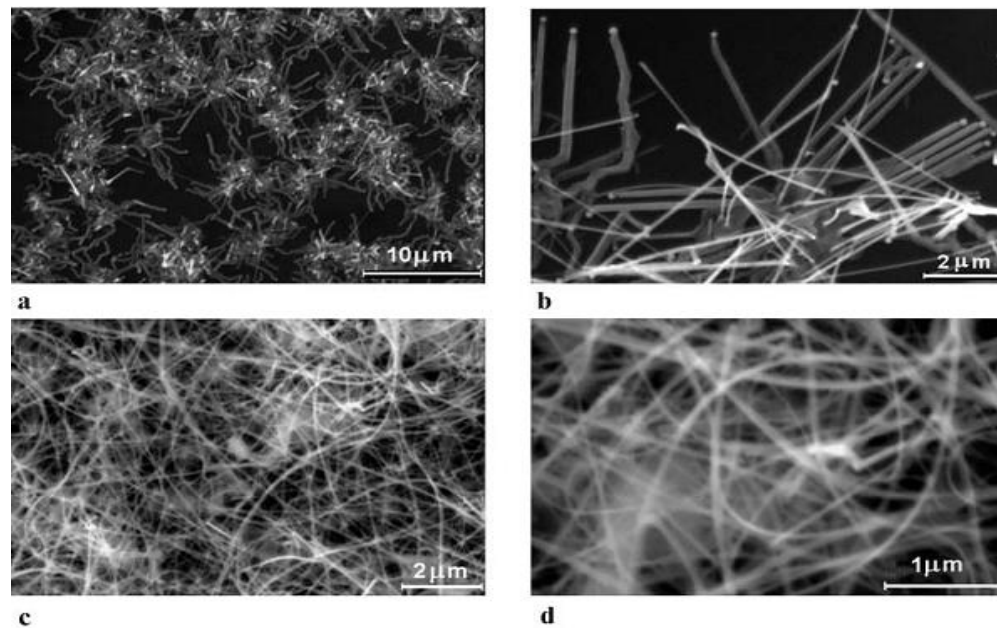


Figure 2.8: SEM images of grown nanostructures using different SnO₂: C ratios of (a) 1:2 at $\times 3000$, (b) 1:2 at $\times 10,000$, (c) 1:4 at $\times 10,000$ and (d) 1:4 at $\times 30,000$ (from [182])

2.3.4 Gold thickness

Gold serve as catalyst to the growth of nanowires by VLS mechanism. It provides reactive sites for vapour to condense, supersaturate, crystallize and nucleate as nanowires. Thin layer of gold is usually coating the substrates, which is carried out by thermal sputtering prior to the nanowires growth. S.Y Lee et al. have shown that thickness of gold thin film affects the morphology of the nanowires [183]. In the studies, the increase in gold thickness contributed to the increase in the diameter of the nanowire (refer Figure 8). During the heating process, the gold thin film will form liquid droplets, scattering all over the substrate. These droplets act as the adsorption sites for the vapour, so that liquid phase can be created. Increasing the gold thickness results in the increase in the size of the droplets formed. The diameter of the wire is dependence on the size of the droplets [184-185]. Therefore the nanowire grown from smaller size droplets will have smaller diameter than the big ones.

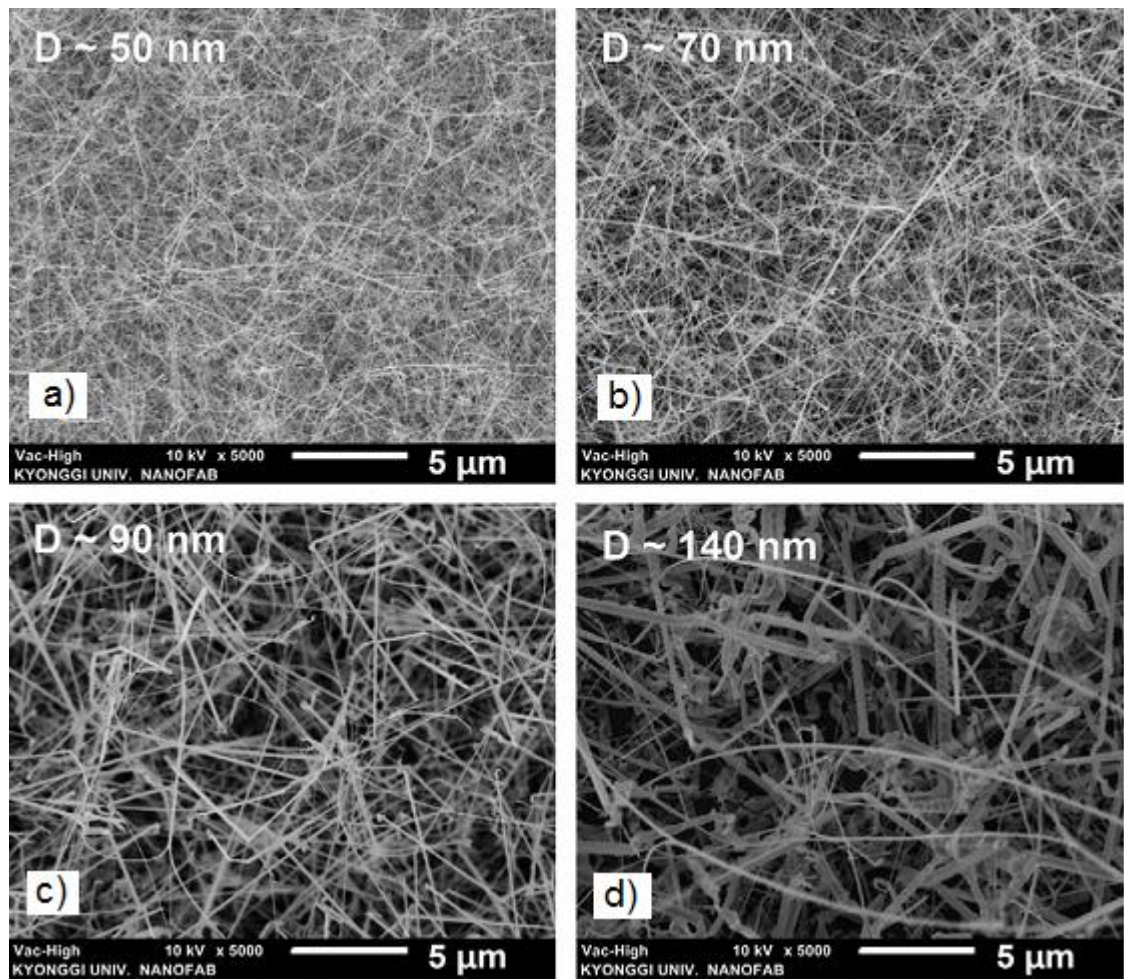


Figure 2.9: FESEM images of SnO₂ nanowires grown on different gold thin film thickness; a) 2nm, b) 5nm c) a 10nm and d) a 15nm. The average diameters of nanowires are 50 nm, 70 nm, 90 nm and 140 nm, respectively. (from [183]).

The size of gold nanoparticles also determines the size of the nanowires during growth. S. Budak et al [158] have demonstrated that reducing the gold colloids size would produce nanowires with a narrow size distribution. Since the nucleation of the nanowires is determined by the gold nanoparticles that act as catalytic centers on the surface of the substrate, the nanowires density can as well be easily controlled by changing the concentration of the dispersed nanoparticles. A report [186] suggested that SnO₂ nanowires branches can be controlled by manipulating the gold thickness. Hong Wan and Harry E. Ruda [187] reported that both of density and diameter of the

nanowires synthesized increase with the increasing of the Au thickness. However, this report is based on ZnO nanowires, and not SnO₂ (refer Figure 2.10).

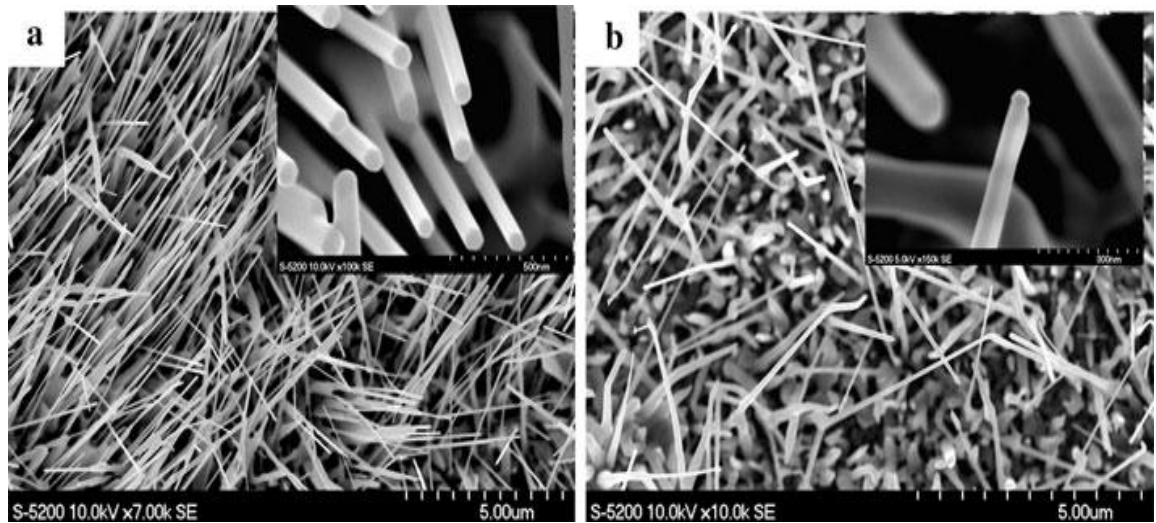


Fig. 2.10: SEM images of ZnO nanowires grown at different thickness of Au film: a) 50 nm, b) 10 nm (from [187])

2.3.5 Inert Gas Flow rate

Inert gas flow the vapour of the material to the substrates usually placed at the upstream of a furnace. Argon and nitrogen are the gas that widely used in nanostructures fabrication. The flow rate is an important factor as it influences the morphology of the nanostructures formed [188]. Studies by Umair Manzoor [188] suggested that by varying the flow rate, nanostructures of nanocomb, nanowire and nanorods can be produced. This is probably because the change in Ar flow has affected the super saturation, which changes the morphology of the nanostructures [189]. Nanowires synthesized with high Ar flow rates shows better distribution and density compared to the lower ones. The report also shows that the diameter increases with the increase in Ar flow rate. It was concluded that the increase was because higher flux of carbothermal reaction products were generated and also the supersaturation conditions

changes, consequently increasing the deposition rate and ultimately size of the nanostructures.

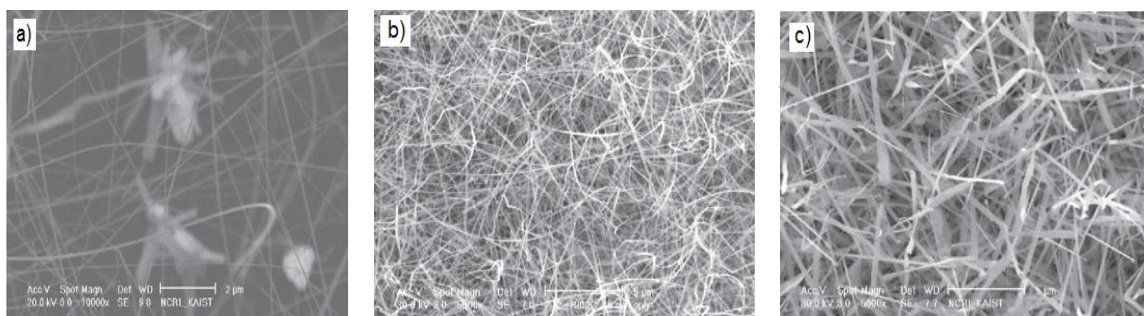


Figure 2.11: ZnO nanowires grown on Au-coated Si substrates with different Ar flowrate ; (a) 10 sccm, (b) 25 sccm and (c) 150 sccm (from [188]).

2.3.6 Oxygen in Argon Gas Carrier

It is believed that the presence of oxygen in nanowire synthesis is very important. This is demonstrated by Jae-Hwan Park et al who synthesized ZnO and SnO₂ nanowire with variation in the percentage of oxygen [190]. No ZnO nanowires were produced if there was only Ar gas. Moreover, the report suggests that it is impossible to get SnO₂ nanowires by the conventional carbothermal process due to the absence of oxygen in the surrounding. However, SnO₂ nanowires were fabricated when more than 0.01% of oxygen and nanoribbons were readily fabricated with additional 1% of oxygen. The successful synthesis of ZnO and SnO₂ nanowires in other reports could be attributed to the air leakage in the processing gas line or lower gas purity used.

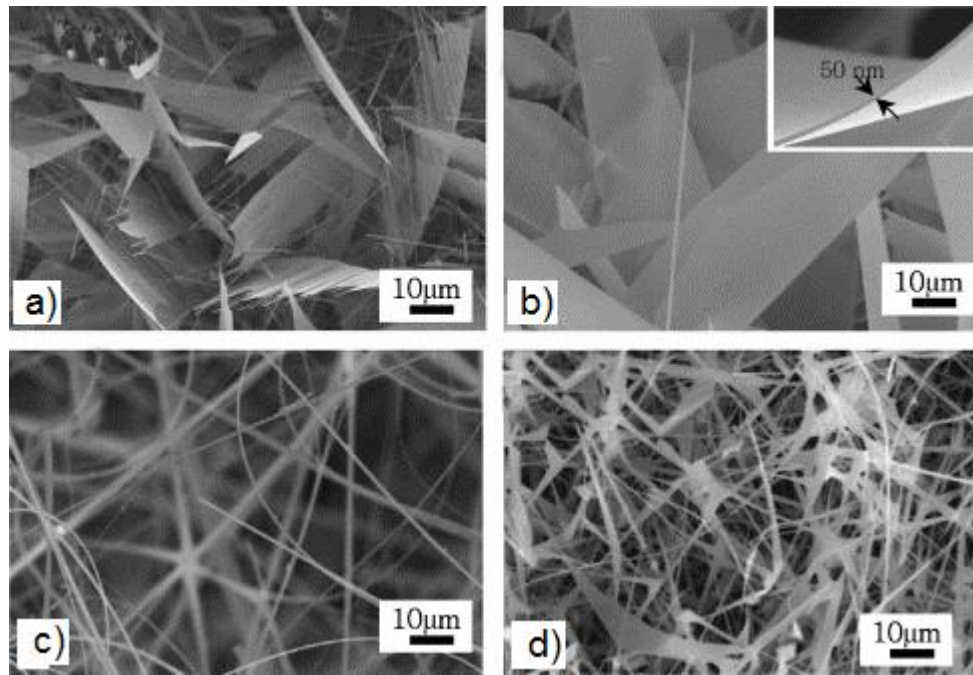


Figure 2.12: (a), (b) ZnO combs and nanosheets fabricated by a MOCVD process. (c) SnO₂ nanowires obtained under a flow of O₂ (0.01%)/Ar gas and (d) SnO₂ nanoribbons fabricated under a flow of O₂ (1%)/Ar gas. (from [190])

2.4 Thermal Ramping As A Facile Nanowires Synthesis Technique

As we have looked through various nanowires synthesis technique, we notice that the established techniques still have room for improvement particularly in term of complexity and parameters required. In size reduction lithography for example where mask is required to transfer pattern before etching can be carried out, designing a defect-free mask is problematic [185]. The mask may also undergo degradation [123]. Moreover the optical system used to project radiation is extremely expensive [123,191].

Template method suffers from inhomogeneity size and branching nanowires [192], which could lead to distinct physical properties among the nanowires and anomalous behaviours [193]. Furthermore, the use of precise anodic voltage and membranes type makes this method complex. In the case of solvothermal, it is low cost and easy to carry out. However problem in uniformity of size and shape of nanoparticles could arise. This is due to long time to raise the temperature of solution which then

results in the inability to uniformly control the nucleation stage of the crystal growth [194]. Sol gel method on the other hand is a low cost technique. However, it possesses several disadvantages such as expensive sol [195], impurities and unstable gel [196] which later affect the nanostructures.

Carbothermal reduction has proven to be an effective technique to produce nanowires[135-137]. It is also a low cost technique except for the furnace equipment. This technique consists of several important parameters such as the use of inert gas, gas flow rate, distance of source material to substrate and many more as we have reviewed in subchapter 2.3. These parameters are indispensable in the conventional approach. Therefore due to the dependency to all of this parameter, we consider the technique to be complex as well, which then perhaps can be regarded as one of its disadvantage.

Therefore it is our objective to improve and simplify the present technique by tackling some of its disadvantages, definitely by not ignoring the fact that the methods and techniques do have their own advantages. We chose carbothermal reduction technique as our method to be simplified due to its wide range of parameters to be explored. Moreover it has been widely used in yielding SnO₂ nanowires, the material that we intend to use in the research.

CHAPTER 3

EXPERIMENTAL SETUP

3.1 Introduction

The research methodology can be divided into two different main parts ; (i) Synthesis of SnO₂ nanowires (section 3.2), (ii) Characterisation of the nanowires (section 3.3), and (iii) Gas sensing measurement and analysis (section 3.4). The first part was carried out first to obtain the nanowires before the samples were later tested for their sensing properties.

In the section 3.2, since this technique is related to the ordinary carbothermal reduction method, only certain parameters which are newly introduced and thought to be producing different results from the conventional carbothermal method were emphasized, studied and analysed. The parameters are temperature, usage and thickness of Au-coated substrates and the most importantly the incorporation of ramp parameter. They were analysed by Field Effect Scanning Electron Microscopy(FESEM), Elemental Diffraction X-ray (EDX) and X-ray diffraction(XRD).

Gas sensing properties of tin dioxide nanowires were tested for their optimum operating temperature and concentration of gas detectable. The measurements from these two experiments were used to analyse sensitivity, selectivity, response and recovery time of the sensor in Chapter 4.

The result would be used to demonstrate that the synthesis technique used is simpler, capable and at par with other technique of producing nanowires for sensing devices.

3.2 Synthesis Of SnO₂ Nanowires

3.2.1 Substrate preparation

Substrates used was n-type silicon wafer. The silicon wafer was cut into 1cmx1cm size using appropriate cutter to obtain the required size for the substrates. The substrates were then immersed in a mixture solution of H₂SO₄ and H₂O₂ with ratio of 5 : 1 for 20 minutes at the temperature of 70° c. The substrates were then rinsed in distilled water before being cleaned in ultrasonic bath. Later, they were dried in the flow of inert gas, argon. All substrates were then coated with Au by thermal sputtering. The thickness of the coating was approximately 25 nm.

3.2.2 SnO₂ Nanowires Synthesis and Depositing Technique

The synthesis of the SnO₂ nanowires was carried out using horizontal tube furnace which consists of an alumina tube process of 2'' outer diameter and length 64 cm and a temperature controller. The furnace was thermally ramped up and down to a desired temperature according to the ramping profile in Fig. 3.1. The heating rate of the up and down rampings was set to be 10 °C/min. As an emulation of the carbothermal low-temperature region, 300 °C is chosen as the ramp down temperature to condense the vapor. The ramp up temperature is also an important value as it must be able to vaporize the SnO₂. Thus, it is chosen based on the reported value of the carbothermal technique in synthesizing SnO₂.

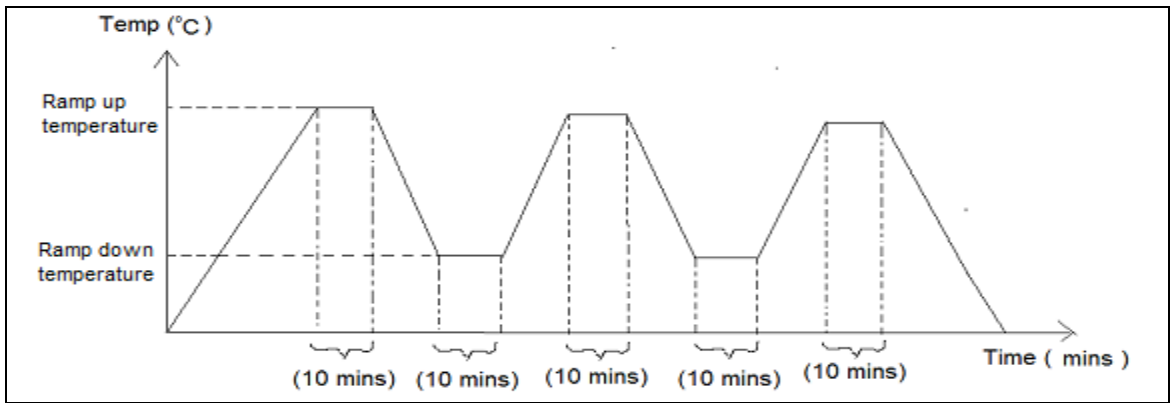


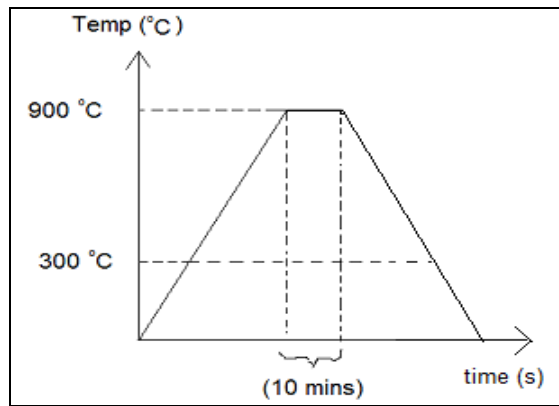
Figure 3.1 : Thermal ramping profile for 900 °C

The precursor materials were mixtures of grounded SnO₂ and carbon powders with 1 : 2 molar ratio. The precursor materials were placed in the same porcelain boat where substrates were in. Prior to the heating process, the porcelain boat was placed at the centre of the horizontal tube furnace.

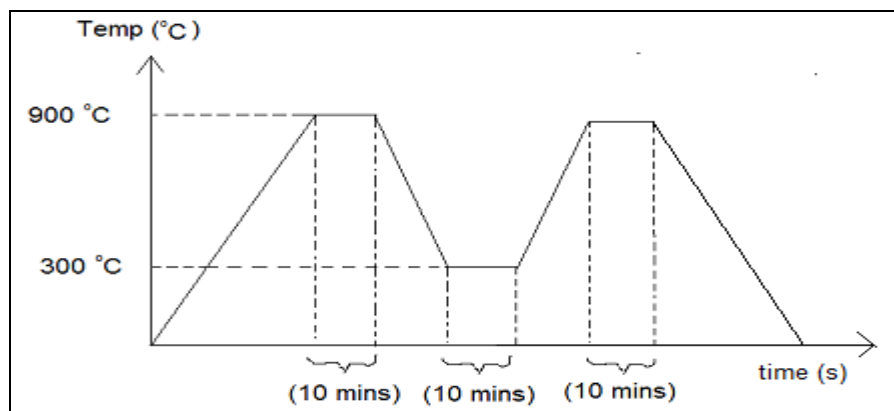
3.2.3 Factors Affecting The Nanowires Formation

3.2.3.1 Number of Ramping

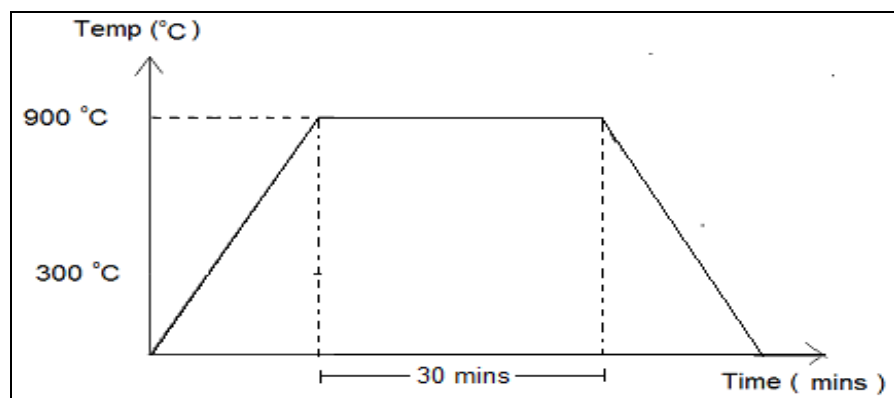
To understand the effects of ramp number in the formation of the SnO₂ nanowires, the experiments were carried out by varying the number of ramping (as in Fig. 3.2); single ramping, double ramping, long-single ramping and triple ramping (as in Fig. 3.1) while maintaining the same temperature at 900 °C, heating rate (10 °C), molar ratio of SnO₂ : C (1 : 2), and deposition time (10 minutes for each ramp up temperature) for each of the ramping.



(a)



(b)



(c)

Figure 3.2 : Heating pattern ; (a) Single ramp , (b) Double ramp, and (C) Long-Single ramping profile

3.2.3.2 Deposition Temperature

To investigate the effect of temperature in thermal ramping technique, the experiments were repeated at 700 °C, 800 °C, 900 °C and 1000 °C. The Au thickness, molar ratio (SnO₂ : C), heating rate were 25 nm, 2 : 1 and 10 °C/min respectively.

3.2.3.3 Au as Growth Catalyst

There have been numerous reports discussing about the role of Au as a catalyst in the formation of nanowires. As widely understood, the presence of a very thin layer of Au capable to induce the nanowires formation by vapor-liquid-solid (VLS) mechanism.

Therefore, two samples with one is coated with Au and the other is uncoated are prepared for the SnO₂ nanowire synthesis. Prior to this, both of the samples are cleansed according to method mentioned in 3.2.1. The molar ratio of 1 : 2 (SnO₂ : C), depositing temperature at 900 °C and thermal ramp heating as in Fig 3.1 were used.

The effect of Au thickness was also studied by preparing two samples with different Au thickness; (i) 10 nm and (ii) 25 nm. In this experiment, ZnO was used instead of SnO₂ as the precursor material. This has been arranged to observe the technique flexibility and capability of synthesizing nanowires from material other than SnO₂.

3.2.3.4 Summary For Synthesizing Parameter

The table below summarizes the whole SnO₂ nanowires synthesizing experiment.

Table 3.1 : All parameters used in the synthesization experiment.

Temperature (°C)	Heating rate (°C/min)	Au thickness (nm)	Ramp
700	10	25	Triple
800	10	25	Triple
900	10	a) 25/10 (ZnO powder) b) With and without Au (SnO ₂ powder)	Single, Double, Triple, Long-Single
1000	10	25	Triple

3.3 Characterisation of SnO₂ Nanostructures

3.3.1 X-ray Diffraction (XRD)

X-ray diffraction is a non-destructive technique to asses the chemical composition and crystallographic structure of the nanowires. Siemens D-5000 diffractometer with copper-monochromatized Cu K α 1 X-ray source was used in the x-ray diffraction measurement. The scan angle was varied from 2-theta 5° to 80° for each sample. The graph of intensity versus angle 2-theta was plotted for every data obtained.

3.3.2 Field Effect Scanning Electron Microscopy (FESEM)

All samples were assessed by Field Effect Scanning Electron Microscopy, FESEM (FEI-Quanta 200 FEG) for featural and structural (morphology) studies. By carrying out the FESEM analysis, identification of the type, size and pattern of the nanostructure formed can be obtained. For each sample, the magnification were set to be 8000, 60 000 and 120 000.

3.3.3 Energy Dispersive X-ray Spectroscopy (EDX)

Energy Dispersive X-ray (EDX) was carried out to evaluate the elemental analysis of the nanowires. The ratio of weight of each element present in the nanowire can be obtained. The present of Au and Si in the nanowire can be attributed to the Au catalyst and Si substrate used, respectively.

3.4 Gas Sensing Measurement

3.4.1 Gas Sensing Setup

A simple chamber was designed to accomodate the SnO₂ thin film, heating equipments, digital multimeter probes and gas flows. Gas was allowed to flow in and out through the aperture at the top and bottom of the chamber respectively. The composition and proportion of the gas mixture were controlled and regulated using flowmeter.

The heating equipment was set to a desired temperature to provide heat to the thin film sample. As the temperature reached the temperature set, air was let to flow into the chamber. The initial resistance of the SnO₂ thin film was measured through the probes which was connected to a digital multimeter. Desired amount of hidrogen was then flown into the chamber. The value of resistance was measured for any changes.

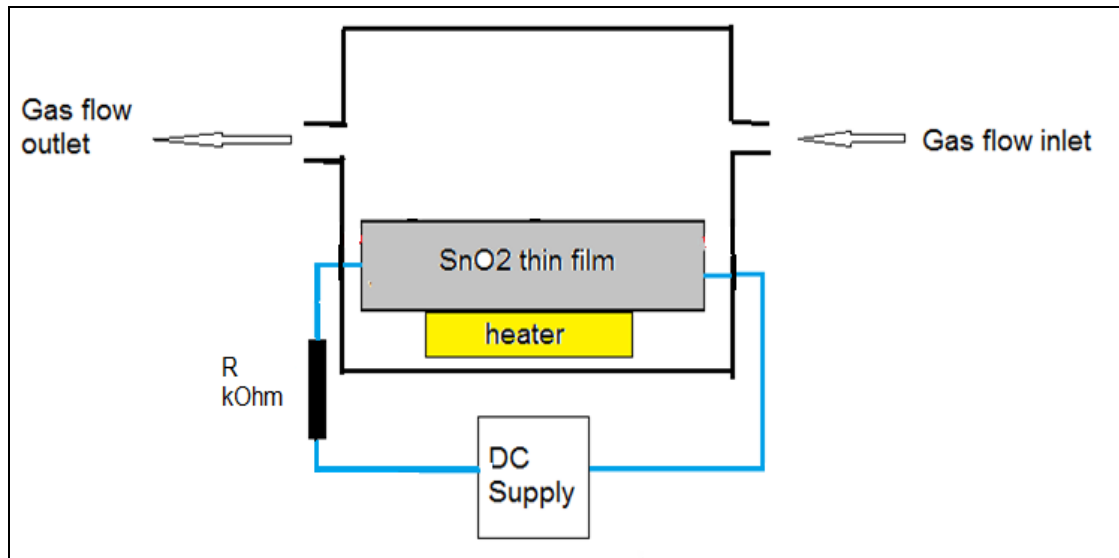


Figure 3.4 : Cross section of the sensing chamber

3.4.2 Effect of Heating Temperature

The equipment was setup and prepared as in the Figure 3.4. Then, the heater was set to heat up the thin film to 200 °C. As the thermal equilibrium was reached, air was flown into the chamber. The measurement of the thin film initial resistance was taken for approximately few minutes to ensure the reading was stable. Hydrogen gas was then flown into the chamber with the proportion was set to be 1000ppm. Any changes in the resistance value was automaticly monitored, measured and recorded by the digital multimeter. The experiment was repeated with different temperature; 250 °C and 300 °C. A graph of Resistance($k\Omega$) Vs Time(s) was plotted to identify the best operating temperature. The temperature at which the changes of the resistance is the most signifant most was selected.

3.4.3 Effect of Hydrogen Gas Concentration

The concentration of hydrogen in the air was sequentially set to be 1000, 800, 600, 500, 400, 300 and 200 ppm. Their effect towards the changes in the resistance was measured. The temperature to operate the experiment was based on the best result obtained in the first experiment.

CHAPTER 4

RESULTS AND DISCUSSIONS

Synthesis of SnO₂ Nanowires

4.1 Introduction

Nanowires of SnO₂ have been successfully synthesized using thermal ramping technique. It is a new technique based on carbothermal evaporation method. As has been mentioned in the previous chapter, this technique requires the precursor material to be vaporized and condensed onto the substrates. Contrary to the ordinary carbothermal method, no inert gas is required hence making the technique less complicated and low cost.

Effect of different vaporising temperature (ramp up temperature), ramp number, Au thickness and the possible mechanism of the nanowires growth will be discussed. Apart from SnO₂, ZnO powder was also used as precursor to yield nanowires in order to expand and demonstrate the capability and flexibility of the technique to synthesize nanowire.

4.2 Effect of Deposition/Ramp Up Temperature

The effect of deposition or ramp up temperature is studied by synthesizing SnO₂ nanowires at different temperatures. The temperatures were 600 °C, 700 °C, 800 °C, 900 °C and 1000 °C. The deposition conditions were kept as follows; SnO₂: C molar ratio was 1 : 2 , apply triple ramp pattern, ramp up and down duration was 10 minutes each. Fig. 4.1 shows the images of the nanowires yielded.

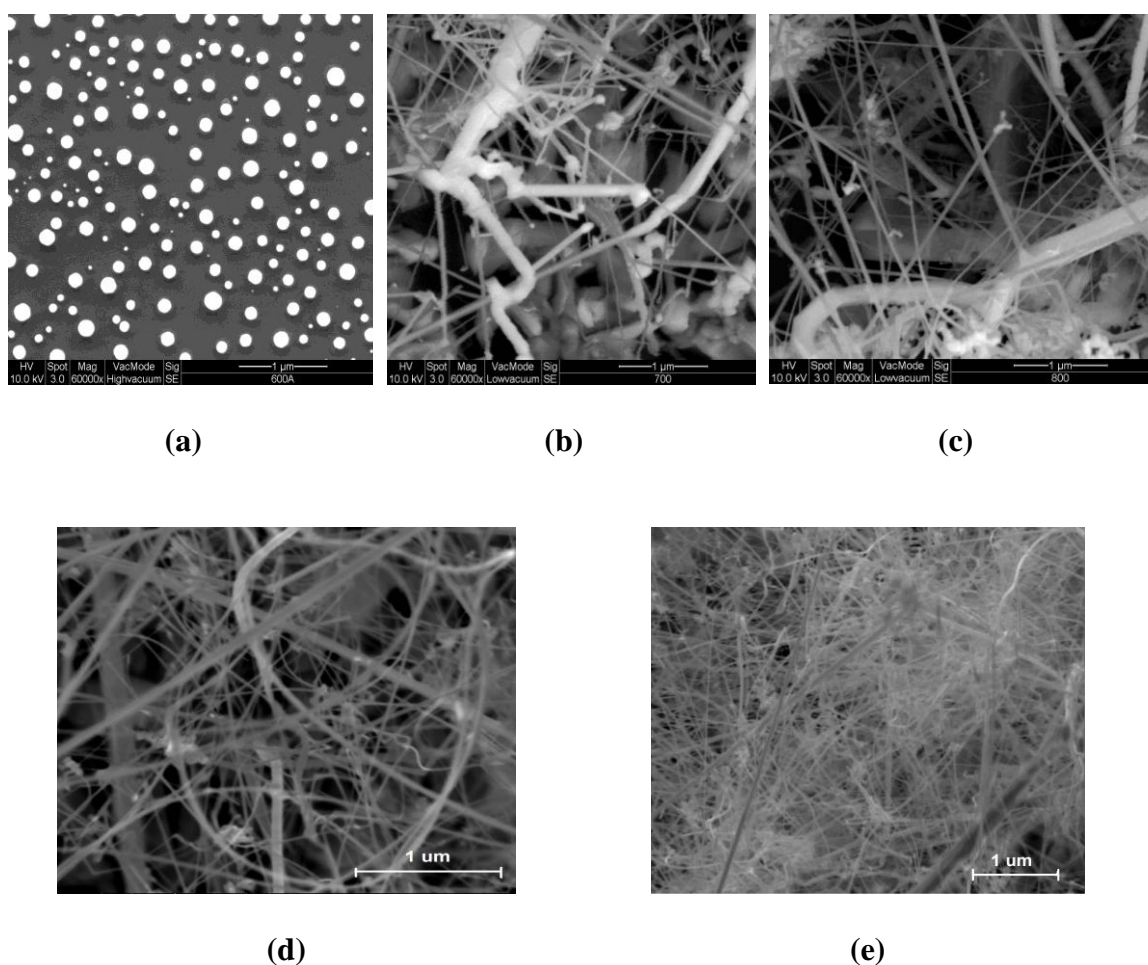


Figure 4.1: FESEM images of SnO₂ nanowires grown on Si substrates at different deposition/ramp up temperature; (a) 600 °C, (b) 700 °C, (c) 800 °C, (d) 900 °C and (e) 1000 °C.

At 600 °C, no nanowire is observed. Only at 700 °C onwards it is observed. With an increment of 100 °C, the density of the nanowire is observed to be increased. The

diameter of the nanowire is steadily decreased as the temperature increased. For nanowires developed at 700 °C and 800 °C, the diameter is in the range of 50-300 nm whereas at 900 °C and 1000 °C, it is approximately 25-100 nm. The length of the nanowires is approximately to be more than 5 μm .

Table 4.1: The weight ratio of the SnO₂ nanowires obtained by EDX analysis

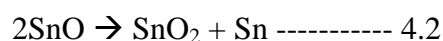
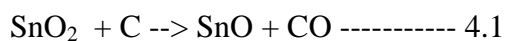
Element	Weight Ratio Percentage (%)				
	600 °C	700 °C	800 °C	900 °C	1000 °C
Sn	-	10.35	24.46	36.99	66.91
O	8.68	21.72	49.72	46.47	30.00
Si	54.36	65.20	25.05	15.66	3.09
Au	36.96	2.73	0.77	0.68	-

Elemental diffraction X-ray (EDX) test revealed that the nanowires are composed of Sn, O, Si and Au. The Si and Au can be attributed to the Si substrates used and gold catalyst respectively. No Sn was detected at 600 °C shows that SnO₂ is not vaporized at this temperature although carbon is employed to reduce the vaporizing temperature. In contrast, the percentage of Sn increases from 10.35 % at 700 °C to 66.91 % at 1000 °C. The percentage of O is also increased as the temperature increases except at 1000 °C it is lesser than the ones at 800 °C and 900 °C. Both Si and Au are reduced as the temperature increases. This indicates that as more nanowires of SnO₂ formed, they overwhelmed and covered the Au-coated-Si substrate.

The densification process of the SnO₂ nanowires can be seen closely related to the temperature because more SnO vapour would be produced at higher temperature compared to the lower one. More vapour means more nanowires could be produced. The FESEM images and EDX have revealed the densification and composition of the nanowires, respectively with regard to the temperature. This is consistent with result

from other people works which show the comparison of nanowires yielded at different temperature [177-178].

Since this experiment was carried out not in a sealed condition (pressure was not regulated), SnO₂ powder would vaporize at normal boiling point temperature, 1800-1900 °C. This temperature is not reachable by the furnace, thus carbon was employed to reduce the vaporizing temperature. The reaction of carbon and SnO₂ produce SnO and CO vapours. Due to its metastability, the SnO decomposed into SnO₂ and Sn. The chemical reaction is as follow:



Employment of Au coated substrate has induced the nanowires formation by vapour-liquid-solid (VLS) mechanism. This is confirmed by the presence of droplet-like at the tip of the nanowires[196]. Generally, the nanowires formation can be explained by the reaction of Sn and SnO₂ vapour with the Au thin film on the substrates. The Au thin film forms sphere-shape-like liquid droplets at elevated temperature. These droplets act as adsorption sites for the vapour to condense and deposit [197]. This creates formation of Sn, SnO₂ and Au alloy. The Sn reacts with traces of oxygen from surrounding or dissolved oxygen in the droplets itself to form SnO₂. This could probably be the reason as of no Sn element was detected from the XRD analysis because all Sn elements have been oxidised by oxygen. As more vapour is condensed and dissolved in the alloy, the alloy droplets supersaturated. This results in the crystallisation of the SnO₂ which occur at solid/liquid interfaces [198]. The crystallisation and solidification of the SnO₂ at the liquid/solid interface will then initiate and nucleate the nanowires formation. The liquid droplets will continue to act as

vapour absorption points and seeds for the growth. The mechanism will be discussed in detail on the next subchapter.

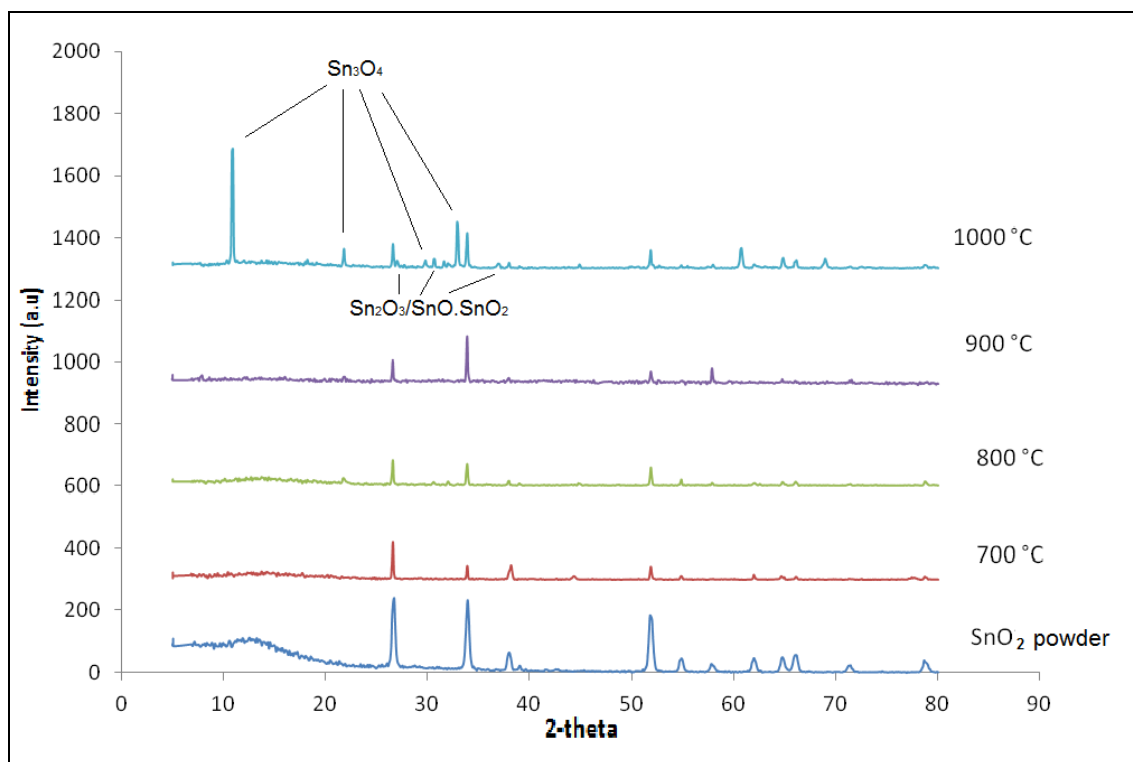


Figure 4.2 : Comparison of XRD patterns of SnO₂ nanowires synthesized at different ramp up temperatures to the SnO₂ powder used as the precursor.

Figure 4.2 shows the result of X-ray diffraction performed on all of the nanowires samples including the SnO₂ starting powder. All the peaks detected in the nanowires synthesized at 700 °C to 900 °C can be indexed to tetragonal rutile structure of SnO₂. The lattice constants are $a = b = 4.738 \text{ \AA}$ and $c = 3.187 \text{ \AA}$. For nanowires at 700 °C, two peaks of Au crystal with cubic structure were also detected at 44.39° and 77.55°. This could be attributed to the usage of Au as catalyst. At 1000 °C, apart from SnO₂ structure, peaks correspond to Sn₃O₄ and Sn₂O₃/SnO.SnO₂ were also detected. The peaks of Sn₃O₄ were detected at 2-theta equals 10.820, 21.765, 30.797, 33.902 and

correspond to triclinic crystal structure with lattice constants $a= 4.800 \text{ \AA}$, $b= 5.880 \text{ \AA}$ and $c= 8.200 \text{ \AA}$. The peaks of $\text{Sn}_2\text{O}_3/\text{SnO}.\text{SnO}_2$ are at 2-theta equals 31.830 and 37.021 and attributed to the triclinic structure with lattice constants $a= 5.457 \text{ \AA}$, $b= 8.179 \text{ \AA}$ and 3.714 \AA .

4.3 Effect of Number of Ramping

Vaporising a material is an endothermic process hence requires sufficient thermal energy to provide atoms or molecules with kinetic energy to escape from intermolecular bond of the solid or liquid. Condensing on the other hand is an exothermic process. It releases out energy. In thermal ramping technique, these two processes have been used or combined to yield the SnO_2 nanowires. As has been reported in Chapter 3 (Table 3.1), they were repeatedly applied one after another to the precursor (grounded SnO_2 and C powder) as well as the substrates.

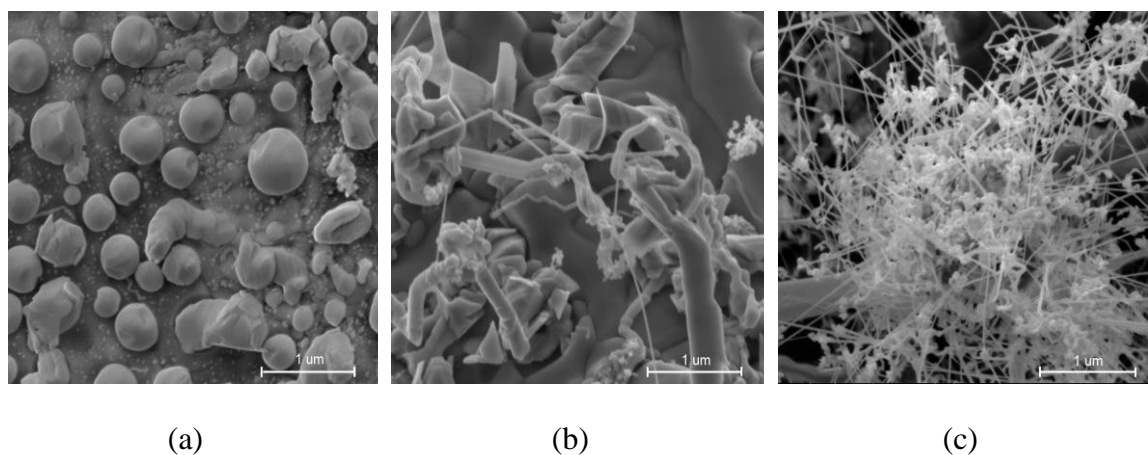


Figure 4.3: FESEM images of nanowires synthesized at different ramp number; (a) Single ramp (1R), (b) Double ramp (2R) and (c) Triple ramp (3R) at $900 \text{ }^\circ\text{C}$.

The figures above show that nanowire starts to appear only in the second ramp (2R). And it flourishes in the third ramp (3R). EDX reveals that the percentage of Sn

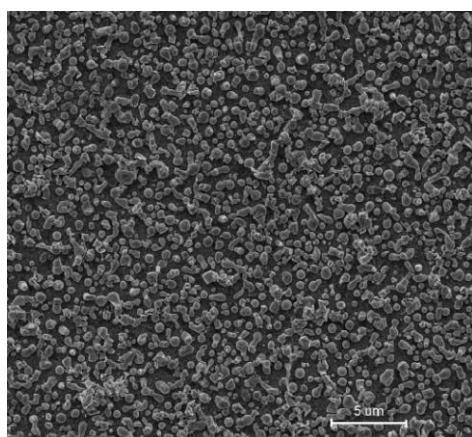
increases from nanostructure in 1R to 3R. Considering the fact this nanostructures and its Sn content is the result of vaporisation (ramp up) and condensation (ramp down), the process could probably be explained as follows. SnO₂ and Sn vapour are produced by increasing up the temperature to 900 °C and remains for 10 minutes. This vaporizes the mixture of SnO₂ and C, producing the vapour of SnO₂ and Sn. The temperature of the furnace is then lowered to room temperature, to emulate the lower temperature region and to condense the vapour onto the Au-coated-substrates (at elevated temperature Au form liquid droplets). Adsorption of these vapours with the Au droplets results in the formation of alloy droplets as shown in Fig. 4.3. This explains the first heating pattern.

The explanation for double ramping pattern can be continued from the single ramp pattern. However in this pattern, instead of room temperature the middle ramp down temperature is set to be 300 °C. This temperature is chosen as according to some carbothermal reports, the low temperature region is around 300 °C – 400 °C [199]. Thus, in order to save energy on cooling it down to room temperature, this temperature is applied instead. After the condensation takes place at 300 °C for 10 minutes (Fig. 3.2b), the temperature is ramped up again to 900 °C so that carbothermal reaction between SnO₂ and C can take place to produce SnO vapour. Thus, the alloy droplets formed earlier would also endure the heating or ramping up process. According to a report [210], a sudden change in temperature can result in the droplets to break. Considering the fact that the temperature will be ramped down again to condense the vapour, this unsteady temperature pattern we applied could cause the droplets' breakup, decay and disintegration. This suggests the irregularity of size and pattern of the nanostructures as in Fig. 4.3b. Apart from that, few nanowires yielded in Fig. 4.3b indicates that some of the alloy droplet have get supersaturated and crystallized at this stage hence nanowires are formed.

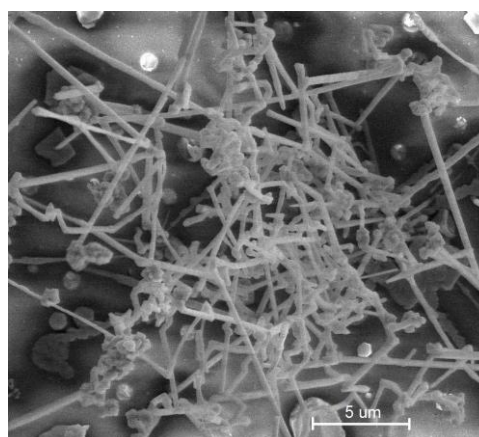
Extending vaporization (ramp up) and condensation (ramp down) pattern as in the triple ramping pattern have further supersaturated the alloy droplets and hence more nanowires are formed as in Fig. 4.3c.

4.4 Effect of Heating Time in Single Ramping

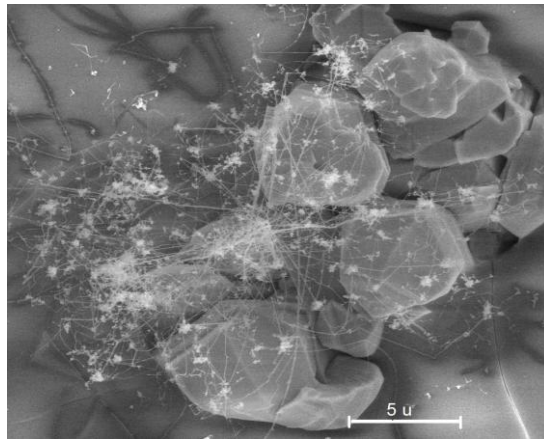
Figure 4.4 below shows the structures obtained when a single ramp was used with variation in the heating/ramp up duration. The ramp up rate was set constant at 10 °C for all the three. No wire-like structures are observed when the heating time is 30 minutes (Fig.4.4a). However, they are observed in Fig. 4.4b and 4.4c., where heating temperature of 1000 °C instead of 900 °C. The wire-like structures in Fig. 4.4b have a diameter approximately 500 nm whereas in Fig. 4.4c it is approximately 50 nm. The wire-like structures in both cases are not well distributed. Their density is very poor. Some macro size rock-like-structures containing Au, Si, Sn and O were even observed as in Fig. 4.4c.



(a)



(b)



(c)

Figure 4.4 : Nanowires yielded from single ramp ; (a) 30 minutes at 900 °C, (b) 30 minutes and (c) 110 minutes at 1000 °C

In comparison, the diameter of the nanowires in Fig. 4.4c (50 nm) is approximately 10 times smaller than in Fig.4.4b (500nm). It is known that smaller diameter of nanowires can be produced by controlling the size of the Au catalyst droplets [200]. We believe that prolonged exposure to the high temperature (without any ramp down) at 1000 °C for 110 minutes has dried up most of the Au catalyst compared to 30 minutes of heating at the same temperature. This reduced the thickness or amount of Au on the substrates. Less or thinner amount of Au would form smaller droplets size of Au [10] which then would serve as adsorption sites for Sn and SnO₂ vapor to deposit and get supersaturated. Having small size of Au droplets would result in small diameter of nanowires [201].

In term of different in the nanowires density, we also believe that it is closely related to the reduced amount of Au catalyst due to the prolonged heating duration. Reduced amount of Au droplets have resulted in the lesser platform for VLS mechanism to take place, hence less nanowire was formed.

4.5 Effect of Au Catalyst Thickness (Based on ZnO precursor)

The effect of Au catalyst thickness towards nanowires formation is studied by synthesizing nanowires from ZnO precursor with 10 nm and 25 nm of Au thickness were employed respectively. The temperature used was 900 °C. As can be seen in the figures below, the density of nanowires in Fig. 4.5a is higher than nanowires in Fig 4.5b. In both cases, the nanowires are not well distributed, aligned and do not follow any specific growth pattern. The diameter is in the range of 70 - 100 nm.

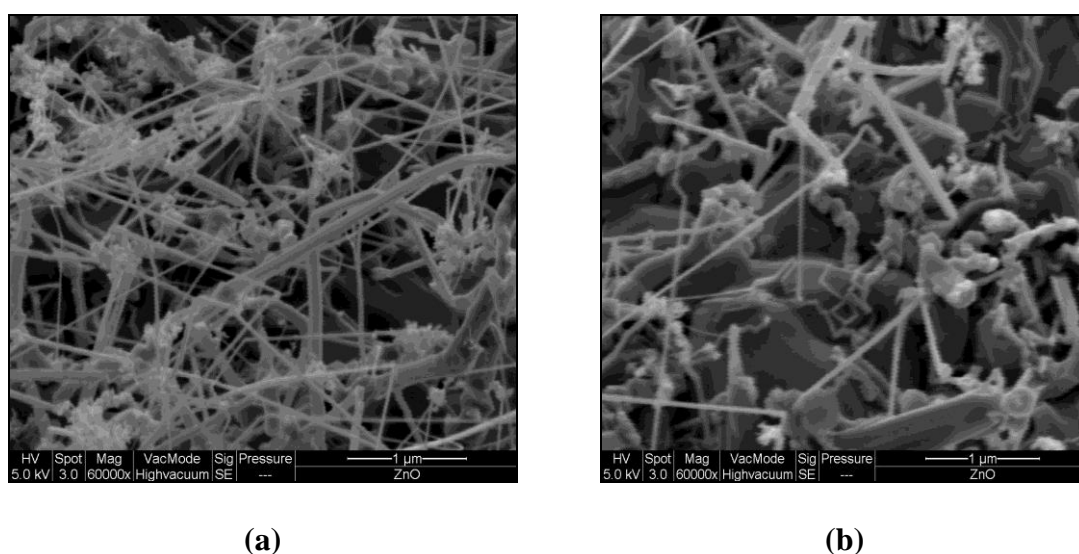


Figure 4.5 : Nanowires synthesized using different Au thickness ; (a) 10 nm and (b) 25 nm

As shown in Fig. 4.6, the x-ray diffraction peaks can be assigned to (3 0 0), (2 2 0), (1 1 3), (2 2 3), (1 4 3) and (4 0 4) reflection facets. These peaks can be indexed to Zn_2SiO_4 compound with lattice constants $a = b = 13.948 \text{ \AA}$ and $c = 9.315 \text{ \AA}$ which corresponds to rhombohedral structure. Unfortunately, no ZnO element is detected.

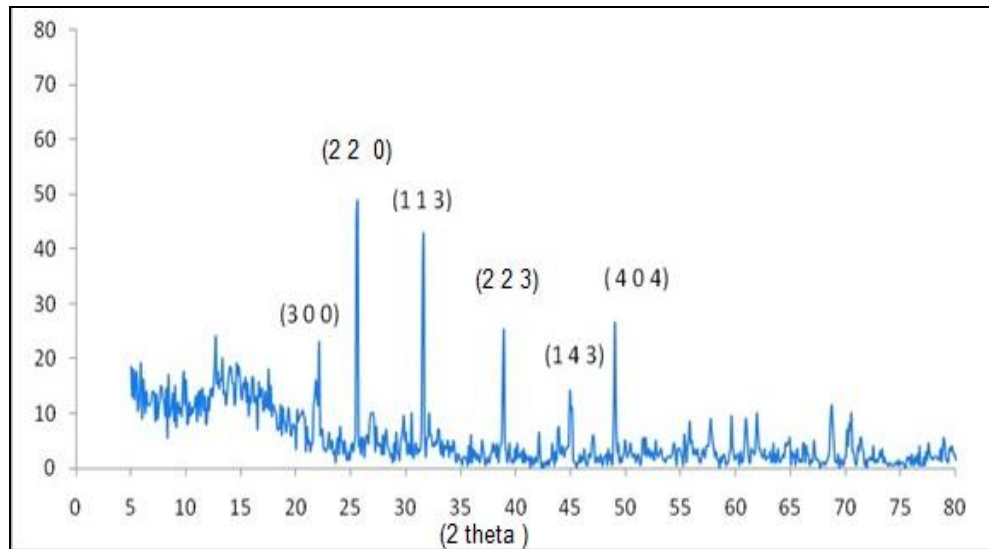
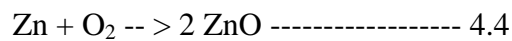
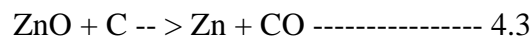


Figure 4.6: XRD pattern of nanowires formed using ZnO as the precursor.

The formation of Zn_2SiO_4 can be explained as follow. The Zn vapors which are produced by carbothermal reaction are condensed onto Au-coated substrates and later get oxidised back to ZnO by the O in the surroundings. The ZnO droplets are then reacted with Si-O from the substrates (oxidised Si melted surface) and Au catalyst to form ZnO/SiO₂/Au alloy. Due to exposure of the mixtures to a very high temperature, the alloy quickly combines to form Zn_2SiO_4 [202]. There is another possibility that instead of ZnO/SiO₂/Au alloy formation, Zn/Si/Au alloy is formed. This alloy droplets will then get oxidised by the O in the surrounding to directly formed Zn_2SiO_4 [203].



Continuous supply of Zn vapor (by ramp up and down) results in the supersaturation of the alloy and thus crystallisation of Zn_2SiO_4 takes place. The crystallisation then acts as the nucleation sites and initiates the growth of the Zn_2SiO_4 nanowires. We assume the

Au catalyst has been left out without forming any bond with Zn or Si since there is no Au-Zn or Au-Si intermetallic compound detected by the XRD analysis.

Although ZnO nanowires were not successfully synthesized, the effect and role of Au thickness towards the density of the nanowires has been demonstrated.

4.6 Effect of Au Catalyst in Thermal Ramping Technique

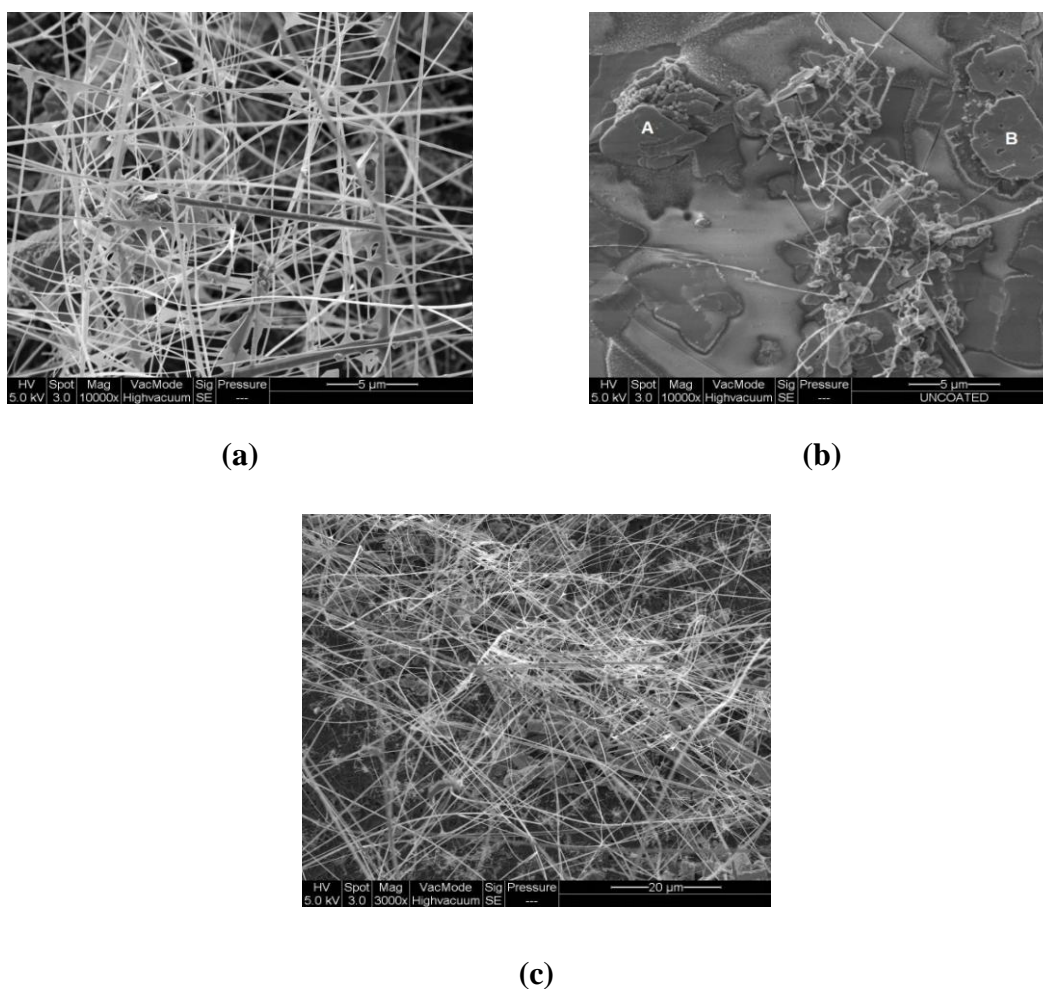


Fig 4.7: FESEM images of SnO₂ nanowires synthesized (a) with and (b) without Au catalyst. Images of nanowires (c) with Au catalyst at 3000 x magnification

In this experiment, nanowires of SnO₂ were synthesized with and without Au catalyst using the thermal ramping technique. The ramp up temperature was 950 °C. Fig. 4.7a shows the FESEM image of the SnO₂ nanowires grown with Au catalyst on

the Si substrates. The diameters and lengths of the nanowires are 150-400 nm and almost 100 μm (refer Fig. 4.7c), respectively. Fig. 4.7b shows the FESEM image of the nanowires grown without Au catalyst. The diameters and lengths are 50-100 nm and more than 5 μm , respectively. In comparison, the density of the nanowires grown with Au catalyst is higher than that of Au catalyst-free nanowires.

In the ordinary carbothermal technique, nanowires grown without Au catalyst are usually explained by vapour-solid (VS) mechanism [204-206] because there is no liquid phase during the formation. However, there is probability that there exist liquid phase during the nanowires formation in our technique. The explanation is as follows. The vapour of SnO produced by the reaction of SnO₂ and C would get condensed on the Si substrates. Since the SnO is metastable, it will decompose to Sn and SnO₂ [207]. Considering the low melting point of Sn which is 231.9 °C, the Sn is probably exist as liquid throughout the whole experiment as in the thermal ramping technique, the temperature is always kept above 300 °C. Therefore the SnO₂ is probably mixed in the Sn liquid droplets. More vapour of Sn and SnO₂ cause the liquid droplets to supersaturate and trigger the crystallisation process. As can be seen in Fig 4.6b, apart from the nanowire structures, the substrate's surface is also covered by rocky-like structures (marked by A and B). Elemental diffraction x-ray (EDX) reveals that they are consist of Sn, O, Si and Au which are the same content as the nanowires.

The SnO₂ nanowires synthesized with Au catalyst follows vapour-liquid-solid (VLS) mechanism, which has been explained in part 4.1. In comparison, although the diameter of the SnO₂ nanowires is not much difference in the both cases, its density and length are highly enhanced when Au catalyst is used. Thus, we have demonstrated that the Au catalyst is very instrumental in synthesizing high density and long nanowires.

4.7 Conventional Carbothermal Technique

Figure 4.8a and 4.8b below show the premature SnO₂ nanowires synthesized using the conventional carbothermal technique. Ar gas was used as vapour carrier from source material to the Au-coated silicon substrates. The distance of source material to the silicon used was 10 cm and 15 cm respectively. From the FESEM images, it is clear that at 10 cm distance, more nanowires are formed than at 15-cm-distance. The presence of the liquid droplets at the tip of the nanowires indicates that VLS mechanism governed the nanowires formation [196].

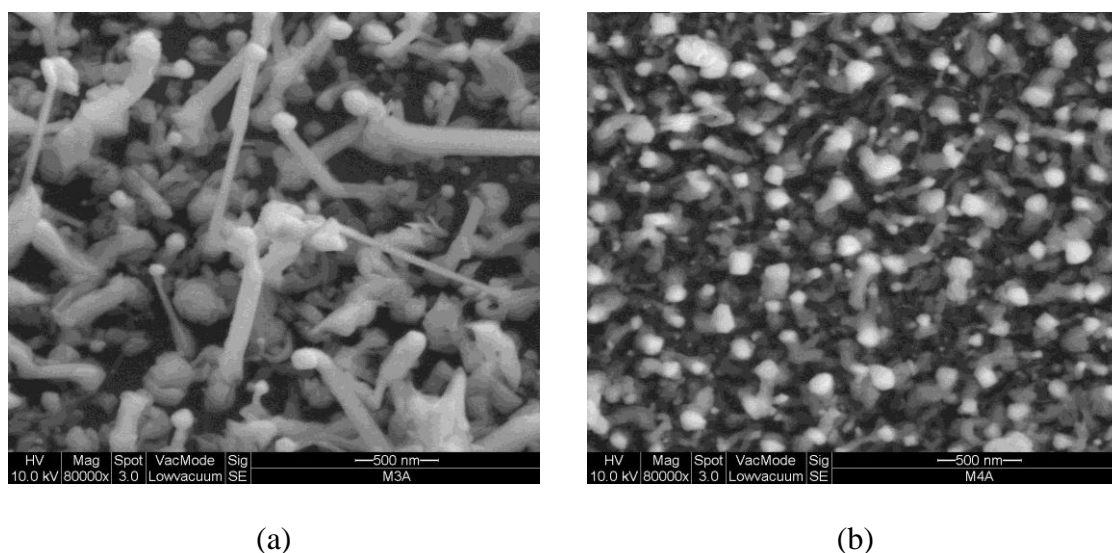


Figure 4.8 : FESEM images of nanowires synthesized using the conventional carbothermal technique with the distance of source material to substrates was varied ; (a) 10 cm and (b) 15 cm

This suggests that the stage of the nanowires formation appears to be advance when shorter distance was used rather than the longer ones in our experiment. In our case, the shorter distance probably provided a more suitable environment for the vapour to get condensed and rightly fell onto the Au-coated silicon. This led to the formation of

Au and SnO₂ mixture or alloy which is the early stage in the nanowires formation in the VLS mechanism.

In the carbothermal technique, nanowires formation is also highly affected by the inert gas flowrate[188-189]. Different flowrate would require different distance of source material to the substrate [179]. Although no studies were carried out to study the relation between these two factors, we believe this result is sufficient to prove that in the conventional carbothermal technique, the source material to substrate distance is very critical in the nanowires formation.

4.8 Growth Mechanism of SnO₂ Nanowires In Thermal Ramping Technique

Vapor liquid solid (VLS) mechanism has been widely used to explain the formation of nanowires by carbothermal technique or techniques involving vapour phase. In our case where the synthesizing technique is based on the established carbothermal technique, presence of droplet at the tips of nanowires has confirmed that the VLS mechanism governed the SnO₂ nanowires growth.

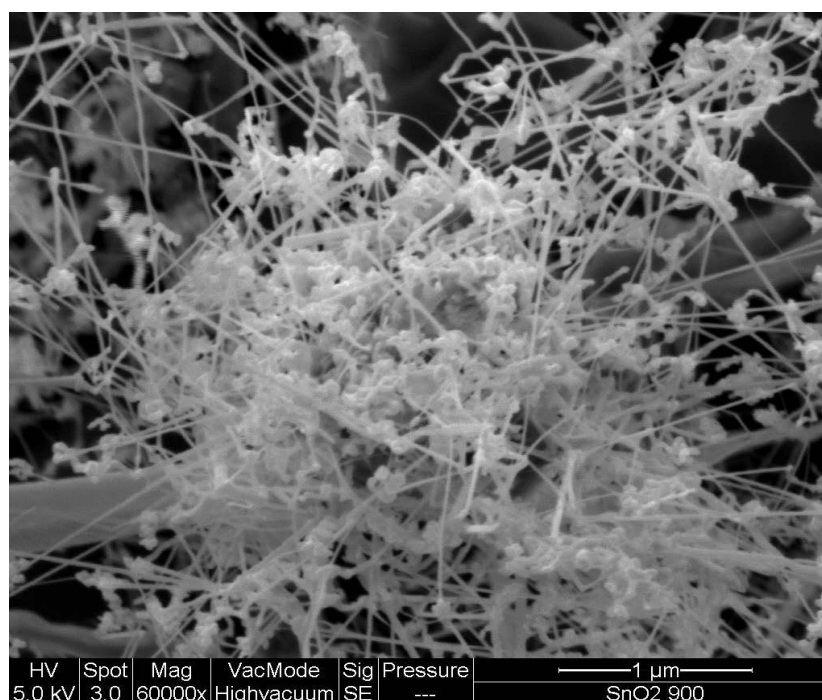
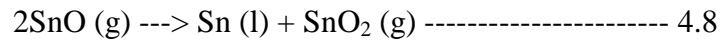
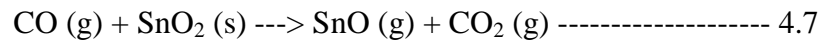
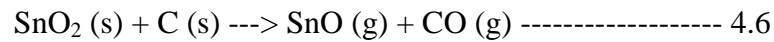


Figure 4.9: Presence of droplets at the tip of the nanowires confirmed the growth was governed by VLS mechanism.

In the same way as the carbothermal reduction method, the thermal ramping technique employs carbon to lower the vaporising temperature of the source material, SnO₂ powder so that vapour may be formed at lower heating temperature. Rafael Padilla [113] outlined that this is possible because SnO₂ will be reduced by C at any temperature above 903 K or 630 °C. The products of the redox reaction, SnO (1080 °C) has lower vaporising temperature than the SnO₂ (1800 °C – 1900 °C). Therefore, the

SnO will be the one to get evaporated and proceeds in the next chemical reaction for the nanowire growth of SnO₂.



As mentioned, the SnO₂ powder is first reduced by carbon to yield SnO and CO in the form of gaseous. Then, the CO will react with other remaining SnO₂ powder to form SnO and CO₂. Due to its metastability, SnO decomposes into Sn and SnO₂. Normally, the phase transformation from SnO to SnO₂ occurs at temperature above 600 °C. Considering the low melting point of Sn (231.9 °C), Sn particles are still liquid at this reaction temperature. These Sn droplets could fell on the substrate and provide the energetically favoured sites for adsorption of SnO₂ vapor [208].

Considering the fact that the substrate is pre-coated by Au thin film, at elevated temperature, the Au will melt and form liquid droplets. Therefore Sn droplets and SnO₂ will be adsorbed on the Au surface before diffuse to the liquid/solid interface. During the diffusion and adsorption on the Au surface, both Sn and SnO₂ can coexist. However, there is also a probability that all the Sn will get oxidised by O₂ presence in surrounding to form SnO₂ [209]. At liquid/solid interface, the SnO₂ will get supersaturated and solidified. This solid will be the seed for the initiation of the nanowire growth, in which its position is just underneath the tip of the Au droplets. Continuous supplies of SnO₂ vapor and Sn liquid will continue the process of adsorption and diffusion of the vapour from the Au surface to the liquid/solid interfaces (which is now is the nanowire seed that has been formed previously). Subsequently, solidification will increase the length of the nanowires vertically. Figure 4.10 illustrates the VLS mechanism growth.

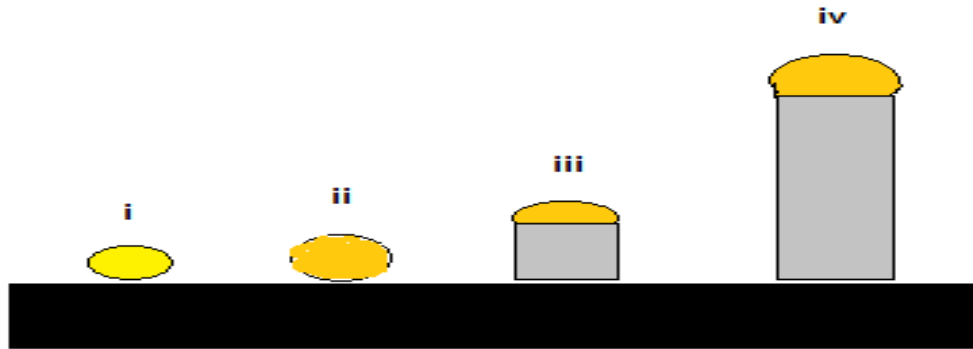


Figure 4.10: Established VLS diagram illustrating the growth of nanowires ; (i) Au melts and forms droplet, (ii) liquid alloy droplet, (iii) crystal nucleation due to vapor adsorption and supersaturation and (iv) axial growth to form nanowires.

According to Muhammad [210], during the nanowires growth if vapour of one element is excessively supplied with regards to the other elements, it can affect the shape of the nanowires. For example, if Sn is flown excessively onto the Au droplets and get integrated into it, cone-shape nanowires are produced (Figure 4.11). Apart from that, in usual VLS mechanism explanation, it is always being assumed that the vapour would fall directly onto the Au catalyst seeds. In the same report, Muhammad illustrated the growth of nanowires if the vapour falls on the substrates and not on the Au catalyst seeds. The diffusion of the vapour species from the substrate to the droplets will then occur via the nanowires sidewalls (S4 in Figure 4.11). Moreover, there is also possibility that the growth will not even occur vertically. Due to the variation in the temperature, the droplets containing Au, Sn, SnO₂ and SnO may become unstable and break up, resulting in no medium for the vertically ordered growth. Therefore the growth occurs randomly. This could be the explanation for our case; multiple thermal ramping numbers might have caused the droplets to break up and therefore growth occurred in random manner. We use FESEM images in Figure 4.3 to support our argument.

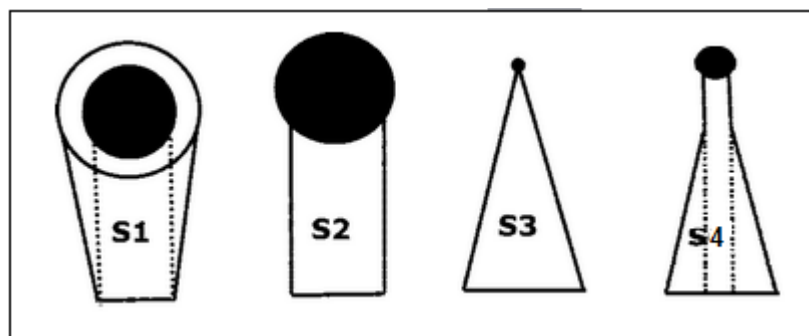


Figure 4.11: Schematic examples of possible nanowire structures formed under a variety of growth conditions. S1, S2 and S3 are the cone shaped structures whereas S4 is due to the vapour diffusion via nanowires sidewall.

In our case where elements of Sn_3O_4 and Sn_2O_3 complex were also detected along with the SnO_2 at $1000\text{ }^\circ\text{C}$, the explanation can be as follows. The Sn_3O_4 and Sn_2O_3 are intermediate oxidation states when SnO oxidizes to SnO_2 through indirect transition. They are not formed if transition is direct from SnO to SnO_2 . It was suggested [211-212] that if the distance, $d(\text{nm})$ values of two sets of parallel planes belonging to the separate phases SnO and SnO_2 are nearly the same, then the direct phase transformation from SnO to SnO_2 occurs without the involvement of intermediate oxidation states Sn_2O_3 or Sn_3O_4 . According to [213], the deposition parameters such as annealing temperature and duration are the factors. They must be sufficiently high and long, respectively.

In VLS mechanism, the diameter of the nanowire produced is dependent on the surface tension energy of the gold droplets. This surface tension energy is actually dependent to the gold droplets radius. This relation has been demonstrated by Wagner and Ellis [38] who determined that the limitation of VLS whisker lower diameters is the consequence of the dependency of liquid surface energy upon the change of liquid droplet radius. According to J. Weyher [115], surface tension energy can be controlled

during VLS growth, by vapour phase composition, substrate type and its crystallographic orientation, growth temperature, liquid phase composition and liquid phase initial amount. For example, decreasing the growth temperature will decrease the droplets diameter. Smaller wire size is then produced. Therefore, different values of the surface tension energy can result in different crystal morphology, and structure (or structure perfection).

Chapter 5

Gas Sensing Results and Discussions

5.1 Gas Sensing Results

In this part, we will be observing through the data and results obtained from the SnO₂ nanowires sensor tested under different operating temperature and H₂ concentration. As has been mentioned in Chapter 3, by testing the sensor at several operating temperature, the optimum operating temperature of the sensor will then be decided and used for the rest of the gas sensing test. The discussion of the results and sensing mechanism will be followed in 5.2.

5.1.1 Different operating temperature

Figure 5.1 shows the response of the SnO₂ nanowire sensor at different operating temperature. The operating temperature was varied to analyse at which temperature the sensor works best. The temperatures used were 200 °C, 250 °C and 300 °C. Hydrogen gas concentration used was 1000 ppm in synthetic air. Throughout the experiment, the resistance of the sensor was monitored and recorded using digital multimeter. The response of the sensor is measured by analysing the degree of change in the sensor's resistance values when hydrogen gas is flown into the chamber.

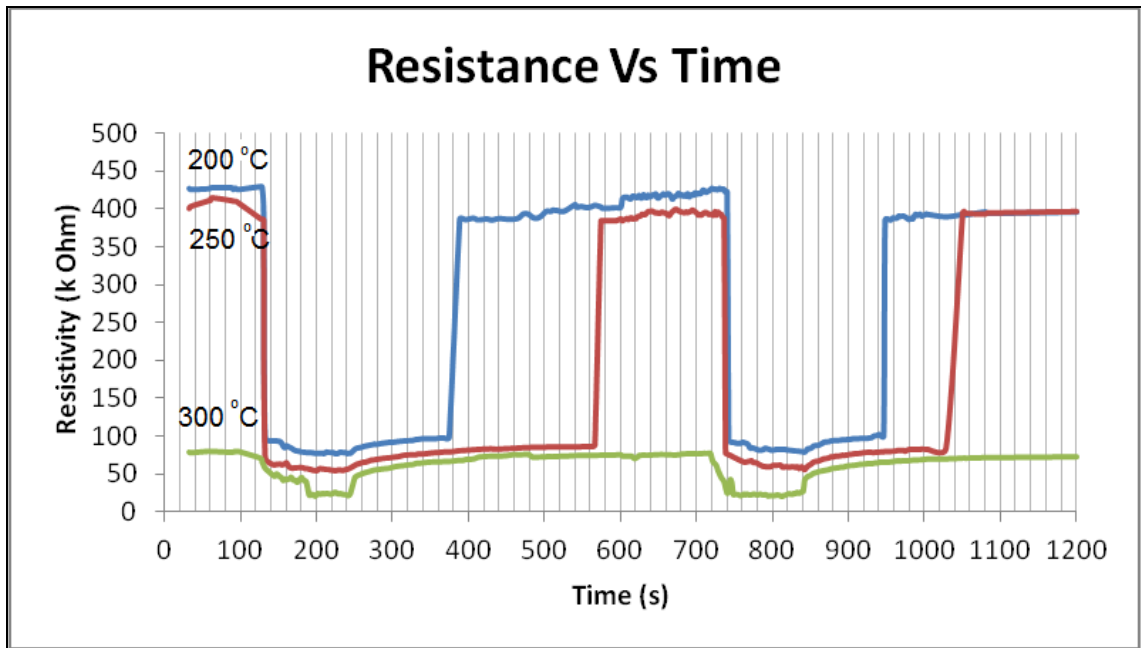


Figure 5.1: Electrical response at different operating temperature and constant hydrogen concentration (1000 ppm).

In all the three cases, the hydrogen gas was flown into the gas chamber after 120 second of exposure to the synthetic air. The sensor started to respond approximately at 140th second, which means the response time is 20 s. The sensor was exposed to the presence of the hydrogen gas for a period of 120 s. The long period of exposure (120 s) is intended to see how well the sensor manages to keep the response. The hydrogen supplied was stopped at 240th second. The resistance value for the sensor operating at 200 °C, 250 °C and 300 °C returned back to the initial resistance value after 140s, 340s and 20s the hydrogen supplied was stopped, respectively. This lagging time to regain their initial resistance value indicates the recovery time of the sensor at the three different operating temperatures. At 200 °C and 250 °C, the responses towards the hydrogen presence are very significant when compared to the response at 300 °C. However, no further studies were carried out to investigate the reason for such response at 300 °C.

Table 1 : The response and recovery times of SnO₂ nanowires sensor upon gas sensor exposure

Temperature (°C)	Response time (s)	Recovery time (s)
200	≈ 20	≈ 140
250	≈ 20	≈ 340
300	≈ 20	≈ 100-150 s

5.1.2 Different gas concentration

Figure below shows the electrical response of the SnO₂ nanowires sensor towards different hydrogen gas concentration. The operating temperature was set constant at 200 °C. The temperature is chosen based on the analysis in the 1st section. Although at 200 °C and 250 °C, both showed almost the same response time, however the recovery time for operating temperature 200 °C was shorter and better.

Different hydrogen gas concentration results in different resistance response. The most significant response is observed when the sensor is exposed to 1000 ppm. The response decreases as the hydrogen gas concentration decreases. Yet the resistance curves are still steadily response towards the hydrogen. However starting from 400 ppm to 200 ppm, the resistance values when hydrogen gas is detected give unstable readings. This is portrayed by the fluctuation resistance values at all the three gas concentration.

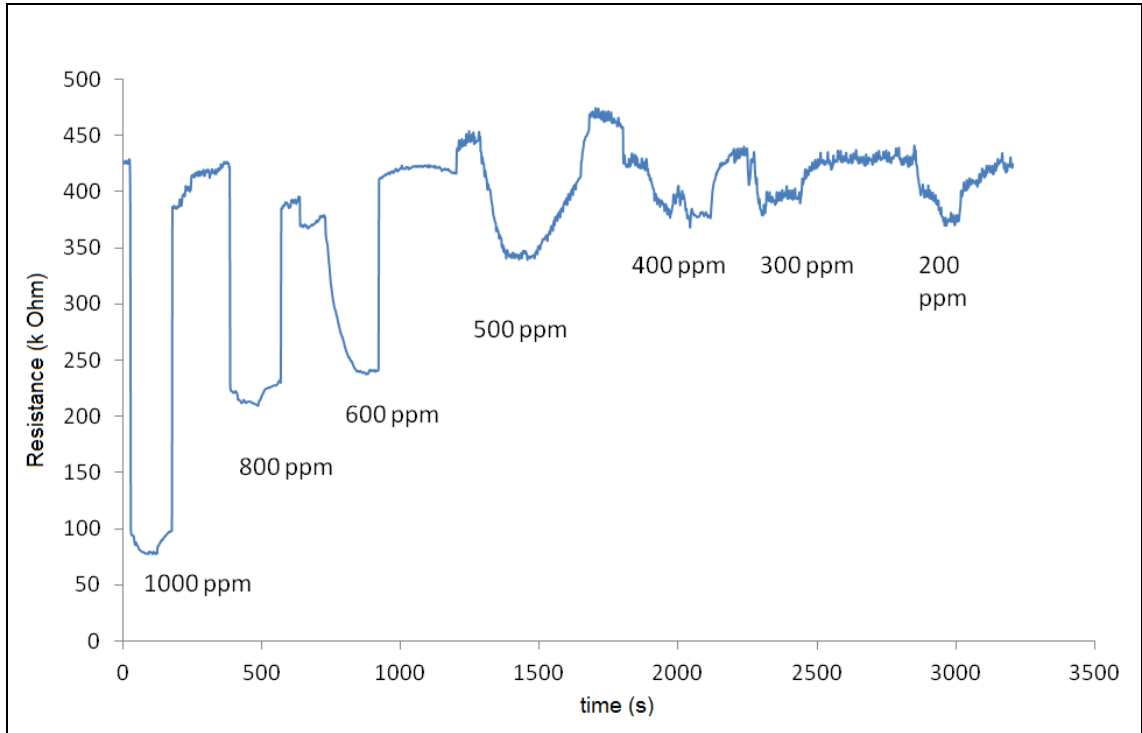


Figure 5.2: Electrical response of SnO₂ nanowires thin film towards hydrogen gas at different concentration and constant operating temperature (T= 200 °C).

5.1.3 Gas Sensor Sensitivity

Figure 5.3 and 5.4 show the sensitivity curves of the SnO₂ sensors. The sensitivity of the sensor is defined as $[(R_g - R_o) / R_o \times 100]$, where R_o and R_g are the sensor resistance before and after H₂ exposure, respectively [214]. The sensitivity of the sensor upon different operating temperature is different for each temperature, with the lowest being at the 300 °C and the highest at 250 °C. However, as has been justified in 5.1.2, the temperature of 200 °C was chosen as the operating temperature based on the recovery time result.

The sensitivity of the sensor shows decrement as the concentration of H₂ decreases. This is consistent with the results of other available reports [57, 38, 68]. The highest and the lowest sensitivity are registered as approximately 82 and 8 when the

sensor was exposed to 1000 ppm and 300 ppm of H₂, respectively. The sensitivity at 200 ppm, 300 ppm and 400 ppm is approximately the same, which is in the range of 8 to 12.

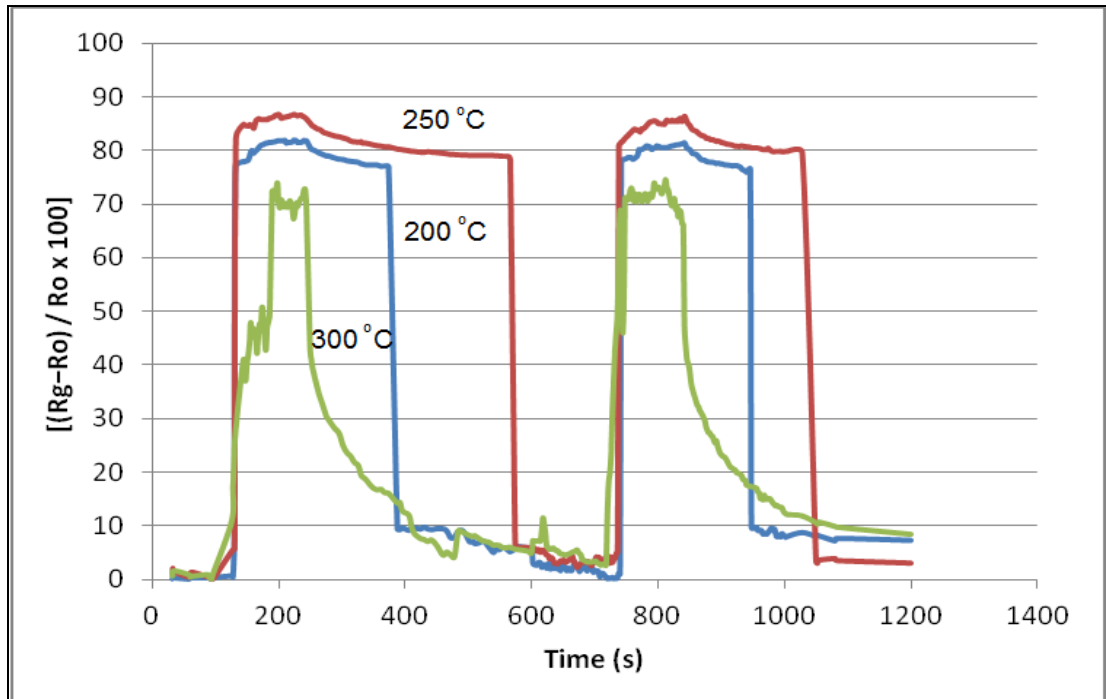


Figure 5.3 : Sensitivity of SnO₂ nanowires sensor at different operating temperature

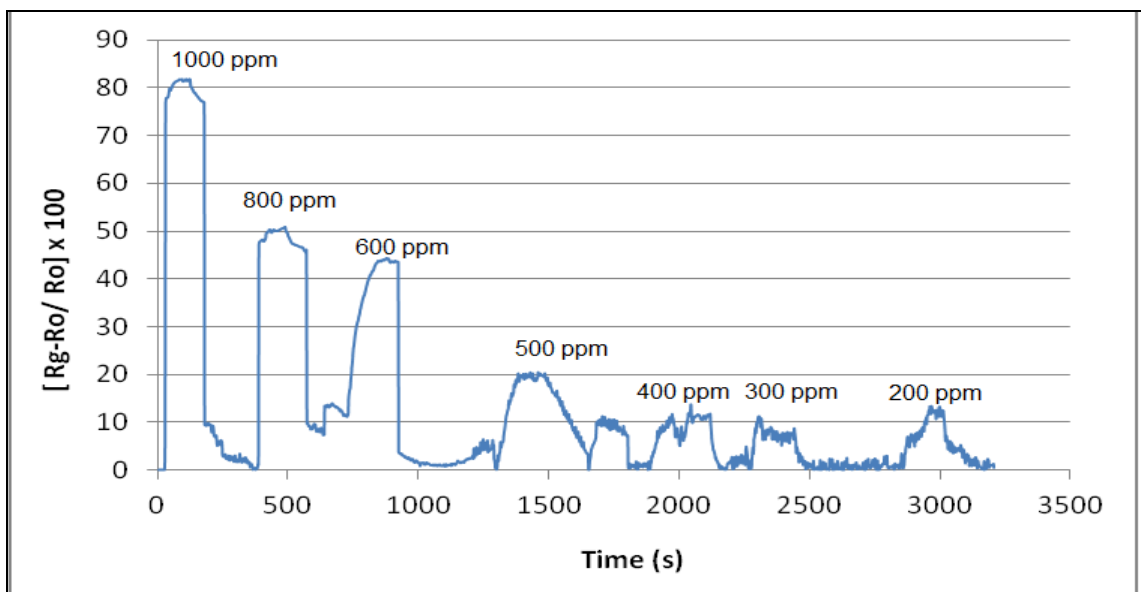


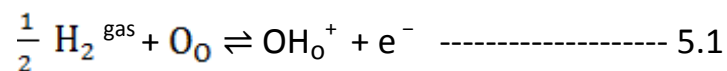
Figure 5.4 : Sensitivity of SnO₂ nanowire sensor at different gas concentrations

5.2 Sensing Mechanism of SnO₂ Nanowires Sensor

Temperature is an important factor in metal oxide gas sensor. It involves in the chemisorption of gas which directly affects the surface reaction of the sensor [215]. Most of the sensors exhibit working temperature of 150 °C-400 °C [57, 216, 217]. The temperature also affects the amount of oxygen and water adsorbed on the surface. As has been mentioned in Chapter 1, negatively charged of O⁻, O₂⁻ and O²⁻ will covered the metal oxide surface as the sensor is exposed to the environment. According to S.H. Hahn et al. [218] at operation temperature 200 °C and above, O⁻ is the main species adsorbed on the surface. Their presence will reduce the charge carrier (electron) at the surface, causing the surface's resistance to increase. In our case, the operation temperature was 200 °C, which means that the main oxygen species adsorbed was O⁻. Presence of reducing gas will decrease the resistance as the H₂ will donate some of its electron to the surface.

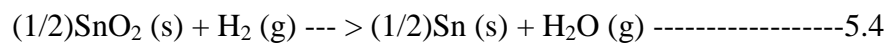
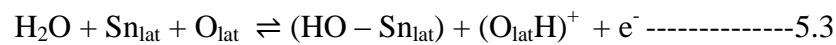
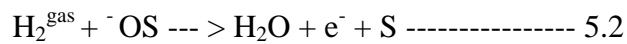
In our case where the SnO₂ nanowires sensor was exposed to synthetic air and hydrogen gas alternately, the resistance was high when synthetic air was flown into the test chamber. This is because, the oxygen molecules from the synthetic air adsorbed and took away electrons from the SnO₂ surface, forming negatively charged of oxygen ions (eg; O⁻, O₂⁻ and O²⁻) which covered the surface. This produces a dipole layer associated with the charged surface and a corresponding depletion region inside the surface of the grain, resulting in a highly resistive inter-granular contact [215]. The sensing part began when the resistance value (as monitored through multimeter) dropped as H₂ molecules was flown onto the chamber and started to adsorb on the SnO₂ surface. It has been proposed [219] that the H₂ will adsorb on the oxygen vacancies (intrinsic defects) sites, which is the SnO₂ surface, while other [215] suggested it will adsorb on the negatively charged oxygen ions. The latter explained that H₂ which is a reducing agent reacts with

the surface oxygen ions, re-injecting electrons into the oxide interior and decreasing the width of the depletion layer [215], thereby decreasing the resistance value. For the former case, J. Z. Larese et al. [220] reported that H₂ can form binding to the oxides surface through the interaction, although he based his experiment using MgO and not SnO₂. This is probably the reason to as why a sensor has recovery time. The H₂ molecules cling to the surface and their presence results in the continuous sensing signal although no more H₂ was flown in the chamber. Variation of recovery time between various sensors could also probably because of how well H₂ cling to the oxide surface, which obviously depend on the binding strength. Apart from that, based on the [215] and [220] reports, it is safe to infer that the re-injection route can possibly be either from the H₂ molecules to the negatively charged oxygen before gained by the oxide surfaces or directly from H₂ to the oxide surface.



Apart from the oxygen, humidity or water in the air as well as the product of combination of H₂ with the pre-adsorbed oxygen ions may as well appear on the surface. This is given by equation 5.1 [221]. They might affect the sensing signal by competing and interfering in the interaction between H₂ and the surface. However, compare to oxidizing gas such as CH₄, water has been proven not to compete with the reducing gas, H₂ to interact with the negatively charged oxygen [222] but it interferes to the signal. This is because the water itself disassociates and donates electrons [218], producing ‘extra signal’ which can obscure the real signal of H₂ detection. Another reports [223, 221] suggested that adsorbed water causes electrons to accumulate at the surface and therefore increases the conductivity. Because of the mixed signal; one caused by H₂ and the other one caused by water, it is said that the sensor performance (recovery time) towards H₂ decreases with increasing humidity [218]. This is

manifested as in Figure 5.2, where we notice that the recovery times at 200 ppm, 300 ppm and 400 ppm are long. This is probably due to presence of water on the SnO₂, even after the H₂ flow was stopped. The question then arises why only at those particular H₂ concentrations and not at 1000 ppm, 800 ppm and 600 ppm (afterwards referred as high concentration). The experiment of these different concentrations was carried out in a successive and continuous manner, where it started with highest and ended with the lowest one, because we intended to test its durability. Therefore the water vapour accumulation at high concentration may not be as much as accumulated at the lower ones. Although there was no comparison measurement on the water accumulation to support our argument, however, we did observe the presence of water on the sensor at the end of the experiment.



The SnO₂ nanowires may also reduced by the H₂ adsorption on the surface [224], and produce water and electron, but unlikely to have occurred in our case due to the conditions which were not met. Therefore, up to this point we understand that there are three (3) ways on how water can form and present as on the sensor; (i) from air humidity, (ii) from hydrogen reaction with pre-adsorbed electrons and (iii) reduction of SnO₂ by hydrogen molecules (referred eq. 5.4 [224]). There are also three ways on how electrons are originated; (i) from hydrogen (referred eq. 5.2 [221]), (ii) water disassociation (referred eq. 5.3 [218]) and (iii) reaction of hydrogen and oxygen pre-adsorbed. As has been written, there are two routes of how electron can reach the surface; direct and indirect. Therefore, it is quite clear on how oxygen and water involve

in gas sensing mechanism. A review report [26] also emphasizes and explains that the sensing characteristics of metal oxide are widely considered to be related with chemisorbed oxygen and water, which can act as intermediates catalyzing the charge transfer processes between gas species and the bulk and which complicates the study of gas sensing mechanisms. The major way they interfere with the gas sensing process is through fluctuations in the concentration and the charges of oxygen vacancies. According to [225], increase in presence of pre-adsorbed oxygen increases the sensitivity of the sensor whereas increase in the amount of water vapour decreases the sensing performance.

As conclusion for this section, we have successfully demonstrated the gas sensing properties of the SnO₂ nanowires sensor synthesized using the thermal ramping technique. The sensing behaviour and electrical response were also consistent with other reports, although it might not be as perfect as theirs, which could be attributed to our moderate and simple sensing equipment or method of sensor fabrication.

Chapter 6

Conclusion

The effect of temperature, ramp number and Au thickness towards SnO₂ nanowires growth were studied. Field emission scanning electron microscopy (FESEM), elemental diffraction x-ray (EDX) and x-ray diffraction (XRD) were used to analyse the morphology, elemental composition and crystal structure of the nanowires. Gas sensing properties of the nanowires were analysed by carrying out a resistivity test upon hydrogen exposure at different operating temperature and gas concentration.

For the nanowires synthesized at different temperature, it was discovered that density was increased as the temperature increased. The increase in the density could be attributed to the increased in the Sn, SnO, SnO₂ and CO/CO₂ vapour supply to the substrates. This is supported by the EDX analysis revealing that the content of Sn and O were increased as the temperature increased. In contrast, diameter decreased at higher temperature is probably due to the fact that at higher temperature, since there is thermodynamic limit for the minimum radius of Au liquid clusters, given by $r_{\min} = 2r_{LVVL}/RT\ln s$, in which at higher temperature, smaller size of droplets or seeds are formed, therefore resulting in thinner diameter size. Apart from that, it was discovered that by slightly changing the thickness of Au, density of Zn₂SiO₄ nanowires were affected. The lower thickness resulted in higher density growth.

SnO₂ nanowires were also observed to increase in density with increase in ramp number. No nanowires were observed in the first ramp. It started to appear in the second ramp and densified in the third ramp. The presence of droplets-like at the tip of the nanowires confirmed that vapour liquid solid (VLS) mechanism governed the growth process. As opposed to vertically growth of the nanowires commonly observed in VLS

mechanism, the nanowires growth direction could have been occurred in random direction. This is concluded based on the fact that liquid droplets break up and disintegrate in the FESEM images of the second ramp. As has been explained by various reports, vertical growth requires the seeds to maintain the vertical shape so that the growth could occur vertically.

No nanowires were observed in single ramp at 900 °C for 30 minutes. They only appeared when the temperature was increased to 1000 °C. Prolonging the annealing time to 110 minutes at 1000 °C has reduced the size of the nanowires formed. It is believed that heating process at high temperature and extended time has dried up and reduced the thickness of the Au catalyst on the substrates. The reduced Au thickness results in the nanowires diameter to decrease. The reduction in the density could also be attributed to the same factor.

SnO₂ nanowires were synthesized with and without Au catalyst on the silicon substrates at 950 °C to study the importance of the Au catalyst. It was observed that only small amount of nanowires were grown when no Au catalyst was applied. Coating the substrates with Au has increased the density of the nanowires significantly. With Au catalyst, the diameter of the nanowire is bigger than the one without Au, approximately 150-400 nm and 50-100 nm respectively. With Au, the lengths of the nanowires are almost 100 μm, whereas without Au catalyst, the lengths are approximately 5 μm. Growth of the nanowires on the bare substrates was probably dominated by vapour-solid (VS) mechanism, whereas the one with Au followed vapour-liquid-solid (VLS) mechanism.

The XRD results revealed that the nanowires obtained at temperatures 700 °C to 900 °C can be indexed to tetragonal rutile structure of SnO₂, with lattice constants are

$a = b = 4.738 \text{ \AA}$ and $c = 3.187 \text{ \AA}$. For nanowires at $700 \text{ }^\circ\text{C}$, peaks for Au crystal with cubic structure were also detected. This is probably due to the less dense of the SnO_2 nanowires formed. At $1000 \text{ }^\circ\text{C}$, SnO_2 , Sn_3O_4 and $\text{Sn}_2\text{O}_3/\text{SnO}.\text{SnO}_2$ were detected. The Sn_3O_4 and Sn_2O_3 are intermediate oxidation states when SnO oxidizes to SnO_2 through indirect transition. They are not formed if transition is direct from SnO to SnO_2 . Therefore, since all the three structures appeared, the nanowires formed at $1000 \text{ }^\circ\text{C}$ could be said to follow both indirect and direct oxidation states, resulting in the mixture structures. In the experiment of investigating the effect of Au thickness where ZnO was used as the precursor material instead of SnO_2 , Zn_2SiO_4 nanowires were formed instead of the ZnO. This is probably due to the high temperature of the environment which caused the mixture or alloy of $\text{ZnO}/\text{SiO}_2/\text{Au}$ or $\text{Zn}/\text{Si}/\text{Au}$ to quickly form Zn_2SiO_4 .

Sensor based on the synthesized SnO_2 nanowires have been fabricated and tested under different operating temperature and hydrogen gas concentration. The sensor was observed to display the optimum performance at $200 \text{ }^\circ\text{C}$, with response and recovery times were approximately 20 s and 140 s, respectively. Although the sensitivity at $250 \text{ }^\circ\text{C}$ was found to be slightly higher compared to the one at $200 \text{ }^\circ\text{C}$, its long recovery time which was 340 s makes the sensing parameter at $200 \text{ }^\circ\text{C}$ considered superior than at $250 \text{ }^\circ\text{C}$. At different hydrogen concentration, the sensitivities were observed to be highest and lowest at 1000 ppm and 200 ppm, respectively. Therefore, the sensitivity can be said to be directly related to the hydrogen concentration. The unstable and fluctuated electrical response and sensitivities of the sensor observed at 400 ppm, 300 ppm and 200 ppm could be attributed to the presence of water vapour on the sensor and complex reaction occurred between the vapour with the oxygen and hydrogen.

Based on the results obtained, it can be observed that the introduction of ramp to the carbothermal reduction technique has successfully eliminated the dependency

towards the usage of gas carrier in the synthesis of SnO₂ nanowires. The distance between source material and substrates was eliminated as well. The sensing performances of the SnO₂ nanowires synthesized were in agreement with other research reports in term of sensitivity, response and recovery times. Therefore, it is concluded that the main objective of the research which is; to develop a new nanowire synthesis technique for H₂ gas sensing application and to demonstrate that this technique is suitable and at par with other nanowires synthesis technique, is achieved.

REFERENCES

1. D.J. Maxwell, S.R. Emory, and S. Nie, *Chemistry of Materials* 13 (3), 1082 (2001).
2. M. Hafeez, T. Zhai, A.S. Bhatti, Y. Bando, and D. Golberg, *The Journal of Physical Chemistry C* 116 (14), 8297 (2012).
3. E.S. Kooij and B. Poelsema, *Phys. Chem. Chem. Phys.* 8 (28), 3349 (2006).
4. K.E. Drexler, New York, NY: John Wiley & Sons, Inc, 1992. (1992).
5. G. Edman Jonsson, H. Fredriksson, R. Sellappan, and D. Chakarov, *International Journal of Photoenergy* 2011 (2011).
6. K. Zhu, N.R. Neale, A. Miedaner, and A.J. Frank, *Nano Letters* 7 (1), 69 (2007).
7. R.A. Pala, J. White, E. Barnard, J. Liu, and M.L. Brongersma, *Advanced Materials* 21 (34), 3504 (2009).
8. B.K. Nayak and M.C. Gupta, *Optics and Lasers in Engineering* 48 (10), 940 (2010).
9. M. Shen, J.E. Carey, C.H. Crouch, M. Kandyla, H.A. Stone, and E. Mazur, *Nano Letters* 8 (7), 2087 (2008).
10. M.C. Lechmann, S.A.L. Weber, J. Geserick, N. Hüsing, R. Berger, and J.S. Gutmann, *J. Mater. Chem.* 21 (21), 7765 (2011).
11. D.T. Schoen, A.P. Schoen, L. Hu, H.S. Kim, S.C. Heilshorn, and Y. Cui, *Nano Letters* (2010).
12. L. Hu, H.S. Kim, J.Y. Lee, P. Peumans, and Y. Cui, *ACS nano* 4 (5), 2955 (2010).
13. F. Patolsky, G. Zheng, and C.M. Lieber, *Nanomedicine* 1 (1), 51 (2006).
14. J. Hahn and C.M. Lieber, *Nano Letters* 4 (1), 51 (2004).
15. G.S. Aluri, A. Motayed, A.V. Davydov, V.P. Oleshko, K.A. Bertness, N.A. Sanford, and M.V. Rao, *Nanotechnology* 22, 295503 (2011).
16. C. Drake, S. Deshpande, D. Bera, and S. Seal, *International Materials Reviews* 52 (5), 289 (2007).
17. Z. Fan and J.G. Lu, *Nanotechnology*, *IEEE Transactions on* 5 (4), 393 (2006).
18. R. Burch, *Catalysis Reviews* 46 (3-4), 271 (2004).
19. M. Law, L.E. Greene, J.C. Johnson, R. Saykally, and P. Yang, *Nature materials* 4 (6), 455 (2005).
20. E. Garnett and P. Yang, *Nano Letters* 10 (3), 1082 (2010).
21. L. Tsakalacos, J. Balch, J. Fronheiser, BA Korevaar, O. Sulima, and J. Rand, *Applied Physics Letters* 91 (23), 233117 (2007).
22. L.S. Zhong, J.S. Hu, H.P. Liang, A.M. Cao, W.G. Song, and L.J. Wan, *Advanced Materials* 18 (18), 2426 (2006).
23. Y. Dong, H. Yang, K. He, S. Song, and A. Zhang, *Applied Catalysis B: Environmental* 85 (3), 155 (2009).
24. X. Lu, D. Zheng, J. Gan, Z. Liu, C. Liang, P. Liu, and Y. Tong, *Journal of Materials Chemistry* 20 (34), 7118 (2010).
25. P. Gouma, G. Sberveglieri, R. Dutta, JW Gardner, and EL Hines, *MRS Bulletin-Materials Research Society* 29, 697 (2004).

26. J. Huang and Q. Wan, *Sensors* 9 (12), 9903 (2009).
27. C. Drake, S. Deshpande, D. Bera, and S. Seal, *International Materials Reviews* 52 (5), 289 (2007).
28. K. Kim and S.M. Cho, 2004 (unpublished).
29. X. Wang, Z. Xie, H. Huang, Z. Liu, D. Chen, and G. Shen, *J. Mater. Chem.* (2012).
30. F. Hernandez-Ramirez, A. Tarancón, O. Casals, J. Arbiol, A. Romano-Rodriguez, and JR Morante, *Sensors and Actuators B: Chemical* 121 (1), 3 (2007).
31. V. Guidi, MC Carotta, M. Ferroni, G. Martinelli, L. Paglialonga, E. Comini, and G. Sberveglieri, *Sensors and Actuators B: Chemical* 57 (1-3), 197 (1999).
32. Y. Dan, S. Evoy, and AT Johnson, *Arxiv preprint arXiv:0804.4828* (2008).
33. A.K. Wanekaya, W. Chen, N.V. Myung, and A. Mulchandani, *Electroanalysis* 18 (6), 533 (2006).
34. Y. Dan, S. Evoy, and AT Johnson, *Arxiv preprint arXiv:0804.4828* (2008).
35. H. Uda, S. Shahrir, S. Fatimah, and A. Rahman, (2008).
36. J. Melngailis, A. Motayed, A. Davydov, D. Tvetkov, and N. Mohammad, 2010.
37. Available online at : <http://www.nist.gov/pml/nanowire-042607.cfm>
38. B. Wang, LF Zhu, YH Yang, NS Xu, and GW Yang, *The Journal of Physical Chemistry C* 112 (17), 6643 (2008).
39. B. Wang, LF Zhu, YH Yang, NS Xu, and GW Yang, *The Journal of Physical Chemistry C* 112 (17), 6643 (2008).
40. JS Wright, W. Lim, BP Gila, SJ Pearton, J.L. Johnson, A. Ural, and F. Ren, *Sensors and Actuators B: Chemical* 140 (1), 196 (2009).
41. O. Lupan, G. Chai, and L. Chow, *Microelectronic Engineering* 85 (11), 2220 (2008).
42. P. Xu, Z. Cheng, Q. Pan, J. Xu, Q. Xiang, W. Yu, and Y. Chu, *Sensors and Actuators B: Chemical* 130 (2), 802 (2008).
43. J. Xu, Y. Chen, and J. Shen, *Materials Letters* 62 (8-9), 1363 (2008).
44. W. Han, S. Fan, Q. Li, and Y. Hu, *Science* 277 (5330), 1287 (1997).
45. A.T. Bell, *Science* 299 (5613), 1688 (2003).
46. P. Hohenberg and W. Kohn, *Physical Review* 136 (3B), B864 (1964).
47. P. TRANSLOCATION, (1990).
48. ID Brown and D. Altermatt, *Acta Crystallographica Section B: Structural Science* 41 (4), 244 (1985).
49. O. Lupan, G. Chai, and L. Chow, *Microelectronic Engineering* 85 (11), 2220 (2008).
50. Z. Fan, J.C. Ho, Z.A. Jacobson, R. Yerushalmi, R.L. Alley, H. Razavi, and A. Javey, *Nano Letters* 8 (1), 20 (2008).
51. T. Seiyama, A. Kato, K. Fujiishi, and M. Nagatani, *Analytical Chemistry* 34 (11), 1502 (1962).
52. J. Campbell, *International Materials Reviews* 39 (3), 125 (1994).
53. K.J. Choi and H.W. Jang, *Sensors* 10 (4), 4083 (2010).

54. E. Kanazawa, G. Sakai, K. Shimanoe, Y. Kanmura, Y. Teraoka, N. Miura, and N. Yamazoe, *Sensors and Actuators B: Chemical* 77 (1-2), 72 (2001).
55. G. Korotcenkov, *Materials Science and Engineering: B* 139 (1), 1 (2007).
56. J. Campbell, *International Materials Reviews* 39 (3), 125 (1994).
57. N. Barsan and U. Weimar, *Journal of Physics: Condensed Matter* 15, R813 (2003).
58. H. Drost, *Zeitschrift für Physikalische Chemie* 177 (Part_1), 123 (1992).
59. N. Yamazoe, J. Fuchigami, M. Kishikawa, and T. Seiyama, *Surface Science* 86, 335 (1979).
60. J. Bardeen and SR Morrison, *Physica* 20 (7-12), 873 (1954).
61. M.E. Franke, T.J. Koplín, and U. Simon, *Small* 2 (1), 36 (2006).
62. VE Bochenkov and GB Sergeev, (2010).
63. KD Schierbaum, U. Weimar, W. Göpel, and R. Kowalkowski, *Sensors and Actuators B: Chemical* 3 (3), 205 (1991).
64. S. Phadungthitidhada, S. Thanasanvorakun, P. Mangkorntong, S. Choopun, N. Mangkorntong, and D. Wongratanaphisan, *Current Applied Physics* (2011).
65. Y.J. Choi, I.S. Hwang, J.G. Park, K.J. Choi, J.H. Park, and J.H. Lee, *Nanotechnology* 19, 095508 (2008).
66. Q. Wan and TH Wang, *Chemical Communications* (30), 3841 (2005).
67. V. Kumar, S. Sen, KP Muthe, NK Gaur, SK Gupta, and JV Yakhmi, *Sensors and Actuators B: Chemical* 138 (2), 587 (2009).
68. Y. Shen, T. Yamazaki, Z. Liu, D. Meng, and T. Kikuta, *Journal of Alloys and Compounds* 488 (1), L21 (2009).
69. O. Lupan, G. Chai, and L. Chow, *Microelectronics Journal* 38 (12), 1211 (2007).
70. C. Wang, L. Yin, L. Zhang, D. Xiang, and R. Gao, *Sensors* 10 (3), 2088 (2010).
71. C. R. Henry, C. Chapon, and C. Duriez, *J. Chem. Phys.* 95, 700 (1991).
72. K. Tsu and M. Boudart, *Can. J. Chem.*, 39, 1239 (1961).
73. C. Li, D. Zhang, B. Lei, S. Han, X. Liu, and C. Zhou, *The Journal of Physical Chemistry B* 107 (45), 12451 (2003).
74. F. Lu, Y. Liu, M. Dong, and X. Wang, *Sensors and Actuators B: Chemical* 66 (1-3), 225 (2000).
75. C. Li, D. Zhang, X. Liu, S. Han, T. Tang, J. Han, and C. Zhou, *Applied Physics Letters* 82 (10), 1613 (2003).
76. SG Ansari, P. Boroojerdian, SR Sainkar, RN Karekar, RC Aiyer, and SK Kulkarni, *Thin solid films* 295 (1-2), 271 (1997).
77. G. Korotcenkov, *Materials Science and Engineering: R: Reports* 61 (1), 1 (2008).
78. N. Barsan and U. Weimar, *Journal of Electroceramics* 7 (3), 143 (2001).
79. G. Korotcenkov, S.D. Han, BK Cho, and V. Brinzari, *Critical Reviews in Solid State and Materials Sciences* 34 (1-2), 1 (2009).
80. B. Timmer, W. Olthuis, and A. Berg, *Sensors and Actuators B: Chemical* 107 (2), 666 (2005).
81. X. Wang, S.S. Yee, and W.P. Carey, *Sensors and Actuators B: Chemical* 25 (1-3), 454 (1995).

82. N. Barsan, *Sensors and Actuators B: Chemical* 17 (3), 241 (1994).
83. H. Liu, S.P. Gong, Y.X. Hu, J.Q. Liu, and D.X. Zhou, *Sens. Actuat. B*, 140, 190 (2009).
84. E. Strelcov, S. Dmitriev, B. Button, J. Cothren, V. Sysoev, and A. Kolmakov, *Nanotechnology* 19, 355502 (2008).
85. LC Tien, DP Norton, SJ Pearton, H.T. Wang, and F. Ren, *Applied surface science* 253 (10), 4620 (2007).
86. S.J. Pearton, D.P. Norton, and F. Ren, *Small* 3 (7), 1144 (2007).
87. S. Verhelst and R. Sierens, *International journal of hydrogen energy* 26 (9), 981 (2001).
88. AZ Sadek, W. Wlodarski, YX Li, W. Yu, X. Li, X. Yu, and K. Kalantar-Zadeh, *Thin solid films* 515 (24), 8705 (2007).
89. YM Wong, WP Kang, JL Davidson, A. Wisitsora-At, and KL Soh, *Sensors and Actuators B: Chemical* 93 (1-3), 327 (2003).
90. W. Shin, K. Imai, N. Izu, and N. Murayama, *Japanese Journal of Applied Physics* 40, 1232 (2001).
91. T. Watanabe, S. Okazaki, H. Nakagawa, K. Murata, and K. Fukuda, *Sensors and Actuators B: Chemical* 145 (2), 781 (2010).
92. M. Batzill and U. Diebold, *Progress in surface science* 79 (2-4), 47 (2005).
93. ETH Tan, GW Ho, ASW Wong, S. Kawi, and ATS Wee, *Nanotechnology* 19, 255706 (2008).
94. H. Huang, YC Lee, CL Chow, CY Ong, MS Tse, and OK Tan, 2008 (unpublished).
95. Y. Shen, T. Yamazaki, Z. Liu, D. Meng, and T. Kikuta, *Journal of Alloys and Compounds* 488 (1), L21 (2009).
96. J. Xu, D. Wang, L. Qin, W. Yu, and Q. Pan, *Sensors and Actuators B: Chemical* 137 (2), 490 (2009).
97. E. Galoppini, J. Rochford, H. Chen, G. Saraf, Y. Lu, A. Hagfeldt, and G. Boschloo, *The Journal of Physical Chemistry B* 110 (33), 16159 (2006).
98. H. Chen, A. Du Pasquier, G. Saraf, J. Zhong, and Y. Lu, *Semiconductor Science and Technology* 23, 045004 (2008).
99. K.S. Shankar and AK Raychaudhuri, *Materials Science and Engineering: C* 25 (5), 738 (2005).
100. C. Wang, X. Chu, and M. Wu, *Sensors and Actuators B: Chemical* 113 (1), 320 (2006).
101. R. Wang, H. Li, M. Pan, and D. Chen, 2009 (unpublished).
102. C. Wang, X. Chu, and M. Wu, *Sensors and Actuators B: Chemical* 113 (1), 320 (2006).
103. Available at: <http://www.aip.org/tip/INPHFA/vol-5/iss-3/p18.pdf> 1
104. U. Hashim, S. Salleh, E.A. Shohini, and S.F.A. Rahman, 2008 (unpublished).
105. Y. Jiang, *E-Beam and Conventional Lithography*, Retrieved May 21, 2012 from <http://www.dssc.ece.cmu.edu/news/seminars/lunch05/headsmidia/041205.pdf>
106. N.S. Ramgir, I.S. Mulla, and K.P. Vijayamohan, *Sensors and Actuators B: Chemical* 107 (2), 708 (2005).

- 107.Y. Zhang, A. Kolmakov, S. Chretien, H. Metiu, and M. Moskovits, *Nano Letters* 4 (3), 403 (2004).
- 108.A. Kolmakov, Y. Zhang, G. Cheng, and M. Moskovits, *Advanced Materials* 15 (12), 997 (2003).
- 109.O. Jessensky, F. Muller, and U. Gosele, *Applied Physics Letters* 72 (10), 1173 (1998).
- 110.B.J. Murray, E.C. Walter, and R.M. Penner, *Nano Letters* 4 (4), 665 (2004).
- 111.R.B. Sadeghian and M. Kahrizi, *Sensors and Actuators A: Physical* 137 (2), 248 (2007).
- 112.Z. Liu and P.C. Searson, *The Journal of Physical Chemistry B* 110 (9), 4318 (2006).
- 113.Y. Im, C. Lee, R.P. Vasquez, M.A. Bangar, N.V. Myung, E.J. Menke, R.M. Penner, and M. Yun, *Small* 2 (3), 356 (2006).
- 114.Y. Dan, Y. Cao, T.E. Mallouk, A.T. Johnson, and S. Evoy, *Sensors and Actuators B: Chemical* 125 (1), 55 (2007).
- 115.R.B. Sadeghian and M. Kahrizi, *Sensors and Actuators A: Physical* 137 (2), 248 (2007).
- 116.Z. Liu and P.C. Searson, *The Journal of Physical Chemistry B* 110 (9), 4318 (2006).
- 117.Y. Im, C. Lee, R.P. Vasquez, M.A. Bangar, N.V. Myung, E.J. Menke, R.M. Penner, and M. Yun, *Small* 2 (3), 356 (2006).
- 118.D. Routkevitch, T. Bigioni, M. Moskovits, and J.M. Xu, *The Journal of Physical Chemistry* 100 (33), 14037 (1996).
- 119.J. Fu, S. Cherevko, and C.H. Chung, *Electrochemistry communications* 10 (4), 514 (2008).
- 120.Y. Xia, P. Yang, Y. Sun, Y. Wu, B. Mayers, B. Gates, Y. Yin, F. Kim, and H. Yan, *Advanced Materials* 15 (5), 353 (2003).
- 121.N.I. Kovtyukhova and T.E. Mallouk, *Nanoscale* 3 (4), 1541 (2011).
- 122.GX Wang, JS Park, and MS Park, *Journal of Nanoscience and Nanotechnology* 9 (2), 1144 (2009).
- 123.J. Fu, S. Cherevko, and C.H. Chung, *Electrochemistry communications* 10 (4), 514 (2008).
- 124.J. Spooren, A. Ruplecker, F. Millange, and R.I. Walton, *Chemistry of Materials* 15 (7), 1401 (2003).
- 125.C. Cheng, B. Liu, H. Yang, W. Zhou, L. Sun, R. Chen, S.F. Yu, J. Zhang, H. Gong, and H. Sun, *ACS nano* 3 (10), 3069 (2009).
- 126.G. Zou, H. Li, Y. Zhang, K. Xiong, and Y. Qian, *Nanotechnology* 17, S313 (2006).
- 127.K.B. Tang, Y.T. Qian, J.H. Zeng, and X.G. Yang, *Advanced Materials* 15 (5), 448 (2003).
- 128.J. Chen, K. Wang, and W. Zhou, *Nanotechnology, IEEE Transactions on* (99), 1 (2011).
- 129.C. Cheng, B. Liu, H. Yang, W. Zhou, L. Sun, R. Chen, S.F. Yu, J. Zhang, H. Gong, and H. Sun, *ACS nano* 3 (10), 3069 (2009).

- 130.Z. Miao, D. Xu, J. Ouyang, G. Guo, X. Zhao, and Y. Tang, *Nano Letters* 2 (7), 717 (2002).
- 131.GS Wu, T. Xie, XY Yuan, Y. Li, L. Yang, YH Xiao, and LD Zhang, *Solid state communications* 134 (7), 485 (2005).
- 132.Q. Tang, Y. Tong, T. Jain, T. Hassenkam, Q. Wan, K. Moth-Poulsen, and T. Bjørnholm, *Nanotechnology* 20, 245205 (2009).
- 133.Q. Tang, Y. Tong, T. Jain, T. Hassenkam, Q. Wan, K. Moth-Poulsen, and T. Bjørnholm, *Nanotechnology* 20, 245205 (2009).
- 134.T.J. Hsueh, Y.W. Chen, S.J. Chang, S.F. Wang, C.L. Hsu, Y.R. Lin, T.S. Lin, and I. Chen, *Sensors and Actuators B: Chemical* 125 (2), 498 (2007).
- 135.Z. Fan, D. Wang, P.C. Chang, W.Y. Tseng, and J.G. Lu, *Applied Physics Letters* 85 (24), 5923 (2004).
- 136.J.M. Wu and C.H. Kuo, *Thin solid films* 517 (14), 3870 (2009).
- 137.Z.L. Wang, *Advanced Materials* 15 (5), 432 (2003).
- 138.T.J. Hsueh, C.L. Hsu, S.J. Chang, and I. Chen, *Sensors and Actuators B: Chemical* 126 (2), 473 (2007).
- 139.D.I. Suh, C.C. Byeon, and C.L. Lee, *Applied surface science* 257 (5), 1454 (2010).
- 140.TI Kamins, X. Li, R.S. Williams, and X. Liu, *Nano Letters* 4 (3), 503 (2004).
- 141.XS Peng, YW Wang, J. Zhang, XF Wang, LX Zhao, GW Meng, and LD Zhang, *Applied Physics A: Materials Science & Processing* 74 (3), 437 (2002).
- 142.P.C. Chen, G. Shen, H. Chen, Y. Ha, C. Wu, S. Sukcharoenchoke, Y. Fu, J. Liu, A. Facchetti, and T.J. Marks, *ACS nano* 3 (11), 3383 (2009).
- 143.CNR Rao, G. Gundiah, F.L. Deepak, A. Govindaraj, and AK Cheetham, *J. Mater. Chem.* 14 (4), 440 (2004).
- 144.J.M. Velazquez and S. Banerjee, *Small* 5 (9), 1025 (2009).
- 145.TI Kamins, X. Li, R.S. Williams, and X. Liu, *Nano Letters* 4 (3), 503 (2004).
- 146.J.M. Velazquez and S. Banerjee, *Small* 5 (9), 1025 (2009).
- 147.A.M. Morales and C.M. Lieber, *Science* 279 (5348), 208 (1998).
- 148.J. Westwater, DP Gosain, S. Tomiya, S. Usui, and H. Ruda, *Journal of Vacuum Science & Technology B: Microelectronics and Nanometer Structures* 15 (3), 554 (1997).
- 149.Y. Wu and P. Yang, *JOURNAL-AMERICAN CHEMICAL SOCIETY* 123 (13), 3165 (2001).
- 150.I. Castro-Hurtado, J. Herrán, GG Mandayo, and E. Castaño, *Thin solid films* (2011).
- 151.T.Y. Kim, S.H. Lee, Y.H. Mo, H.W. Shim, K.S. Nahm, E.K. Suh, JW Yang, KY Lim, and GS Park, *Journal of crystal growth* 257 (1), 97 (2003).
- 152.L. Bachmann and JJ Shin, *Journal of Applied Physics* 37 (1), 242 (1966).
- 153.S. Budak, GX Miao, M. Ozdemir, KB Chetry, and A. Gupta, *Journal of crystal growth* 291 (2), 405 (2006).
- 154.R.S. Wagner and W.C. Ellis, *Trans. AIME*, 233(1965) 1053.
- 155.I. Castro-Hurtado, J. Herrán, GG Mandayo, and E. Castaño, *Thin solid films* (2011).

- 156.J.C. Lee, K.S. Park, T.G. Kim, H.J. Choi, and Y.M. Sung, *Nanotechnology* 17, 4317 (2006).
- 157.M. Comotti, W.C. Li, B. Spliethoff, and F. Schüth, *Journal of the American Chemical Society* 128 (3), 917 (2006).
- 158.L. Wen, J.K. Fu, P.Y. Gu, B.X. Yao, Z.H. Lin, and J.Z. Zhou, *Applied Catalysis B: Environmental* 79 (4), 402 (2008).
- 159.S.C. Lyu, Y. Zhang, H. Ruh, H.J. Lee, H.W. Shim, E.K. Suh, and C.J. Lee, *Chemical Physics Letters* 363 (1), 134 (2002).
- 160.T. Hanrath and B.A. Korgel, *Journal of the American Chemical Society* 124 (7), 1424 (2002).
- 161.L. Luo, B.D. Sosnowchik, and L. Lin, *Applied Physics Letters* 90, 093101 (2007).
- 162.P.H. Suman and M.O. Orlandi, *Journal of Nanoparticle Research* 13 (5), 2081 (2011).
- 163.B. Wang, YH Yang, and GW Yang, *Nanotechnology* 17, 4682 (2006).
- 164.J. Geurts, S. Rau, W. Richter, and FJ Schmitte, *Thin solid films* 121 (3), 217 (1984).
- 165.Y. Rosenfeld Hacoheh, R. Popovitz-Biro, E. Grunbaum, Y. Prior, and R. Tenne, *Advanced Materials* 14 (15), 1075 (2002).
- 166.WK Choi, H. Sung, KH Kim, JS Cho, SC Choi, H.J. Jung, SK Koh, CM Lee, and K. Jeong, *Journal of materials science letters* 16 (19), 1551 (1997).
- 167.M. Salehi, B. Janfeshan, and SK Sadrnezhaad, *Applied Physics A: Materials Science & Processing* 97 (2), 361 (2009).
- 168.S K.L. Lin and T.P. Liu, *Oxidation of metals* 50 (3), 255 (1998).
- 169.J. Weyher, *Materials Science and Engineering* 20, 171 (1975).
- 170.H.W. Kim and S.H. Shim, *Key Engineering Materials* 336, 2160 (2007).
- 171.S. Luo, J. Fan, W. Liu, M. Zhang, Z. Song, C. Lin, X. Wu, and P.K. Chu, *Nanotechnology* 17, 1695 (2006).
- 172.MK Fung, KK Wong, XY Chen, YF Chan, AMC Ng, AB Djurišić, and WK Chan, *Current Applied Physics* (2011).
- 173.P. Nguyen, S. Vaddiraju, and M. Meyyappan, *Journal of electronic materials* 35 (2), 200 (2006).
- 174.SH Sun, GW Meng, MG Zhang, XH An, GS Wu, and LD Zhang, *Journal of Physics D: Applied Physics* 37, 409 (2004).
- 175.S. Thanasanvorakun, P. Mangkorntong, S. Choopun, and N. Mangkorntong, *Ceramics International* 34 (4), 1127 (2008).
- 176.A. Kar, M.A. Stroschio, M. Dutta, J. Kumari, and M. Meyyappan, *Semiconductor Science and Technology* 25, 024012 (2010).
- 177.M. Salehi, B. Janfeshan, and SK Sadrnezhaad, *Applied Physics A: Materials Science & Processing* 97 (2), 361 (2009).
- 178.SY Lee, YH Shin, Y. Kim, S. Kim, and S. Ju, *Journal of Luminescence* (2011).
- 179.J. Weyher, *Materials Science and Engineering* 20, 171 (1975).
- 180.T. Yanagida, K. Nagashima, HS. Tanaka, and T. Kawai, *Journal of Applied Physics* 104 (1), 016101 (2008).

- 181.J. Huang, A. Lu, B. Zhao, and Q. Wan, *Applied Physics Letters* 91 (7), 073102 (2007).
- 182.H. Wan and H.E. Ruda, *Journal of Materials Science: Materials in Electronics* 21 (10), 1014 (2010).
- 183.U. Manzoor and D.K. Kim, *Physica E: Low-dimensional Systems and Nanostructures* 41 (3), 500 (2009).
- 184.Z. Chen, N. Wu, Z. Shan, M. Zhao, S. Li, C.B. Jiang, M.K. Chyu, S.X. Mao, *Scr. Mater.* 52 (2005) 63.
- 185.Synthesis of ZnO nanowires and nanosheets by an O₂-assisted carbothermal reduction process Jae-Hwan Park, Young-Jin Choi, Jae-Gwan Park, *Journal of Crystal Growth* Volume 280, Issues 1–2, 15 June 2005, Pages 161–167.
- 186.OH Elibol, D. Morissette, D. Akin, JP Denton, and R. Bashir, *Applied Physics Letters* 83, 4613 (2003).
- 187.C.T. Sousa, D.C. Leitao, J. Ventura, P.B. Tavares, and J.P. Araujo, *Nanoscale Research Letters* 7 (1), 168 (2012).
- 188.DC Leitao, J. Ventura, CT Sousa, AM Pereira, JB Sousa, M. Vazquez, and JP Araujo, *Physical Review B* 84 (1), 014410 (2011).
- 189.H. Chen, S.M. Yu, D.W. Shin, and J.B. Yoo, *Nanoscale Research Letters* 5 (1), 217 (2010).
- 190.Jae-Hwan Park, Young-Jin Choi and Jae-Gwan Park, *Journal of Crystal Growth* 280 (2005) 161–167.
- 191.D. Calestani, L. Lazzarini, G. Salviati, and M. Zha, *Crystal Research and Technology* 40 (10-11), 937 (2005).
- 192.X. Zhang, B. Yao, L. Zhao, C. Liang, L. Zhang, and Y. Mao, *Journal of the Electrochemical Society* 148, G398 (2001).
- 193.DC Leitao, J. Ventura, CT Sousa, AM Pereira, JB Sousa, M. Vazquez, and JP Araujo, *Physical Review B* 84 (1), 014410 (2011).
- 194.PMC US National Libraray of Medicine National Institutes of Health, Retirieved June 15, 2012 from <http://www.ncbi.nlm.nih.gov/pmc/articles/PMC2893607/%206/>
- 195.D. Kopeliovich, *Fabrication of Ceramic Matrix Composites by Sol-gel process, SubsTech Substances and Technologies*, Retrieved June 12, 2012 from http://www.substech.com/dokuwiki/doku.php?id=fabrication_of_ceramic_matrix_composites_by_sol-gel_process
- 196.S.N. Mohammad, *Nano Letters* 8 (5), 1532 (2008).
- 197.E. Durgun, S. Dag, VMK Bagci, O. Gülseren, T. Yildirim, and S. Ciraci, *Physical Review B* 67 (20), 201401 (2003).
- 198.L. Zhang, X. Fang, and C. Ye, *Controlled growth of nanomaterials*. (World Scientific Pub Co Inc, 2007).
- 199.D. Yu, T. Trad, J.T. McLeskey, V. Craciun, and C.R. Taylor, *Nanoscale Research Letters* 5 (8), 1333 (2010).
- 200.M.S. Gudiksen and CM Lieher, *JOURNAL-AMERICAN CHEMICAL SOCIETY* 122 (36), 8801 (2000).
- 201.SY Lee, YH Shin, Y. Kim, S. Kim, and S. Ju, *Journal of Luminescence* (2011).

- 202.H. Q. Wang, G. Z. Wang, L. C. Jia, C. J. Tang, and G. H. Li, *J. Phys. Chem. C*, 111, 14307-14311(2007).
- 203.XD Wang, C.J. Summers, and Z.L. Wang, *Advanced Materials* 16 (14), 1215 (2004).
- 204.JK Jian, XL Chen, WJ Wang, L. Dai, and YP Xu, *Applied Physics A: Materials Science & Processing* 76 (2), 291 (2003).
- 205.JS Jeong, JY Lee, CJ Lee, SJ An, and G.C. Yi, *Chemical Physics Letters* 384 (4), 246 (2004).
- 206.SH Sun, GW Meng, YW Wang, T. Gao, MG Zhang, YT Tian, XS Peng, and LD Zhang, *Applied Physics A: Materials Science & Processing* 76 (2), 287 (2003).
- 207.B. Wang, Y.H. Yang, C.X. Wang, G.W. Yang, *Chem. Phys. Lett.* 407, 347 (2005).
- 208.Y. Chen, X. Cui, K. Zhang, D. Pan, S. Zhang, B. Wang, and JG Hou, *Chemical Physics Letters* 369 (1), 16 (2003).
- 209.M. Zheng, G. Li, X. Zhang, S. Huang, Y. Lei, and L. Zhang, *Chemistry of Materials* 13 (11), 3859 (2001).
- 210.S.N. Mohammad, *Nano Letters* 8 (5), 1532 (2008).
- 211.K. Suzuki and M. Mizuhashi: *Thin Solid Films* 97 (1982) 119.
- 212.J. Geuets, S. Rau, W. Richter and Fj Schmitte, *ibid.* 121 (198) 217.
- 213.WK Choi, H. Sung, KH Kim, JS Cho, SC Choi, H.J. Jung, SK Koh, CM Lee, and K. Jeong, *Journal of materials science letters* 16 (19), 1551 (1997).
- 214.T.V. Cuong, V.H. Pham, J.S. Chung, E.W. Shin, D.H. Yoo, S.H. Hahn, J.S. Huh, G.H. Rue, E.J. Kim, and S.H. Hur, *Materials Letters* 64 (22), 2479 (2010).
- 215.B. Chwieroth, B.R. Patton, and Y. Wang, *Journal of Electroceramics* 6 (1), 27 (2001).
- 216.E. Brunol, F. Berger, M. Fromm, and R. Planade, *Sensors and Actuators B: Chemical* 120 (1), 35 (2006).
- 217.G. J.H. Lee, *Sensors and Actuators B: Chemical* 140 (1), 319 (2009).
- 218.N. SH Hahn, N. Bârsan, U. Weimar, SG Ejakov, JH Visser, and RE Soltis, *Thin solid films* 436 (1), 17 (2003).
- 219.M. Menetrey, A. Markovits, and C. Minot, *Surface Science* 524 (1), 49 (2003).
- 220.R. Hinde, *Physical review letters* 101, 165302 (2008).
- 221.M. Hübner, RG Pavelko, N. Barsan, and U. Weimar, *Sensors and Actuators B: Chemical* 154 (2), 264 (2011).
- 222.X. Wang, S.S. Yee, and W.P. Carey, *Sensors and Actuators B: Chemical* 25 (1-3), 454 (1995).
- 223.J.F. Boyle and K.A. Jones, *Journal of Electronic Materials*, *Iiol.* 6, 6, (1977).
- 224.RM Prasad, A. Gurlo, R. Riedel, M. Hubner, N. Barsan, and U. Weimar, *Sensors and Actuators B: Chemical* 149 (1), 105 (2010).
- 225.Y.T. Jang, S.I. Moon, J.H. Ahn, Y.H. Lee, and B.K. Ju, *Sensors and Actuators B: Chemical* 99 (1), 118 (2004).

PUBLICATION LIST

JOURNAL PAPER

- [1] Zainal Abidin Ali and R. Puteh, “Zn₂SiO₄ and SnO₂ nanowires synthesized by thermal ramping technique”, IJFPS, Vol.1, No.3, pp. 64-67, Sep. 2011.
- [2] W. Ahliah Ismail, Zainal Abidin Ali, and R. Puteh, “Optical and Physical Properties of Methyltrimethoxysilane Transparent Film Incorporated with Nanoparticles,” Advances in Materials Science and Engineering, vol. 2012, Article ID 124820, 6 pages, 2012.
- [3] Zainal Abidin Ali, W. Ahliah Ismail and R. Puteh, Synthesis of ZnO Nanowires for Hydrogen Sensor Application Using Simple Heating Technique (Submitted to Advanced Material Research).